

Design and Implementation of Microwave and Terahertz Material Characterization Methods

by

Saleem Shahid

A dissertation submitted to

Dipartimento di Elettronica, Informazione e Bioingegneria

Politecnico di Milano

in fulfillment of the requirements for the degree of

Doctor of Philosophy in Information Technology

2018

Supervisor:
Professor Gian Guido Gentili

Tutor:
Professor Michele D'Amico

Doctoral Program Coordinator:
Professor Andrea Bonarini

Cycle XXX

© Saleem Shahid 2018

All Rights Reserved

DEDICATION

To my parents

with respect and love

Saleem

ACKNOWLEDGEMENT

Undertaking this PhD has been a truly life-changing experience for me and it would not have been possible to do without the support and guidance that I received from many people. First and foremost, I would like to thank my supervisor Gian Guido Gentili, who has constantly encouraged me to strive for excellence in my career. He has been a continual source of inspiration for me, and has exceeded the call of a supervisor in every possible respect. He is an exceptional scientist, mentor, and friend. Without his guidance and constant feedback this PhD would not have been achievable.

I want also to thank the reviewers of this thesis, Prof. Jordi Romeu from Universitat Politècnica de Catalunya (UPC) Barcelona, Spain, and Prof. Patrizia Savi from Politecnico di Torino, Italy, for their valuable comments that helped me to improve the final version of the thesis.

I also wish to thank my colleagues Kapal, Misagh, Hamid, Naveed, Shahnawaz and Ahmed, and all others. I shared with them the joys and the sorrows of the Politecnico di Milano; and thanks to them and to their support, moral and technical, which I am here today to write these thanks.

Thanks to my great friends, Babar and Rizwan who inspired me to step forward for a new life experience abroad. I am very grateful for all their support and effort to cheer me up.

I would like to thank all the people that went along with me during my study period at PoliMi for making my life in Italy full of wonderful experiences. Finally and most importantly, I would like to thank my family: my parents, my brothers and sisters and my wife, Saba, for supporting me spiritually throughout writing this thesis and my life in general.

ABSTRACT

My PhD research work is focused on characterization of dielectric materials for microwave and terahertz imaging systems. Novel source antenna designs are proposed and a couple of time domain data inversion techniques are implemented in order to study dielectric material characterization of solid objects. Initially, stacked patch microstrip and custom shaped horn antennas are designed to improve the antenna bandwidth and spot focusing characteristics at microwave and terahertz frequencies. A waveguide-horn-waveguide structure scheme is used to model a horn antenna in order to avoid lens correction at horn apertures, which is usually needed to enhance the spot focusing. The presented horn antennas are designed and simulated with an accurate proprietary Body-of-Revolution Finite-Element code. Interaction of electromagnetic waves with materials is studied, where the variation in magnitude and phase of the transmitted and reflected wave has been observed with and without presence of dielectric material for calibration purpose. Different data inversion techniques are developed and tested e.g, Fourier inversion and Bayesian inversion. Time and computation efficiency of the post processing techniques has also been enhanced significantly, by using proprietary code in MATLAB. The analysis and estimation of dielectric properties is mostly based on measured data and simulated results obtained using commercial software (Ansys HFSS and CAD FEKO) for the purpose of comparison.

The dielectric measurement are carried out at PoliMI and UPC Barcelona to validate the results in multiple environments and test benches. Different Vector Network Analyzer (VNA) calibration techniques e.g, TRL, waveguide etc. are realized to minimise the measurement errors. Furthermore, the material thickness is also included in the inverion algorithm to reduce possible errors between ground (reference) and material's scattering parameters. The materials tested have dielectric constant in the range of 2 to 12 thickness ranging from 0.5mm to 10mm. Both single and multi-layered materials at different frequency bands i-e; 26-40GHz, 75-110GHz and 915-925GHz are measured during the experiments. We have successfully verified the accuracy of dielectric estimation as compared to the available data, while the computational power and time is significantly reduced when compared to commercial softwares like Ansys HFSS and CAD FEKO. The bayesian inversion method provides a measure of reliability on material properties since, the probability density is calculated and corresponding eigenvectors are plotted to find the confidence on observed parameters over model parameters. The novel horn antenna designs and improved time domain data inversion techniques made in this research, are very useful contribution in the development of latest dielectric measurement and imaging systems. The possible applications of this research are biomedical imaging for detection and diagnoses of cancer, non-destructive testing of structural defects in objects and communication systems with ultra-high data rates.

Keywords; Dielectrics, Material characterization, Antennas, Bayesian inversion

TABLE OF CONTENTS

Dedication iii

Acknowledgement iv

Abstract v

Table of Contents vi

List of Figures ix

List of Tables xiii

Chapter

1 Introduction 1

1.1 Dielectric Measurement Systems ……..…… 2

1.1.1. Background ……..... 2

1.1.2. Material Characterization Methods ……..……..... 2

1.1.3. Dielectric Measurement Systems…….……..…….. 3

1.2 Motivation and Contribution …….…..... 3

1.3 Applications …….……..... 4

1.4 Thesis Overview ……..... 5

2 Literature Review 8

2.1 Introduction to Dielectrics ……. 9

2.1.1. Dielectric Constant …….. 9

2.1.2. Dielectric Loss Tangent …….. 10

2.2 Antenna Sources …….……...…….……..……. 10

2.2.1. Dipole Antennas ……... 11

2.2.2. Stacked-patch Antennas …….. 11

2.2.3. Horn Antennas …….. 12

2.3 Dielectric Measurements …….. 13

2.3.1 Free Space Technique ……...…... 13

2.3.2 Waveguide Technique …….. 16

2.3.3 Termination of Coaxial Line Probe ……. 17

2.4 Material Characterization Methods ……. 18

2.4.1 Time Domain Fourier Inversion ……..... 18
2.4.2 Time Domain Bayesian Inversion ……... 20

3 Antennas for Dielectric Measurement 24

3.1 Microstrip Antennas ……..…… 25
3.1.1. Microstrip Antenna with Opposite Slots ……..... 25
3.1.2. Stacked Segment Patch Antenna …… 31
3.2 Horn Antennas ……..... 36
3.2.1 Pyramidal Horn Antenna ……..… 37
3.2.2 Conical Horn Antenna ……..……... 39
3.2.3 Exponential Horn Antenna ……..… 41
3.2.4 Shaped Horn Antenna …….. 43

4 Data Inversion Methods 50

4.1 Frequency Domain Technique ……..……. 51
4.1.1. Spot Focusing Characteristics ……..…… 52
4.1.2. TRL Calibration ……..……. 53
4.1.3. S-Parameters Extraction ……..…… 55
4.1.4. Dielectric Constant Estimation ……..……. 57
4.2 Time Domain Technique ……..……. 59
4.2.1. Reflection Method ……..... 59
4.2.2. Parametric Study and Discussion ……... 62
4.3 Measurement Results ……. 67
4.3.1 Frequency Dispersion Analysis ……..…..... 68
4.3.2 W-band Measured Results ……..... 71

5 Bayesian Inversion Method 74

5.1 Theoretical Approach ……. 75
5.1.1. Inversion Procedure and Dielectric Properties ……... 75
5.1.2. Model and Data Space …… 77
5.1.3. Analysis of Uncertainties and Sensitivities …… 78
5.2 Bayesian Inversion Results ……..…….. 79
5.2.1 Single Layer Materials …… 80

5.2.2 Multiple Layer Materials ……. 99

6 Conclusion and Future Work 103

6.1 Conclusion …… 104

6.2 Future Work ……..... 106

List of Publications ……...……..… 108

Bibliography……..……...……..… 110

LIST OF FIGURES

Figure no.	Title	Page
1.1	Applications of dielectric measurement systems	5
2.1	Charge propagation in dielectrics	9
2.2	Relation between complex permittivity and loss tangent	10
2.3	Design of the stacked patch microstrip antenna	11
2.4	Design of lens corrected horn antenna	12
2.5	Free space measurement setup	13
2.6	Measurement method at 68-118GHz	14
2.7	Illustration of waveguide technique	17
2.8	Coaxial probe line method	17
2.9	Measured and derived model for dielectric constant estimation	19
2.10	S11 extraction from reflection method	20
2.11	Illustration of probability density	22
3.1	UWB antenna geometry and prototype	25
3.2	Simulated S11 for different dielectric materials	26
3.3	Simulated S11 for different thickness of dielectric material (FR4)	27
3.4	Simulated S11 for different combinations of L2 & W2	28
3.5	Simulated S11 for different combinations of L1 & W1	28
3.6	Simulated radiation pattern for optimized UWB antenna (a) 4.2GHz (b) 5.5GHz (c) 8.2GHz (d) 9.7GHz	29
3.7	Comparison of simulated and measured S11	30
3.8	Stack segment antenna geometry	31
3.9	Return loss versus frequency analysis for SPA	32
3.10	Simulated S11 for h1=2.6 mm, stacked patch center (0, 0)	33
3.11	Simulated S11 for h1=2.6 mm, stacked patch center (-1,-1mm)	33
3.12	Simulated S11 for h1=2.6 mm, stacked patch center (-1.5, -1.5mm)	34
3.13	Simulated S11 for h1=2.6 mm, stacked patch center (-2,-2mm)	34
3.14	Comparison between FIT and FEM return loss results for widest impedance bandwidth case	35
3.15	The simulated radiation pattern of the proposed antenna at different frequencies (a) X-Z plane (b) X-Y plane	35

3.16	Typical horn antenna profile	36
3.17	Pyramidal horn model	37
3.18	Simulated and measured S11 for pyramidal horn	38
3.19	E-fields for pyramidal horn antenna; (a) E-plane and (b) H-plane	38
3.20	Spot Focusing at different distances from horn face, (a) 6cm and (b) 12cm	39
3.21	Conical horn antenna geometry	40
3.22	Magnitude and phase of E-fields for conical horn antenna	40
3.23	Geometry of the exponential horn antenna	41
3.24	S11 comparison between conical and exponential horn antenna	42
3.25	Magnitude and phase of E-fields for exponential horn antenna	42
3.26	Horn antenna geometry (a) Lens corrected and Shaped horn (b) 3D Shaped horn	43
3.27	Shaped horn antenna with geometry and modelling table	44
3.28	Simulated reflection coefficient of both horn antennas	44
3.29	Radiation magnitude and phase of lens corrected horn at different frequencies in dB (a) 920GHz (b) 940GHz (c) 980GHz (d) 1000GHz	45
3.30	Spot focusing by lens corrected horn at different frequencies in dB	46
3.31	Radiation magnitude and phase of shaped horn at different frequencies in dB (a) 920GHz (b) 940GHz (c) 980GHz (d) 1000GHz	47
3.32	Spot focusing by shaped horn at different frequencies in dB	48
4.1	Measurement setup with proposed shaped horn antenna	51
4.2	S11 of horn antennas (lens corrected horn and shaped horn)	52
4.3	Spot focusing of horn antennas at 2.55mm for 920GHz	52
4.4	Focusing of horn antennas at 920GHz (a) Magnitude (b) Phase	53
4.5	TRL calibration results	54
4.6	Material characteristics estimation in terms of S11, single layer with thickness = 0.01mm. LCH is lens corrected horn and SH is shaped horn	55
4.7	Material characteristics estimation in terms of S11, single layer with thickness = 0.1mm. LCH is lens corrected horn and SH is shaped horn	56
4.8	Material characteristics estimation in terms of S11, multi-layer with thickness = 0.01mm per layer. LCH is lens corrected horn and SH is shaped horn	56
4.9	Material characteristics estimation in terms of S11, multi-layer with thickness = 0.1mm per layer. LCH is lens corrected horn and SH is shaped horn	57

4.10	Material characteristics estimation in terms of Er, single-layer with thickness (a) 0.01mm (b) 0.1mm	58
4.11	The horn antenna model and setup details	59
4.12	S11 extraction from reflection method	59
4.13	Multiple reflective response from the MUT	60
4.14	Time domain post-processing method	60
4.15	Measured and derived model for dielectric constant estimation	61
4.16	S11 extraction from reflection method	62
4.17	Effect of MUT area on the dielectric loss tangent (a) 4cm, (b) 6cm, (c) 8cm	63
4.18	Effect of FR4 thickness on the dielectric loss tangent (a) 0.8mm, (b) 1.6mm	64
4.19	Effect of Roger RT/Duriod 5880 thickness on the dielectric loss tangent (a) 1mm, (b) 3mm	65
4.20	Effect of Silicon thickness on the dielectric loss tangent (a) 2mm, (b) 0.5mm	66
4.21	Experimental setup at PoliMI	67
4.22	Experimental setup at UPC Barcelona	68
4.23	Derived models and experimental time response from MUT	68
4.24	Magnitude and phase of measured data for grounded PEC and MUT	69
4.25	Material properties estimation for the FR4 material at Td = 0.8mm (a) Relative epsilon (b) loss tangent	70
4.26	Material properties estimation for the FR4 material at Td = 1.6mm (a) Relative epsilon (b) loss tangent	71
4.27	Experimental setup for W-band at UPC Barcelona	72
4.28	Material's dielectric constant estimation at W-band	73
5.1	Inversion iterative procedure	76
5.2	Steps involved in the inversion procedure	78
5.3	Matrix G: absolute value of eigenvectors in the model space [11]	79
5.4	Bayesian inversion software (a) Model parameters (b) Inversion parameters	80
5.5	Echo comparison for the case of single layer Rogers AD600	81
5.6	Residual analysis for the cases of single layer Rogers AD600	81
5.7	Dielectric constant (Er) vs thickness (Td) for the cases of single layer Rogers AD600	82
5.8	Matrix G: eigenvectors in the model space for all the cases of single layer Rogers AD600	83
5.9	Echo comparison for the cases of single layer FR4 Epoxy	84

5.10	Residual analysis for the case of single layer FR4 Epoxy	84
5.11	Dielectric constant (Er) vs thickness (Td) for the case of single layer FR4 Epoxy	85
5.12	Matrix G: eigenvectors in the model space for all the cases of single layer FR4 Epoxy	86
5.13	Echo comparison for the case of single layer Rogers RT/Duriod 5880	87
5.14	Residual analysis for the case of single layer Rogers RT/Duriod 5880	87
5.15	Dielectric constant (Er) vs thickness (Td) for the cases of single layer Rogers RT/Duriod 5880	88
5.16	Matrix G: eigenvectors in the model space for all the cases of single layer Rogers RT/Duriod 5880	89
5.17	Echo comparison for the case of single layer FR4 Epoxy (WO)	90
5.18	Residual analysis for the case of single layer FR4 Epoxy (WO)	90
5.19	Dielectric constant (Er) vs thickness (Td) for the case of single layer FR4 Epoxy (WO)	91
5.20	Matrix G: eigenvectors in the model space for all the cases of single layer FR4 Epoxy (WO)	92
5.21	Echo comparison for the case of single layer Rogers RT/Duriod 5880 (WO)	93
5.22	Residual analysis for the case of single layer Rogers RT/Duriod 5880 (WO)	93
5.23	Dielectric constant (Er) vs thickness (Td) for the case of single layer Rogers RT/Duriod 5880 (WO)	94
5.24	Matrix G: eigenvectors in the model space for all the cases of single layer Rogers RT/Duriod 5880 (WO)	95
5.25	Echo comparison for the case of single layer materials – W band	96
5.26	Residual analysis for the cases of single layer materials – W band	96
5.27	Dielectric constant (Er) vs thickness (Td) for the cases of single layer materials – W band	97
5.28	Matrix G: eigenvectors in the model space for all the cases of single layer materials – W band	98
5.29	Residual analysis for the cases of multi-layer materials	100
5.30	Dielectric constant (Er) vs thickness (Td) for the cases of multi-layer materials	100
5.31	Matrix G: eigenvectors in the model space for all the cases of multi-layer materials (a) 2 layers (b) 3 layers	101

LIST OF TABLES

Table no.	Title	Page
3.1	Antenna Dimensions	26
3.2	Summary of Parametric Study	30
3.3	Summary of Spot Focusing Parametric Study	47
4.1	Summary of the Parametric Study	67
5.1	Summary of Analysis – Single Layer Rogers AD600	83
5.2	Summary of Analysis – Single Layer FR4 Epoxy	86
5.3	Summary of Analysis – Single Layer Rogers RT/Duriod 5880	89
5.4	Summary of Analysis – Single Layer FR4 Epoxy (WO)	92
5.5	Summary of Analysis – Single Layer Rogers RT/Duriod 5880 (WO)	95
5.6	Summary of Analysis – Single Layer Materials	98
5.7	Summary of Analysis – Multi-Layer Materials	100

CHAPTER 1

Introduction

This chapter provides the brief introduction of my PhD research work which is focused on design and development of novel approaches for dielectric measurement. The measurement systems such as, free space method, and material characterization techniques such as, time domain bayesian inversion are introduced. The problem statement and motivation behind this research work is well explained, and contribution to the knowledge is presented. The possible applications and overview of the next chapters is also discussed.

1.1. Dielectric Measurement Systems

Dielectric constant measurement has been playing a vital role in various medical, security and non-destructive testing applications from the last few decades. Different type of measurement setups has been developed and improved by enhancing the antenna focusing performance, positioning systems etc. in order to achieve ultra-wideband (UWB) reflected waves or precisely the scattering fields from the object or dielectrics. Microwave and millimetre frequency signals are widely used to measure the s-parameters. The measured data is further processed to estimate the electrical properties of materials, particularly dielectrics. The sub-sections are organized below to briefly introduce the concept of dielectric measurement systems, mainly, background, reported characterization techniques and measurement systems used up till now.

1.1.1. Background

The dielectric material characterization has been divided into various types of measurements which depends on the nature of characterization i-e, (a) measurement in narrow or broad band, (b) the material under test (MUT) is low loss or high loss medium, (c) whether to measure the electrical and/or magnetic properties, etc. [1–2]. The free-space dielectric measurement method have been used widely over the years at microwave and millimetre frequency bands due to easy extraction of the transmission and/or reflection scattering parameters from MUT which is placed between transmitter and receiver antennas [3–5]. The free-space measurement method is mostly used for imaging and material characterization applications which particularly prefers non-destructive evaluation technique in order to avoid physical contact with a sample and reduce extra machining care needed for an MUT [2].

1.1.2. Material Characterization Methods

The conventional free-space measurement method for dielectric material characterization have been first experimented at the MIT Radiation Laboratory [6]. Later, a low-loss dielectric measurement based on the method in [6] at millimetre frequency bands has also been demonstrated by Breeden [7] which provided a comprehensive uncertainty analysis for the characterization of the materials. Similarly, another method is developed for the dielectric permittivity estimation using Brewster's angle and the magnitude of transmission and reflection coefficients are measured from reference metal and MUT [8]. Furthermore, in free-space measurement methods for microwave, millimetre or sub-millimetre frequencies, the dielectric constant of low loss and thinner materials has been estimated from envelopes of measured transmission and/or reflection spectra instead of the whole scattering parameters unlike in visible light or X-rays [9–10]. In most of the studies, we have noticed the use of only normal incidence wave interaction with materials to build the maximal and/or minimal envelopes. Many other interesting discussions on analytical analysis and derivations for the envelope method has been reported and their utilization in the dielectric measurement systems has been studied [11-12].

Another method which is gaining the reputation in material characterization is Bayesian inversion [13]. This method is proven to be efficient when it comes to the reduction of uncertainties in electrical or magnetic parameters estimation. Bayesian inversion can be useful to get the detailed information about the model parameters in terms of a probability density. Later, this probability density can be used to measure the uncertainty in the prior model parameters to build the confidence on observed parameters. In our dielectric measurement work, we have been able to find the uncertainties in the MUT thickness and its positioning. The uncertainty quantification (UQ) may be defined as: the process of quantifying uncertainties associated with extraction of scattering parameters and quantifying the uncertainty contributions of all other sources in data space [14].

1.1.3. Measurement Systems

The dielectric measurements encounter two type of problems; the error in positioning of MUT and data extraction method, and inefficient post-processing techniques to accurately estimate the dielectric properties. It is convenient to implement the measurement system using off-the-self performance instruments such as, commercial vector network analyzers (VNAs) and positioning apparatus [15-17]. The VNA uses the step frequency technique in order to perform the measurement in usually wide frequency range and it transmit each signal at different step frequency which illuminates the MUT individually, and the scattering parameters (transmitted and/or reflection) are received back [18]. We have used frequency domain scattering parameters for dielectric properties estimation as well as we have inverted it to time domain response using Fourier transform and Bayesian inversion. Despite that, the time domain experimental systems are also available where a pulse generator and real time oscilloscope is used instead of VNA [19]. Usually the pulse generator is used to generate the required pulse which illuminates the MUT and the time response is recorded at the oscilloscope [19-20].

1.2. Motivation and Contribution

To our understanding, the antenna systems for dielectric measurement can be further improved which will help to extract more accurate scattering parameters. There is a scope in the designing of UWB microstrip patch antennas as well as horn antennas with lens correction. The lens correction is usually done to achieve the better spot focusing. The antennas with wide bandwidth and directive radiation patterns are needed to get high resolution data from dielectric measurement systems. The lens corrected horn also limits the use of measurement setup at only single distance from transmitter to MUT (where distance is focal length of lens). Avoiding the lens correction will allow us to measure the scattering parameters at variable distance in near field. Furthermore, the measurement setups normally hold inaccuracy in the measured data due to different factors including positioning tolerance and physical limitation in setup, which makes the dielectric properties estimation more challenging. We have found the scope of improvement in the time domain data inversion techniques which can incooperate all the challenges. In this thesis, we have developed couple of time domain data inversion techniques which

are fast in processing and more accurate in dielectric properties estimation making this research work interesting and useful for dielectric measurement and imaging applications.

The contributions of this thesis are divided into two parts; the antenna designing and data inversion methods. The first part presents the designing of microstrip patch and horn antennas for bandwidth and radiation performance enhancement. We have proposed novel designs of microstrip patch antennas i-e; opposite slots and stacked patches, whereas the proposed horn antenna designs allowed us to measure the MUT at variable near field distances which was not possible with lens corrected horns. We have designed two different spot focused horn antennas; one for frequency domain analysis and another for time domain analysis for better removal of all the spurious elements after TRL calibration. In the second part, the research focus is shifted to the characterization of electrical properties of MUT such as, dielectric constant, loss tangent and MUT thickness for single and multi-layered materials at different frequency bands of 26-40GHz, 75-110GHz and 915-925GHz. The free space measurement method is used for data acquisition using commercially available VNA's and custom built positioning system. In order to extend the comprehensive study, the measurement are carried out at PoliMI and UPC Barcelona. The frequency domain analysis is done for 915-925GHz band while the different techniques in time domain analysis are used for 26-40GHz and 75-110GHz bands. The time domain Fourier inversion and Time domain Bayesian inversion techniques are developed with the focus on improvement of the results accuracy as well as reduction of computational power and time. We have successfully achieved convincible accuracy in dielectric properties estimation as compared to the reported techniques whereas the computation power and time is significantly reduced when compared to commercial softwares like Ansys HFSS and CAD FEKO.

1.3. Applications

This research work can be useful for the applications requiring the estimation of physical and/or electrical properties particularly dielectric constant, loss tangent and material thickness (see Fig. 1.1). The possible list of applications can be;

1. Non-destructive test for structural defects detection in small objects as well as buildings.
2. Product quality control e-g, food, drugs and commercial grade items etc.
3. Medical imaging for early cancer diagnoses and detection.
4. Security scanning of the concealed objects at airports and sensitive places.

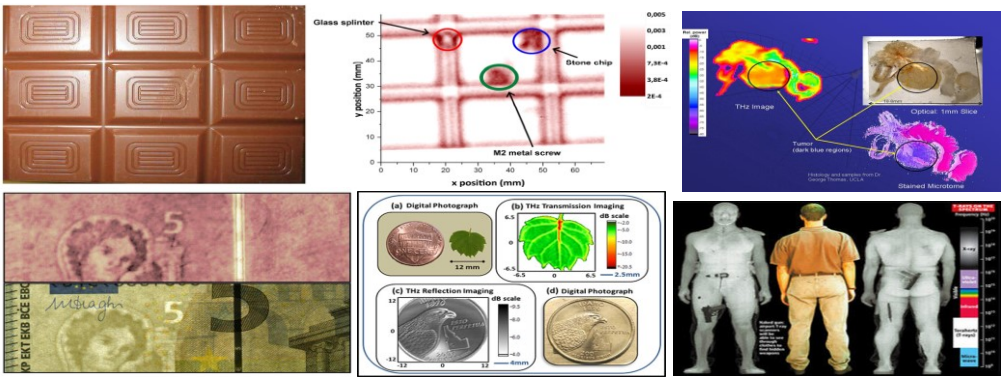

Fig. 1.1 Applications of dielectric measurement systems

1.4. Thesis Overview

The thesis is divided into different chapters where the chapter 2 provides the background needed for those not familiar with the subject and gives a brief introduction of current state of the art. The chapters 3, 4 and 5 present the author's contribution in detail including the appended papers. The PhD dissertation is organised as follows:

Chapter 2 provides a detailed insight about state of the art dielectric measurements. It first presents the basic of dielectric and other important properties of the materials. Later, the discussion is provided on antenna designs and latest dielectric measurement techniques used, precisely the free space method, waveguide based measurements and termination of coaxial probe line. Furthermore, the single and multi-layered data inversion techniques has also been presented.

Chapter 3 mainly focuses on the proposed antenna designs and, improvenemnt in the bandwidth, radiation pattern and spot focusing of the antenna beam. The different antennas are designed and their performance impact on dielectric measurements is explored. The UWB microstrip patch antennas with opposite slots and stacked patch configuration has been proposed. Later, the horn antenna structures has been introduced with the aim of removing the lens correction at horn aperture, which is usually done to enhance the focusing performance. All the simulation work is carried out in MATLAB 2016b and Ansys HFSS for antenna design as well as antenna integration in dielectric measurement setup. The performance and usefulness of each antenna is well explained in this chapter.

Chapter 4 describes the implementation of the dielectric measurement system. The components of the system are introduced first, including the antenna source, the MUT positioning and the setup. Afterwards, the frequency domain dielectric properties estimation is done at higher frequency bands of 915-925GHz band using only simulated scattering parameters. Later, time domain inversion method is presented in detail using Fast Fourier transform. Two different frequency bands; 26-40GHz and 75-110GHz has been used to measure the scattering parameters of different materials e.g., FR4, Roger AD600, RT/Duriod 5880, Bay-blend etc. The permittivity, loss tangent and thickness of the material is

estimated with frequency dispersion over the frequency bands. All the measurement work done at PoliMI and UPC Barcelona is also presented in this chapter.

Chapter 5 presents the implementation of Bayesian inversion method in detail. The same measured data used in chapter 4, is used again material properties estimation at both Ka and W-band. The scattering parameters of single and multi-layer materials are treated as observed parameters and introduced in data space and the desired dielectric properties are assumed as model parameters and included in model space. The materials properties are estimated with and without the ground plane. The probability density is calculated and the corresponding Eigen vectors are plotted to find the confidence on observed parameters.

Chapter 6 concludes the research work done in this PhD thesis. The research is summarized into five contributions and the corresponding future work is also suggested to improve the dielectric measurements especially in multi-layer mediums.

CHAPTER 2

Literature Review

In this chapter, the brief introduction to dielectric materials, antenna sources and measurement systems is presented. Different type of antennas are reviewed which are being used in dielectric measurement systems. The efficient measurement of a material's scattering response from wide band antenna excitation and techniques of material characterization are also studied. The survey on two conventional methods for material properties estimation: frequency domain and time domain inversion, are presented. Theory of Bayesian inversion method is also described in detail.

2.1. Introduction to Dielectrics

The dielectrics are usually insulating or very poor conducting materials because they don't have the loose bounds or free electron which can drift through the material, so only electrical polarization happens [21-22]. The electrical and magnetic parameters of the dielectrics are calculated by illuminating them through the electromagnetic waves and measuring the scattering response.

2.1.1. Dielectric Constant

In dielectrics, the complex permittivity is a major parameter which defines the physical-electrical properties of the materials related to the energy storage and loss [21-23]. The dielectric properties of materials are important to be known for various applications. Measnwhile, the dielectrics are treated as a grounded mediums in our case of study as shown in Fig. 2.1.

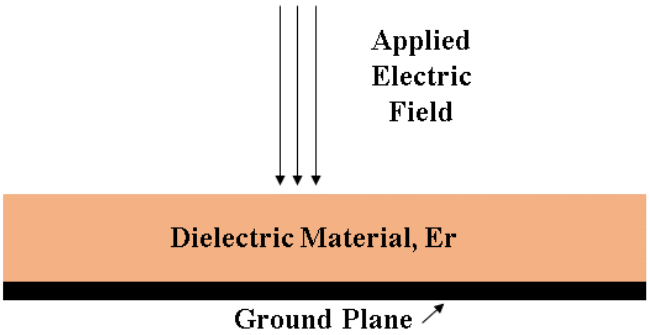

Fig. 2.1 Dielectric materials with ground plane

The real and imaginary parts of complex permittivity can also be defined with respect to free space permittivity (ε_o) as;

$$\varepsilon = \varepsilon_o . \varepsilon_r \qquad (2.1)$$

where ε_r is the relative permittivity which is also defined by the factor through which capacitance of the capacitors increases e.g., the volume between capacitor plates is filled with dielectric material which increases the capacitance relative to the free space capacitance [22, 24]. Moreovere, the dielectric constant of materials is also dependent on frequency and temperature, and it varies between different dielectrics. There are two parameters of the dielectrics which defines the dielectric attenuation are; conductivity, σ, and imaginary part of permittivity, ε. The permittivity is treated as a complex quantity, given as;

$$\varepsilon = \varepsilon' - j\varepsilon'' = D/E \qquad (2.2)$$

Where D is the electric flux density and E is the electric field strength. The real part of complex permitivitty (ε') is defined as dielectric constant and ε_r' the relative dielectric constant. Similarly, the imaginary part of comlex permitivitty (ε'') is defined as dielectric loss factor and ε_r'' the relative dielectric loss factor of the dielectric [21, 24]. The $\varepsilon_o = 8.854191 \times 10^{-12}$ Fm^{-1} is the permittivity of free space.

2.1.2. Dielectric Loss Tangent

The loss tangent of dielectric is defined as ratio (or angle in a complex plane) of the losses in medium w.r.t the applied electric field, E [21]. The angle δ, is very small for some dielectrics i-e, $\delta << 1$, in that case, $\tan \delta = \delta$. The real and imaginary parts of complex permittivity of the dielectric medium and corresponding angle δ, can be represented on x-y axes as shown in Fig. 2.2, below.

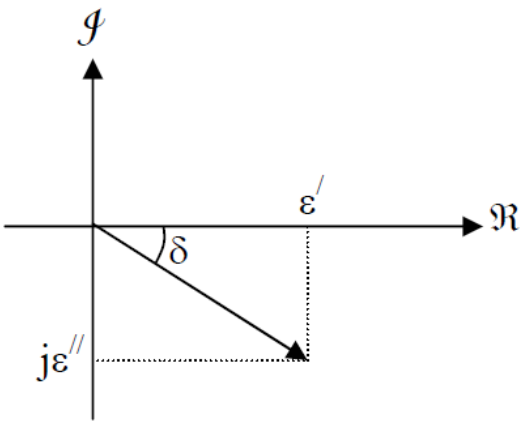

Fig. 2.2 Relation between complex permittivity and loss tangent

The dielectric loss tangent is expressed in terms of loss ratio, as given below;

$$\tan\delta = \varepsilon'' / \varepsilon' = \sigma / \omega \varepsilon_r' \varepsilon_o \qquad (2.3)$$

2.2. Antenna Sources

Antenna is one of the vital component in any wireless system, particularly dielectric measurement systems in our case [25-28]. The antenna source is determined by how well it can radiate and/or receive back the scattering response. Over the years, different type of antennas are designed and tested in dielectric measurement setups especially, microstrip patch and horn antennas. Microstrip patch antennas are used for ultra-wide band (UWB) imaging and material characterization applications at RF and microwave bands whereas horn antennas are mostly used for wide band material characterization at microwave, millimetre and sub-millimetre wave bands [25, 28].

The UWB antennas for imaging and dielectric measurement system needs to be less dispersive and linear phased so that, they can achieve the high resolution scattering response at microwave band [29-30]. Different challenges arises in achieveing UWB performance in microstrip antennas such as, small size, good impedance matching, stable gain and radiation patterns etc. [30]. Similarly, number of horn antenna designs are reported in literature which are being used in microwave material characterization [26-27]. The conical horn antennas with custom structure or lens correction are realized in order to

achieve desired antenna performance for frequency domain and time domain material characterization [27]. The different type of imaging antennas are discussed below in detail.

2.2.1. Dipole Antennas

The dipole antennas are happened to be compact and light weight but they lack the wideband characteristics which is usually desirable in dielectric measurements [28, 31]. When the dipole antenna is excited by an impulse wave, the radiation patterns of antennas are reported as end fire ringing patterns which are not suitable for our study of dielectric measurements. This end reflection problem can be resolved by adding a lossy material at the edges of dipole antenna which reduces the reflected waves and decrease the Q factor [31]. A resistive load can also be placed at a quarter wavelength of the dipole to avoid edge reflections and scattering. These technique were basically used to develop travelling wave antennas, but if we change the electrical distance from resistor to the ends of dipole, it limits the bandwidth of antenna which is again not desirable for our measurements setup [25].

2.2.2. Stacked-patch Antennas

The type of microstrip antennas in which, multiple parasitic patches are stacked, is particularly of our interest due to its wide band characteristics [32-35]. In stacked patch antenna, two or more parasitic patches are piled up with or without air gaps between them and usually fed from the shorting pin technique as shown in Fig. 2.3. The stacked patch antennas exhibits the wide operational bandwidth up to 30% of the band [36-37]. However, the University of Bristol has designed the stacked patch with the impedance bandwidth up to 77% which they have radiated directly into the breast tissues [38].

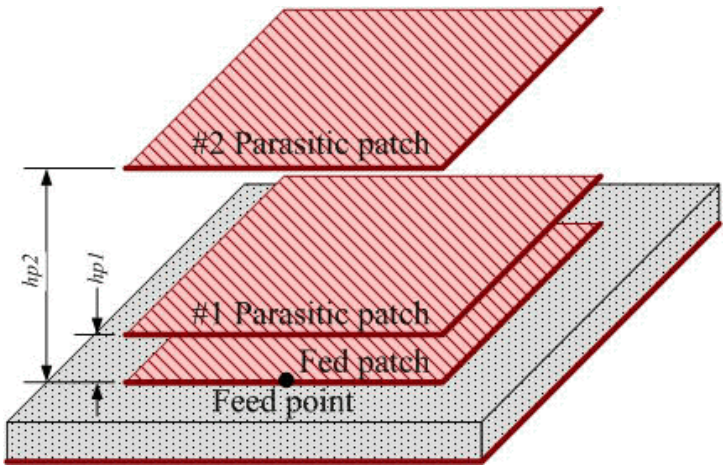

Fig. 2.3 Design of the stacked patch microstrip antenna [32]

Some more stacked patched antennas are reported in [39-40] where the antenna structure starts with design of patches and meandered slots in order to adjust the antenna resonance at desired frequencies. Different substrate materials are used in stacked patches e.g., FR4 Epoxy, Rogers RT/Duriod 5880 etc, patches used the same material or combination of them to achieve the wideband impedance bandwidth.

2.2.3. Horn Antennas

The horn antennas are famous for their directive radiation patterns with high gain that's why they are mostly used in standard gain measurements [27, 41-42]. The horn antenna is also known for its high aperture efficiency but sometimes they have limited bandwidth due to design and application constraints. There are various reported techniques which can be used to enhance the bandwidth of horn antennas such as, adding the metallic ridges in both waveguide and flare sections, where size of the ridges depends on the frequency tuning [43].

Microwave, millimetre wave and THz horn antennas with lens corrections [15], dielectric probing [44], photo-Induced coded aperture [45] and many more [46-49] has been used in order to improve the spot focusing for several dielectric material characterization and imaging applications. Particularly, the lens-correction techniques has gained our interest where the horn antennas with embedded lens has been reported in measurement setups for material characterization of solid objects [50-55]. The example of lens corrected horn antenna is shown in Fig. 2.4. However, this design approach is not found much successful for plane-waves generation, there is a fixed spot focusing point to extract scattering response. It also lack the spatial resolution and showed fabrication complexities. Overall, it has been found that horn antenna are suitable for imaging and material characterization applications.

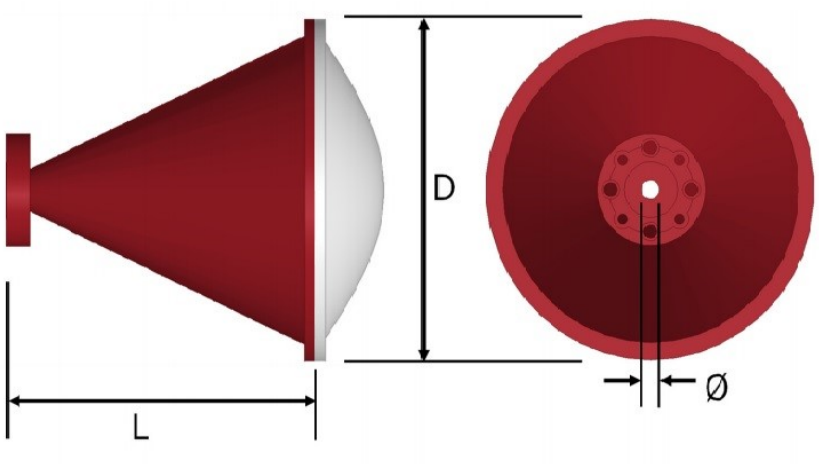

Fig. 2.4 Design of lens corrected horn antenna

2.3. Dielectric Measurements

It is known that, the electrical parameters of materials can't be calculated directly from the measurement but they can be extract from the scattering parameters or similar form of measured data [56-59]. We can estimate the dielectric constant, loss tangent and even thickness of the material from measured scattering data using various type of measurement techniques. Some of the most commonly used techniques are discussion in sub-sections below, with the emphasis on measurement of solid objects in different frequency bands. The detailed review of these techniques is provided in the work of Birch [2], Correia [3] and, Jain and Voss [4].

2.3.1. Free Space Technique

The most conventional method of extracting the dielectric properties of materials is from the reflection and/or transmission parameters which are measured in free space setup consist of one or two horn antennas [1, 7, 10-11]. In free space technique, normally, thickness of the material under test (MUT) is known or assumed within model parameters whereas the area of MUT is kept large enough to cover the full antenna beam which is important in extract of accurate s-parameters. In literature, different experimental setups of free space measurement are reported: Ma and Okamura [8] has measured the scattering parameters of the damp saw dust at 9.4GHz by plotting them in a container and then estimated the dielectric properties from measured data. The minimum size or area of MUT depends on the wavelength and antenna beam, larger the wavelength, larger is the MUT area required. A typical free space measurement setup is illustrated in Fig. 2.5.

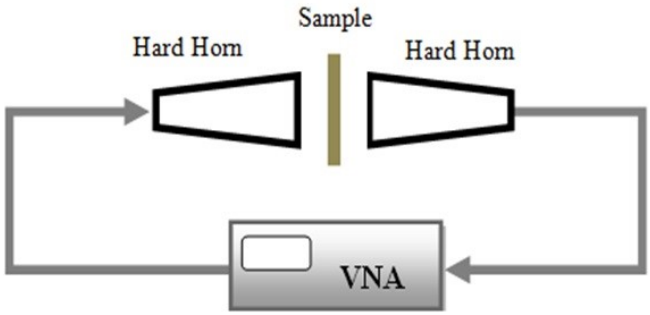

Fig. 2.5 Free space measurement setup

For example, the same free space technique is again used by Okamura et. al [8] for the frequency of 11-12GHz with MUT size of 50cm^2 and, the distance between antenna and MUT of 80cm. Kadaba [9] used the similar techniques to measure material properties at 56 and 94GHz and Cullen et. al [10] exploited the use of lens correction at horn antenna aperture which has significantly reduced the MUT size and also the separation between antenna and MUT. Similarly, Friedsam and Biebl [16] used free space technique for the estimation of higher value dielectric materials at W band. We have found that, the

phase of scattering parameters is useful in determining the accuracy of estimation instead of using only the magnitude of measured data. However, high degree of antenna and MUT positioning is required to measure the correct phase of material's scattering response. The requirement of phase accuracy increases with the increase in measurement frequency. Iijima et. al [17], has proposed a method of phase correction which significantly reduced the phase measurement difficulties. A free space measurement method which uses the precision waveguide reference run and combines it with the free space medium to generate an interferogram with the frequency shift pattern [18]. This method is used at 68-118GHz (W band) measurement to extract the transmission and reflection coefficient of ceramic materials, as shown in Fig. 2.6.

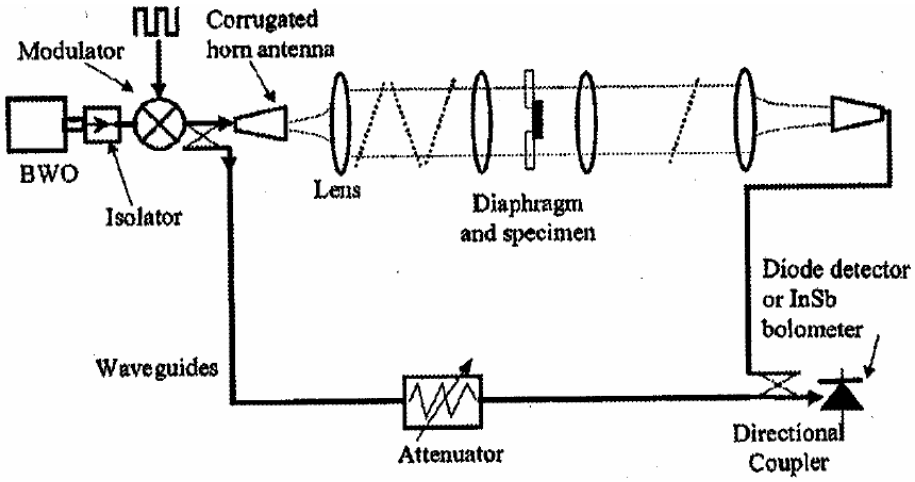

Fig. 2.6 Measurement method at 68-118GHz [18]

The free space measurement method is a non-destructive and contactless technique, to measure an MUT properties. The thickness and area of MUT can also be estimated but only if the antenna beam width is smaller than the MUT area and it passes through a uniform surface of MUT [19-20]. The measured scattering response is defined in terms of transmission and reflection coefficients as given in equations below;

$$S_{11} = \frac{\Gamma\left(1-\mathrm{T}^2\right)}{1-\Gamma^2\mathrm{T}^2} \tag{2.4}$$

$$S_{21} = \frac{\mathrm{T}\left(1-\Gamma^2\right)}{1-\Gamma^2\mathrm{T}^2} \tag{2.5}$$

These parameters are measured using an accurately calibrated VNA. The S_{11} can be extracted by 1-port reflective measurement system but S_{11} and S_{21} are measured by 2-port measurement system. The reflection coefficient is given as;

$$\Gamma = X \pm \sqrt{(X^2 - 1)} \tag{2.6}$$

Where,

$$X = \frac{S_{11}{}^2 - S_{21}{}^2 + 1}{2S_{11}} \tag{2.7}$$

Similarly, the transmission coefficient is given as;

$$T = \frac{S_{11} + S_{21} - \Gamma}{1 - (S_{11} + S_{21})\Gamma} \tag{2.8}$$

The choice of positive or negative reflection coefficient is defined as if $|\Gamma| < 1$, thus;

$$\varepsilon = \frac{\gamma}{\gamma_0}\left(\frac{1-\Gamma}{1+\Gamma}\right) \tag{2.9}$$

$$\mu = \frac{\gamma}{\gamma_0}\left(\frac{1+\Gamma}{1-\Gamma}\right) \tag{2.10}$$

Here, γ is the propagation constant of material, it is given as;

$$\gamma = \frac{\left[log_e(1/T)\right]}{d} \tag{2.11}$$

Where d is the thickness of MUT. The T is complex parameter and the expanded equation for propagation constant of material is given as;

$$\gamma = \frac{\left[log_e(1/|T|)\right]}{d} + j\left(\frac{2\pi n - \Phi}{d}\right) \tag{2.12}$$

Where, n = 1, 2, 3….

The real part of eq. 2.12 is a singular value whereas the imaginary part of eq. 2.12 contains multiple values.

$$\text{Imaginary part of } (\gamma) = \text{phase constant } (\beta) = \frac{2\pi}{\lambda_m} \tag{2.13}$$

$$\frac{d}{\lambda_m} = n - \frac{\Phi}{2\pi} \tag{2.14}$$

If n = 0 and $-2\pi < \Phi < 1$, $\frac{d}{\lambda_m}$ is between 0 and 1. There can be two cases depending on the thickness of material *d,*

- If $d < \lambda_m$, there will a single complex value of dielectric constant
- If $d > \lambda_m$, there will be measurement with two different values of thicknesses

If $d < \lambda_m$, then *i* must be 0, whereas, if $d > \lambda_m$, different values of *n* occurs. The problem of propagation in a material can be easily solved by eq. 2.14 but the thickness of material should remain less than that of λ_m. In general case, the relation between material thickness *d*, measured phase variation Φ and wavelength λ_m, can be defined as;

$$d_i = n_i\lambda_m + \frac{\Phi_i}{2\pi}\lambda_m, 0 < \Phi_i < 2\pi \qquad (2.15)$$

We have found that, most of the free space measurement methods faced problems in processing of the measured data in order to estimate the dielectric properties of material. One common problem which is reported was related to the multiple reflection between the MUT and horn antenna, it can be reduced or eliminated using the time gating technique in which only the desired portion of reflection is filtered out for further processing.

2.3.2. Waveguide Technique

The waveguide method is used to measure the scattering response of the material, where the MUT is placed between or in front of the waveguide and reflection and/or transmission coefficients are extracted [20, 57-59]. This method only considers the dominant mode of propagation, normally TE_{01} mode, and provides the estimation in whole bandwidth of the antenna system. There is one major challenge in this technique, the MUT sample must be placed accurately along the waveguide aperture without any air gaps because this technique assumes that current flows to/from the waveguide walls to the MUT. Hence, the MUT sample must be homogenous and planar surface material in order to provide 100% contact with waveguide walls [56]. The major disadvantage of waveguide technique is that, the sample MUT should be small sized keeping in mind the waveguide dimensions, which is not suitable for most of the industrial applications [20, 57].

There are variety of methods in waveguide technique to measure the reflection and/or transmission coefficients of solid as well as flexible and liquid materials. Reportedly, Sheppard et. al [56] measured the permittivity of human tissues and blood using waveguide technique from 29 to 90GHz band. They have extracted the scattering parameters of the blood by placing it in a container and measuring the reflection coefficient at two different thicknesses. Finsy et. al has also used the similar method to

measure the scattering parametersof the liquid material from 5 to 40GHz band [57], they have noticed the significant inaccuracy above 40GHz due to MUT positioning error and waveguide losses. The typical illustration of waveguide method is shown in Fig. 2.7.

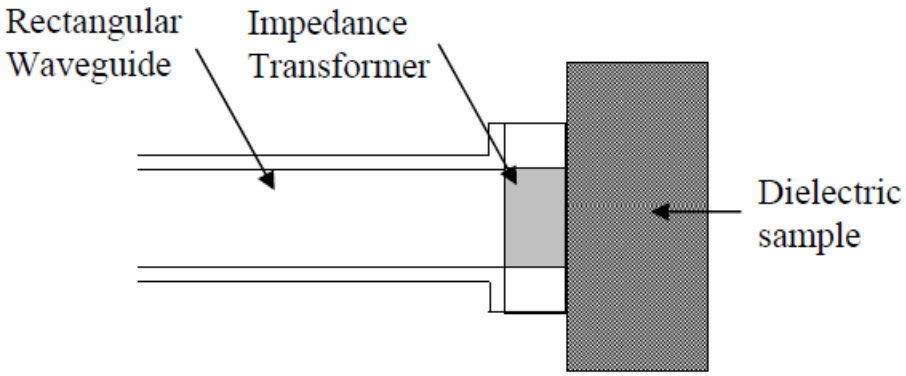

Fig. 2.7 Illustration of waveguide technique

There are many other methods of measurement in waveguide technique in which the MUT is between the transmission lines as a discontinuity e.g., adding MUT as dielectric waveguide or microstrip line [19, 58]. The scattering parameters of MUT are extracted and compared with the modelled parameters, the estimation is considered accurate when the measured data parameters translate the modelled parameters efficiently.

2.3.3. Termination of Coaxial Line Probe

The dielectric properties of MUT can also be measured with the coaxial probe line using commercial network analyser (VNA). In this method, the admittance is measured at the tip of coaxial probe line and calculated as a function of the dielectric constant of MUT [60-64]. Fig. 2.8 shows the experimental setup for the coaxial probe line technique.

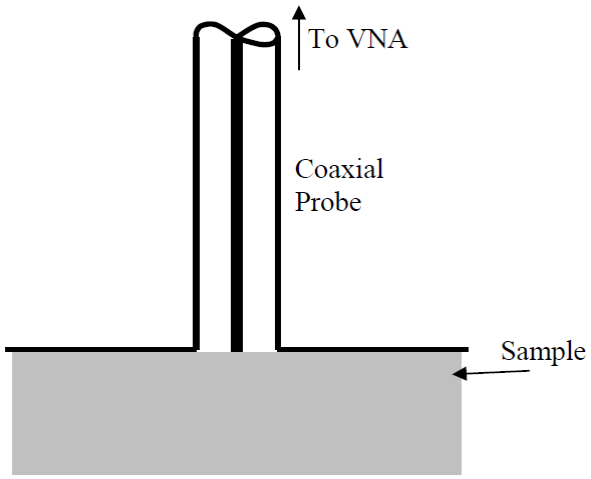

Fig. 2.8 Coaxial probe line method

The coaxial probe termination is one of the easiest method to find the dielectric properties of material, where the measurements doesn't need specific MUT sample dimensions. This method is best suited for the measurement of biological tissues [65]. The probe must be well calibrated with reference to a short circuit load and materials of known dielectric constant. The MUT thickness should also be large enough to in compensate the discontinuities in probe line which can produce inaccurate measurements. The MUT sample would remain in good electrical contact with the coaxial probe in order to avoid scattering from the rough surfaces of MUT. All these difficulties limit the use of coaxial probe method up to 20GHz [62]. However, some further research is reported from Boric-Lubecke et. al [66-67] who have measured the human skin tissues in Ka band (30 to 40GHz) using the typical 2.2mm coaxial probe. Similarly, [68] have also measured the biological tissues at 110GHz using small probe of 1mm diameter. Nevertheless, the calibration of coaxial probe is the major challenge in extracting the correct scattering parameters at such high frequencies.

There are couple of other methods which has been developed and tested for the measurement of scattering parameters of the materials. These methods are time domain spectroscopy [69] and coaxial line with dielectric filling terminated in a short circuit [63]. However, it is concluded that, most of these methods are not suitable for dielectric measurement above 30GHz.

2.4. Material Characterization Methods

There are various methods of material characterization after extracting the scattering parameters of materials from the dielectric measurements [13-14, 70-71]. In some methods, the frequency response of measured data is directly used to extract the dielectric material properties but it is difficult to remove all the spurious components from the data in frequency domain [70]. Thus, the measured data is inverted into time domain response for more accurate estimation of material properties, the time domain methods are discussed below in detail.

2.4.1. Time Domain Fourier Inversion

The scattering parameters are obtained for two type of data sets, one is the reference data set of grounded PEC for particular cases and second is the MUT observed data [72]. The voltage response of reference data is denoted by V_{PEC} and the voltage response for MUT data is denoted by V_{MUT}. The data is normally passed to a post processing system where the time sample (T_p) are defined for each response and kept within the specific defined frequency range (F_p). The time sweep (N_t) is defined as;

$$N_t = 2\text{^}\log_2(T_p x F_p) \qquad (2.16)$$

The conductivity coefficient (δ_{co}) is initially set to the nominal value whereas the conductivity of grounded PEC (δ_{pec}) is set as large as $1x10^4$. The Fourier transform (FFT) of both V_{MUT} and V_{PEC} is taken and divided into half in order to multiple with the spar (zeros) denoted by V1, and then it's further

mirrored on the Ind_f as Spar (Ind_F) and stored as V2 which is the FFT of V1. The conjugate of V2 and the V2 is added again and inverse Fourier transfer (IFFT) is taken to get back the scattering data [71]. The scattering response after the inverse Fourier transform and time windowing is shown in Fig. 2.9. The highest response is normally the reflection from MUT and it should be detected accurately by both prior model and measured S_{11} data. The highest peak is determined and a time window is created around the peak response time value (t_0) and Δt is defined as;

$$\Delta t = \frac{1.7}{\delta_{co}(f2-f1)} \tag{2.17}$$

Where the frequencies f_1 and f_2 are the first and last frequencies of the sweep respectively. The bounds of the time window are defined as;

$$T_1 = t_0 - \frac{\Delta t}{3},\ T_2 = t_0 + \frac{\Delta t}{3} \tag{2.18}$$

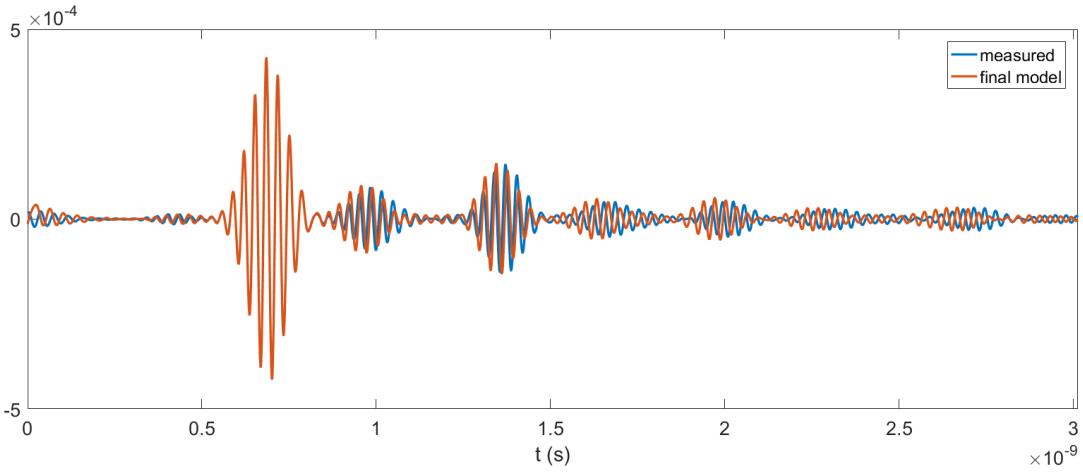

Fig. 2.9 Measured and derived model for dielectric constant estimation

After the comparison of derived model and measured data, the dielectric constant with minimum error percentage is obtained as shown in the graph below, Fig. 2.10. In this particular case, MUT has a dielectric constant 4.4 and thickness 1.6mm. This behaved as the starting point to any material estimation in time domain Fourier inversion.

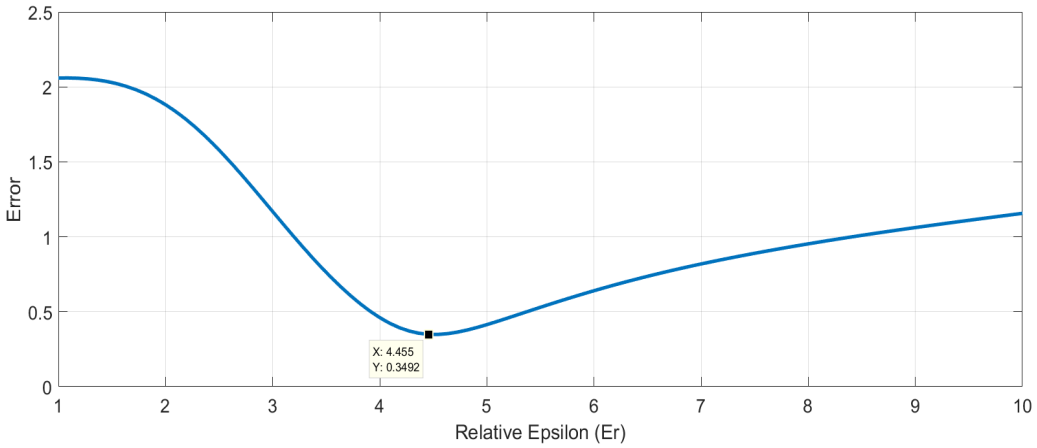

Fig. 2.10 Dielectric constant (Er) estimation from S11

2.4.2. Time Domain Bayesian Inversion

In Bayesian inversion method, the scattering response collected from the measurements is defined as the observed data parameters [13-14, 73]. The prior model is created in the beginning based on theoretical assumptions to define the model parameters. The correlation between the observed parameters and model parameters is described in terms of probability density and the inverse problem is derived on the basis of all the available information.

Every inverse problem is related to a physical system and the procedure to study such systems is divided into following steps [73];

i) Understand the physical system: identify the set of model parameters needed to estimation the system properties in a particular scenario (model space).

ii) Forward model: identify the physical or electrical laws for the given set of model parameters and built a prior model to correlate with the set of observed data parameters.

iii) Inverse modelling: use the real time results of measurements (observed parameters) to estimate the accurate values of the model parameters.

All the three steps are interdependent on each other and, the positive or negative progress in one of them is reflected in other two. In *step i* and *step ii*, the process is inductive and it gives the general conclusion on the model parameters while *step iii* is deductive and it provides the true estimation of model parameters. Therefore, *step iii* develop basis for the Bayesian inversion method.

A. Model Space and Data Space

The choice of model parameters is never easy and it varies depending on the nature of physical or electrical system i-e, the model parameters in our case are dielectric constant, dielectric loss tangent, thickness of MUT and positioning error in measurement setup [73]. This choice of model parameters is called parameterization of the system and it can be identical or equivalent to model parameters of another system [72-73]. We can create a manifold, which contains an abstract space of points which is independent of the parameterized system. Each point in manifold is representing a possible model of the system and this manifold is called model space denoted by *M*. There can be individual models for each point in the model space denoted as M1, M2 … etc. We normally choose a particular parameterization for the system and define certain set of experimental procedure to measure the model parameters in order to characterize the system [73]. Each point M of the model space *M* has a set of values m_1, m_2, …, m_n which are associated to a particular parameterization. We can define a linear model space **M**, if all the components in the model space have no curvature and we can sum two or more model points, m_1 and m_2 and perform their multiplication by a real number λ.

$$(m_1 + m_2)^{\alpha} = m_1^{\alpha} + m_2^{\alpha}\,, \qquad (\lambda m)^{\alpha} = \lambda m^{\alpha} \tag{2.19}$$

Similarly, the measurements are conducted to get the information about the observed parameters and find the correlation between observed parameters and model parameters. Here, we have to define another manifold which contains all the observed or measured data responses and called data space denoted by *D*. Later, all or any reliable result of the measurement will be associated to a particular point D in data space *D*. If the points are equal in both model and data manifold, then the structure is assumed as linear manifold and the data manifold is called the linear data space **D**, where $d = [d^i]$; i is the index set value.

$$(d_1 + d_2)^i = d_1^i + d_2^i\,, \qquad (rd)^i = rd^i \tag{2.20}$$

Each possible realization of d is then named as data vector.

B. Forward Problem

The experiments are conducted to perform empirical studies and propose theories, and these theories are later used to predict the outcome of future experiments [74-75]. These theories provide the comparison between experiments (observed data) and predicted results (model data). In physical theory, we explain the formulation by including the parameters, similarly the inverse problem theory also includes the quantitative analysis about the comparison of model (predicted) parameters and observed parameters. Thus, the forward problem can be defined as the prediction algorithm for accurate estimation of observed parameters which corresponds to the given model m, it can be denoted as;

$$\mathbf{m} \rightarrow \mathbf{d} = \mathbf{g}(\mathbf{m}) \tag{2.21}$$

where **d** = **g*(m)*** represents the set of equations $d^i = g^i(m_1, m_2, \ldots)$. The operator **g** is called the forward operator which describes the model of physical system.

In practice, the estimation of model parameters cannot be exactly accurate because of the measurement uncertainties and modelling errors. This is the reason, an inverse problem cannot be correctly proposed without accurate modelling of the system, and here the probability density comes into consideration [76]. All the measurement contains the uncertainties and therefore, the data set can't be described as the observed value but as a state of information extracted from an observed parameter. If we represent the **d** = $[d_1, d_2, \ldots, d_n]$ as the set of observed data, then the measured data can be defined in terms of probability density ρD(**d**) for the data space *D*.

C. Solution of Inverse Problem

We can define the prior probability density of both model space M and data space D as ρ(**d,m**) for collective space M x D. The theoretical probability density is also described as ρ_t(**d,m**) for the correlation between **m** and **d**. When we combine the information of prior and theoretical probability densities, we get the posterior state of information. The posteriori probability density σ(**d**,**m**) is defined as;

$$\sigma(\mathbf{d},\mathbf{m}) = k\frac{\rho(\mathbf{d},\mathbf{m})\rho t(\mathbf{d},\mathbf{m})}{\mu(\mathbf{d},\mathbf{m})} \qquad (2.22)$$

where μ(**d**,**m**) represents the homogeneous state of information and where k is a normalization constant.

It is concluded that the results obtained from these formulation are confined in the approach as compared to the previously reported methods [77-83]. Once the aposteriori information in the D×M space has been defined, the aposteriori information in the model space is given by the marginal probability density as;

$$\sigma_M(\mathbf{d},\mathbf{m}) = \int_D d\mathbf{d}\,\sigma(\mathbf{d},\mathbf{m}), \qquad (2.23)$$

while the aposteriori information in the data space is given by

$$\sigma_D(\mathbf{d},\mathbf{m}) = \int_M d\mathbf{m}\,\sigma(\mathbf{d},\mathbf{m}), \qquad (2.24)$$

Figure 2.9 illustrates the determination of σM*(**m**)* and σD*(**d**)* from ρ*(**d**,**m**)* and ρ_t(**d,m**) geometrically.

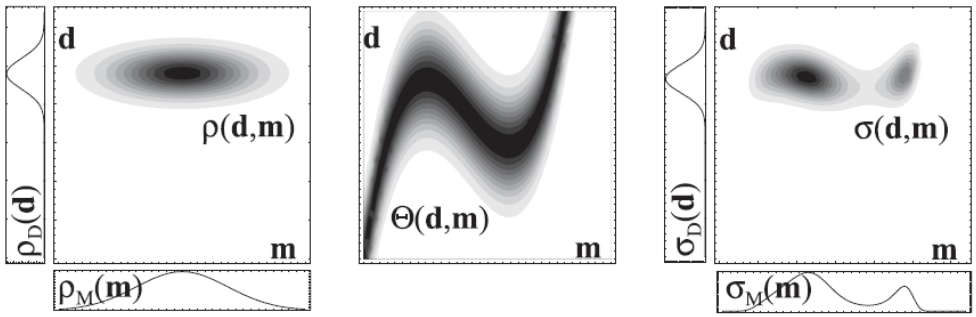

Fig. 2.11 Illustration of probability density [73]

CHAPTER 3

Antennas for Dielectric Measurement

This chapter demonstrate different type of antennas used in dielectric measurement systems. The microstrip patch and horn antennas are used to extract the scattering parameters in the measurement setup. The novel antenna designs are proposed in this chapter for microwave, millimeter wave and terahertz bands. The opposite slot and stacked patch antennas for UWB and custom structured horn antennas for Ka, W and terahertz bands are presented.

3.1. Microstrip Antennas

Dielectric measurement in microwave imaging systems require a compact antenna design which can provide wide operational bandwidth. The microstrip patch antenna (MPA) is suitable for UWB imaging applications due to their advantages of low profile, light weight, easy integration and low manufacturing cost. The growing interest of the researchers in MPA for the microwave imaging and dielectric measurement applications is well reported in [32-35]. In such applications, the antennas are designed to be used both as transmitter and receiver, and transmit the signal with high level of resolution. Microstrip antennas are suitable for this purpose because we can exploit their characteristics such as large impedance bandwidth, low side lobes and low mutual coupling (case of two different antennas for transmission and reception). In recent years, researchers have tried many techniques in order to further increase the input impedance bandwidth of microstrip antenna such as modified patch shapes [32-33], patches with vertical pins [34-35], modified probe configuration [36], and stacked patches [37-39]. Controlling a combination of above mentioned techniques, the impedance bandwidth can be enhanced to cover most of the UWB frequency band, ranging from 3.1-10.6 GHz.

3.1.1. Microstrip Antenna with Opposite Slots

In this section, the proposed antenna uses the meandering technique (opposite slots) to achieve the operational bandwidth of 3.9-10.3 GHz with the gain varying from 4.5-7.5 dB. The proposed UWB microstrip patch antenna (simulated and fabricated) is shown in Fig. 3.1(a-b), all dimensions are in *mm* otherwise indicated. The antenna consists of rectangular patch, 30×40 mm^2. The two opposite slots with dimensions L1×W1, and L2×W2 are entrenched in the radiating patch respectively. A dielectric substrate has the dimensions, 100×100mm^2 and thickness h.

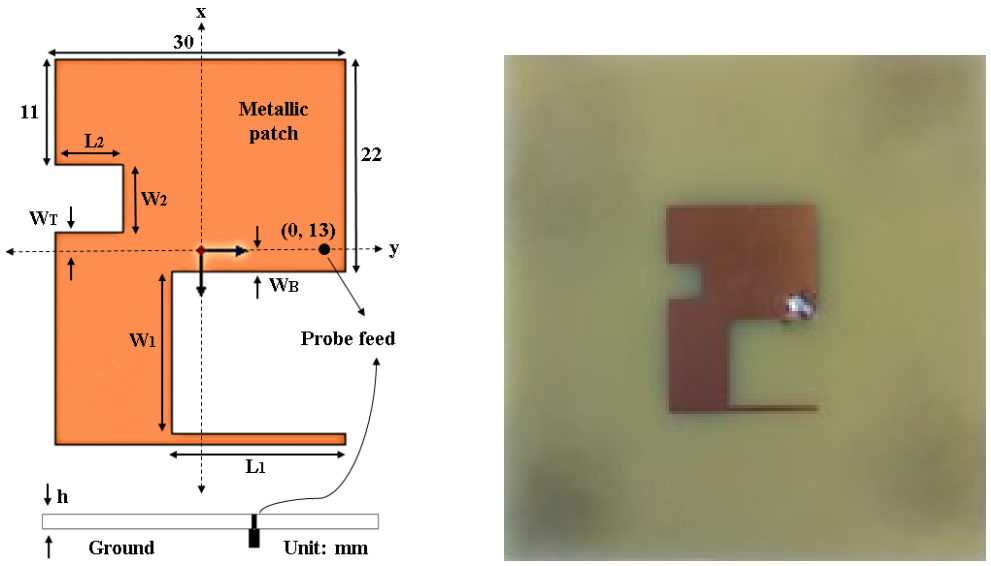

(a) (b)

Fig. 3.1 UWB antenna geometry and prototype

A 50Ω coaxial probe with 0.75mm inner radius is used to excite the proposed antenna centred at (0, 13mm). The design of UWB probe fed MPA with two unsymmetrical opposite slots is studied and briefly analysed for the dielectric measurement applications. The antenna is fabricated using the advance milling machine available at Politecnico di Milano. The optimized dimension of the prototype antenna are shown in Table 3.1.

Table 3.1: ANTENNA DIMENSIONS

Parameter	Dimension (mm)	Parameter	Dimension (mm)
L_1	7	W_1	7
L_2	17	W_2	18
W_T	2	W_B	2

The parametric study of the proposed UWB MPA has been done to analyse the effect of dielectric material and its thickness, and radiating and non-radiating slots. Initially, the antenna resonates at 5GHz with impedance bandwidth from 4.2 to 6.6GHz when the permittivity of dielectric material is 4.4 with thickness (h) of 1.6mm. The parameters which resulted in the enhancement of antenna impedance bandwidth from 3.9GHz to 10.3GHz are optimized slot dimensions and FR4 dielectric material of thickness 4mm. The material of antenna substrate and its thickness (h) were changed, and their effect on the antenna reflection coefficient is observed. In parametric study, the available dielectric materials such as, Rogers RT/Duriod 5880 (Er=2.2), FR4 Epoxy (Er=4.4) and Polyimide Quartz (Er=4) has been used with their distinct parameters. Fig. 3.2 shows the comparison of S11 versus frequency curves, for different dielectric materials.

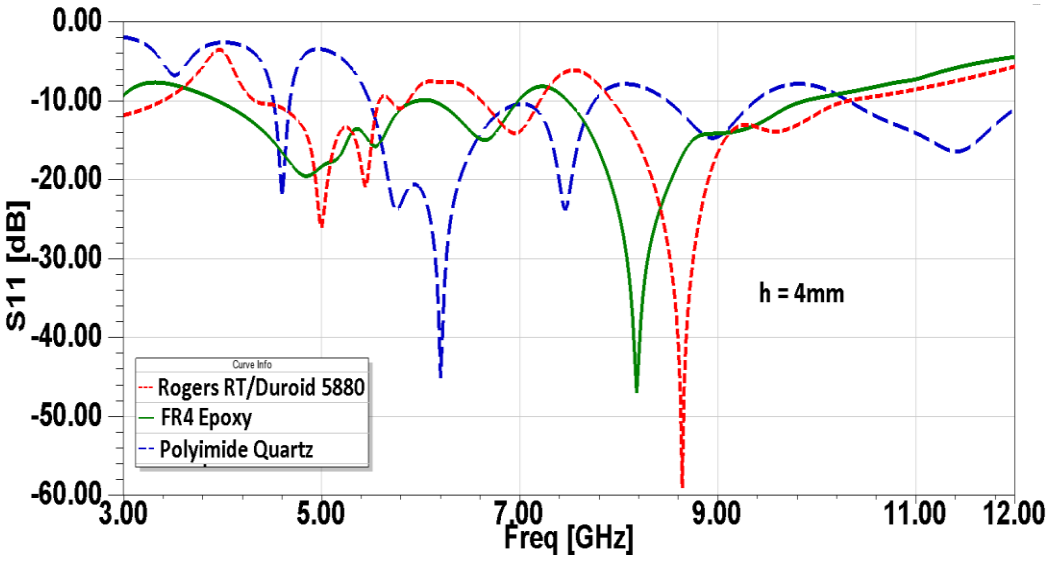

Fig. 3.2 Simulated S11 for different dielectric materials

Increasing the permittivity of dielectric material shifted the resonance band down to the desired frequency range for Rogers RT/Duriod 5880 and Polyimide Quartz but FR4 shows the up shifting with largest impedance bandwidth [40]. Fig. 3.3 shows the effect of thickness in case of FR4 dielectric material. Increasing the thickness of dielectric material has improve the impedance matching in the middle frequency band but leads to a higher mismatch in the lower frequency band. After this study, the best suitable dielectric material thickness is found to be 4mm for FR4 Epoxy, which provided an impedance bandwidth from 4.8 to 10.3GHz. This case has been further studied to enhance the impedance bandwidth in order to achieve UWB characteristics by possible optimizing the slots dimensions.

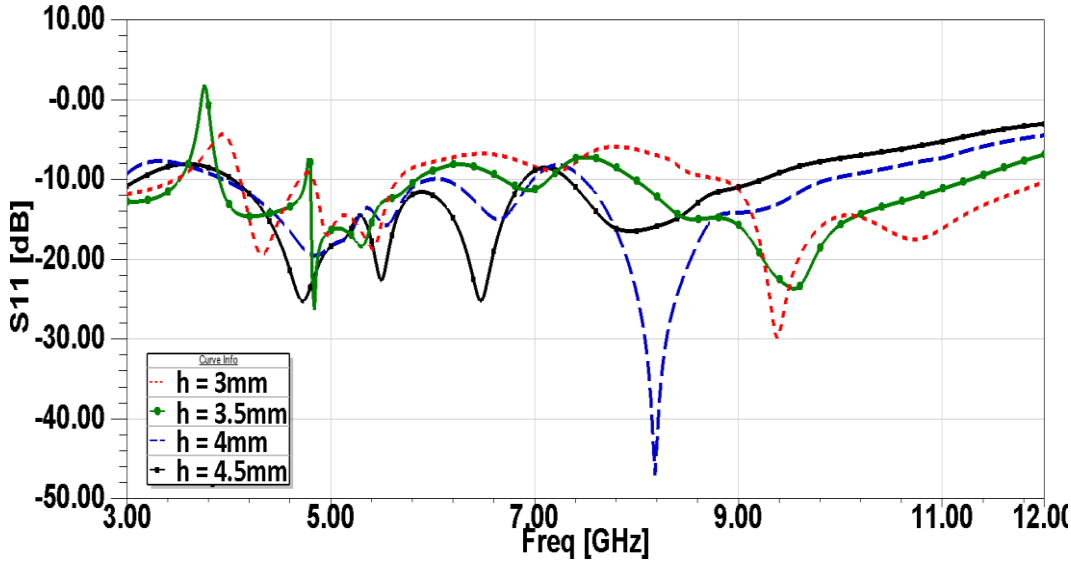

Fig. 3.3 Simulated S11 for different thickness of dielectric material (FR4)

The top slot dimensions (L2 x W2) were optimized first. Fig. 3.4 shows the variation of reflection coefficient (S11) with frequency for different combinations of L2 and W2. Changing the value of L2 and W2 has no effect on the impedance bandwidth of MPA but, at small values of L2, the extra resonance has been observed in lower part of the operational bandwidth. The study reviles that the widest impedance bandwidth has been obtained when L2 = 7 mm and W2 = 7mm, ranging from 4.5 to 10.1GHz, keeping the dimensions of L1 = 12mm and W1 = 13mm.

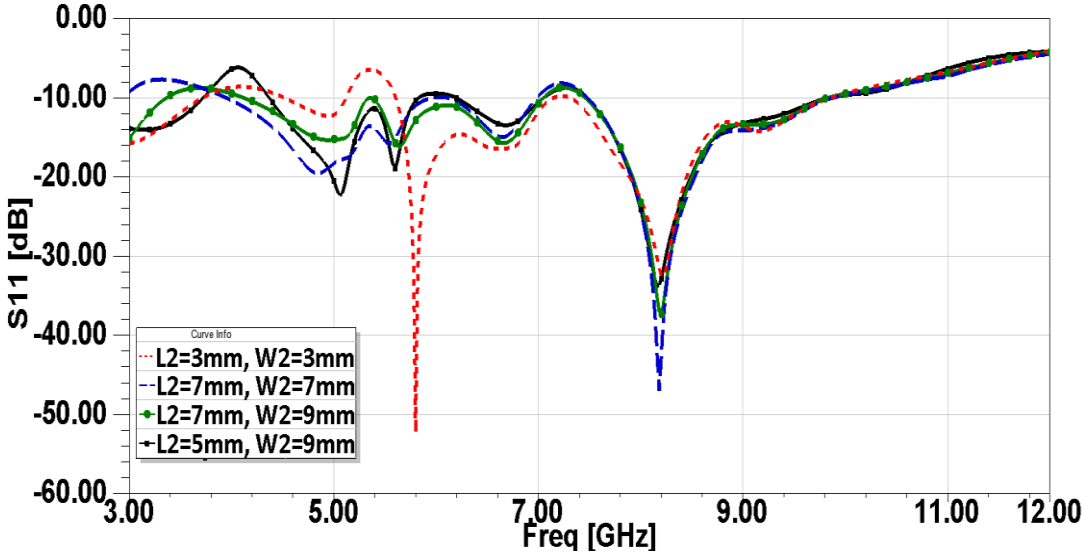

Fig. 3.4 Simulated S11 for different combinations of L2 & W2

The bottom slot dimensions are now optimized, keeping the dimensions of L2 = 7mm and W2 = 7mm. Fig. 3.5 shows the variation of reflection coefficient (S11) with respect to frequency for different combinations of L1 and W1. It can be observed in Fig. 3.5, increasing the value of L1 and W1 improve the operational bandwidth but, with an irregular patterns. The widest impedance bandwidth was obtained when L1 is 12mm and W1 13mm. An impedance bandwidth ranging from 3.9 to 10.3 GHz is obtained with the best optimized structure for proposed UWB antenna.

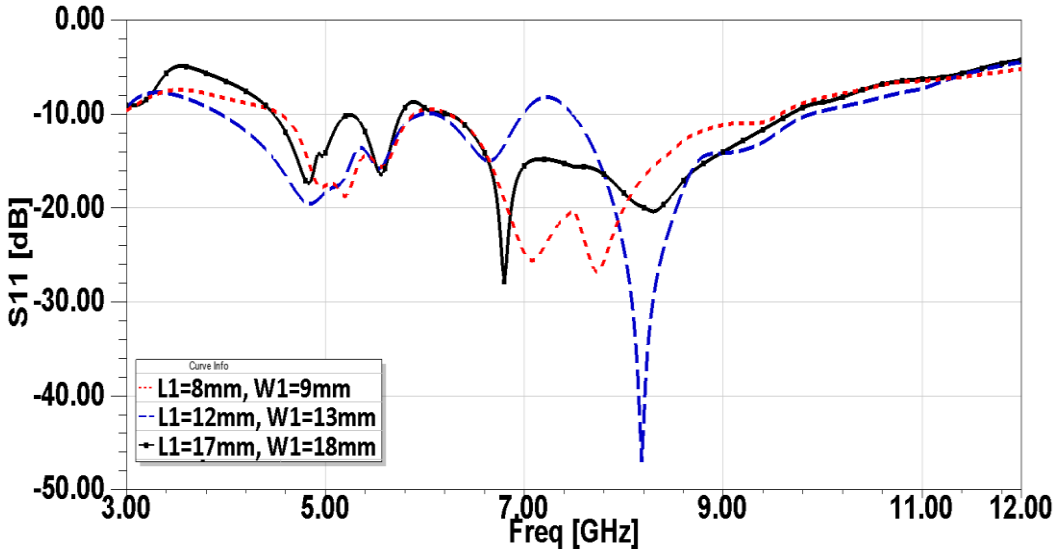

Fig. 3.5 Simulated S11 for different combinations of L1 & W1

The radiation patterns of the proposed antenna structure at four different frequencies has been are shown in Fig. 3.6 (a-d). The peak gain varies from -2.3 dB to 5.5 dB over the operational frequency band. The minimum gain is observed at the lower frequencies from 4 to 5 GHz and highest gain is witnessed from 8.5 to 9.5 GHz.

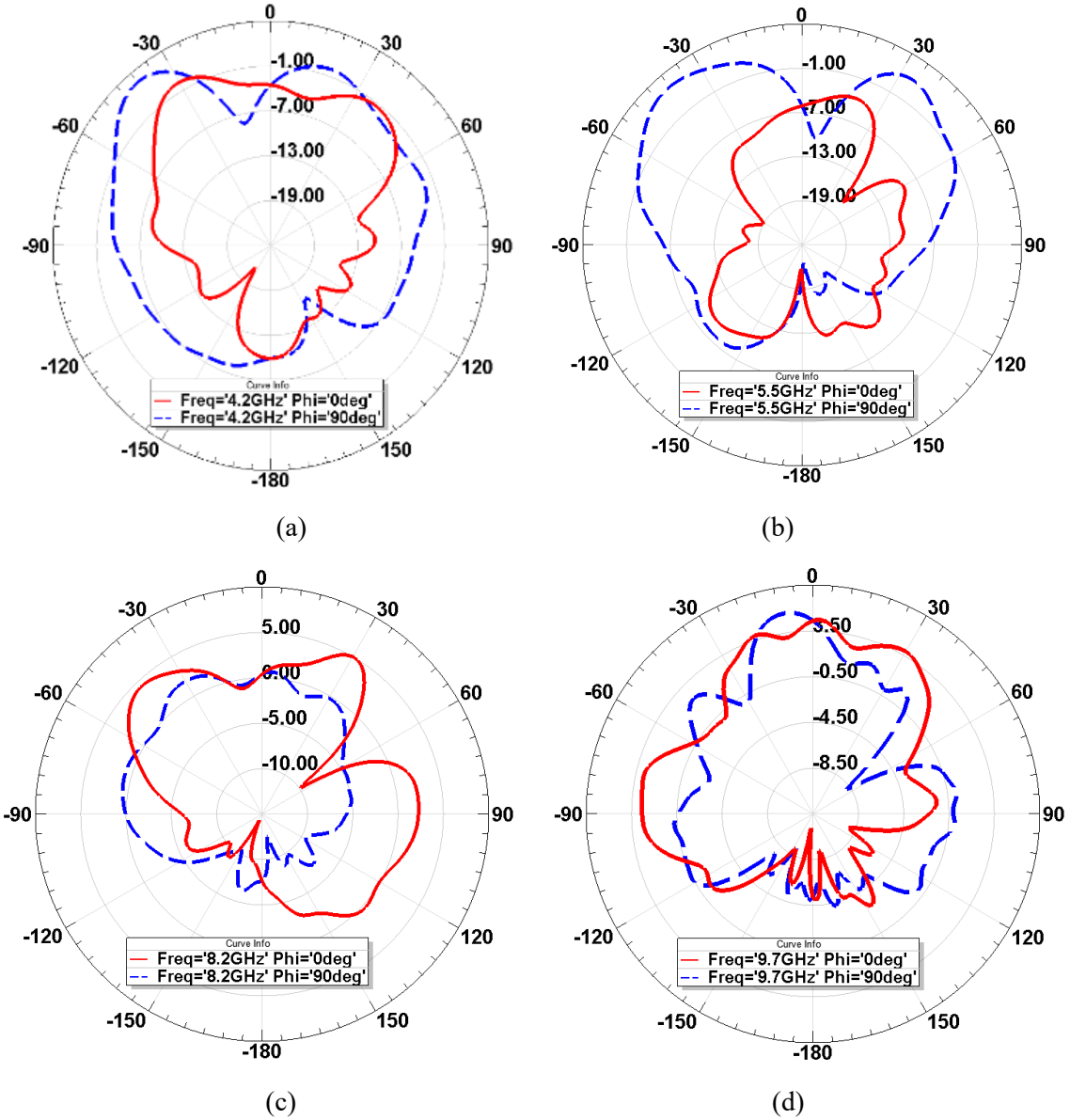

Fig. 3.6 Simulated radiation pattern for optimized UWB antenna (a) 4.2GHz (b) 5.5GHz (c) 8.2GHz (d) 9.7GHz

The optimized MPA has been fabricated using the antenna milling machine and measured using Anritsu Vector Network Analyzer. Fig. 3.7 shows the comparison between simulated and measured reflection coefficient (S11). The measured result seems in good agreement with simulated reflection coefficient but down shifted with some extra resonance notches. The two FR4 sheets of thickness 1.6mm and one sheet of 0.8mm has been stacked to make a 4mm thickness dielectric substrate, this stacking of sheets might have added the reported disagreement in results. Furthermore, the bandwidth variation between

simulated and measured S11 is less than 10% approx. which was considered due to soldering and fabrication tolerance.

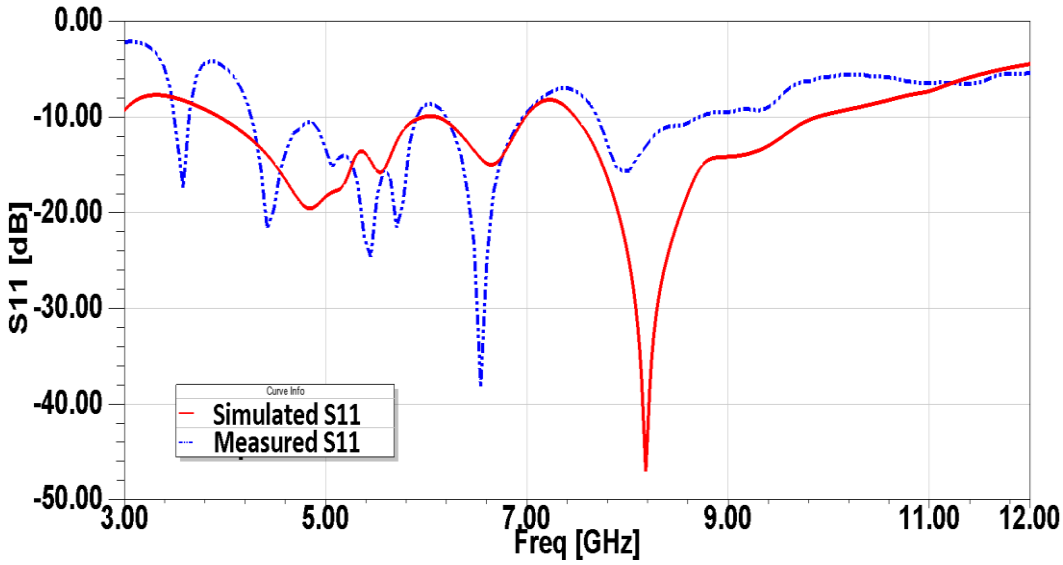

Fig. 3.7 Comparison of simulated and measured S11

The summary of the parametric study with optimized parameters and corresponding impedance bandwidth has been tabulated in Table 3.2. In the table, each optimized value is considered fixed for next optimized value e.g., FR4 Epoxy is considered fixed for dielectric thickness with optimized value 4mm. The UWB operational frequency band makes the antenna, a suitable candidate for variety of dielectric measurement systems.

Table 3.2: SUMMARY OF PARAMETRIC STUDY

Impedance Bandwidth		
Parameter	**Optimized Value**	**Bandwidth Range**
Dielectric Material	FR4 Epoxy	4.8 – 9.7
Dielectric thickness	4mm	4.8 – 10.3
Slot L_2 x W_2	7mm x 7mm	4.5 – 10.1
Slot L_1 x W_1	12mm x 13mm	3.9 – 10.3

3.1.2. Stacked Segment Patch Antenna

In this section, a stacked patch antenna (SPA) with substrate material RT/Duriod (dielectric constants ≈ 2.2 and Loss tangent ≈ 0.0004) is presented with an impedance bandwidth of 2.04:1, corresponding to the frequency range of 9.3-19GHz. Stacked patched antennas are also reported in [36-39] where the antenna structure combines the design of patches and meandered slots in order to optimize the antenna bandwidth at the desired frequencies. In the proposed design, we have added additional resonant structures, like L shaped slots on the excitation patch and two layer stacked patch are then optimally introduced into the antenna structure to realize the UWB impedance bandwidth. The stack centre is shifted at different locations to realize the best impedance bandwidth along with the variable thickness of substrate between the patches. A wide bandwidth of 9.7GHz is obtained with the proposed SPA design over the whole operational band.

The structure of proposed stacked segment antenna is shown in Fig. 3.8. The antenna consists of two square patches with thickness, 0.035mm; the first patch is deposited over the dielectric material at a distance (h1) 2.6mm away from the ground plane which has dimensions 20×20mm^2. It also contains two identical rectangular slots, with dimensions (L2 x S2) 12×1 mm^2, S1= 2 mm, and one square slit with dimensions (D1 x D1) 5×5mm^2. In the excitation slot, smaller square patch has been added with dimensions (D2 x D2) 3×3mm^2. The antenna is excited through a coaxial probe feed through an SMA connector attached to the patch (D2 x D2). The second patch is stacked over the first one at a distance h2 with dimensions (L1 x L1) 15×15 mm^2. Both the substrates use dielectric material Rogers RT/Duriod 5880, with the ground plane (40x40mm^2) at the bottom.

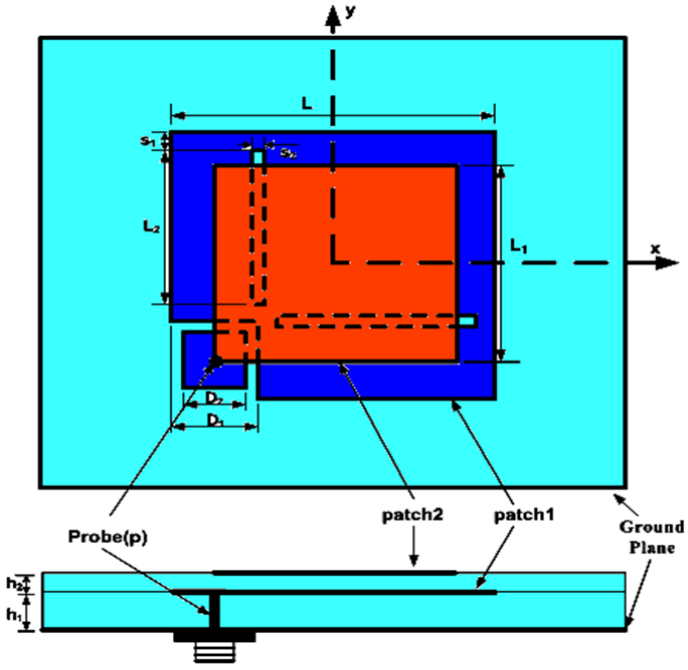

Fig. 3.8 Stack segment antenna geometry

The entire structure without stacking has been first examined using simulation softwares; Ansys HFSS and CST-MWS. The FEM analysis in HFSS and FIT analysis in CST has been carried out to optimize the antenna for best performance [34-35]. The obtained curves for reflection coefficient (return loss) versus frequency is shown in Fig. 3.9. A good agreement between both simulations has been found and the antenna impedance bandwidth for reflection coefficient below –9dB is calculated to be 11.5% between 17.2-19.3 GHz. To improve the operating impedance bandwidth, extensive parametric study have been done to obtain the best thickness and position of the stacked patches, keeping all other antenna parameters constant.

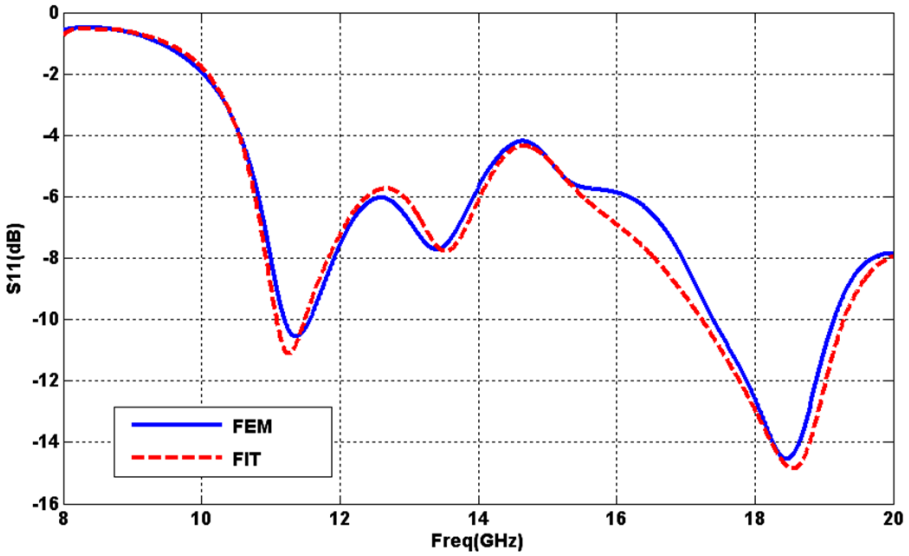

Fig. 3.9 Return loss versus frequency analysis for SPA

The effect of different structural parameters has been studied. The height (h2) is changed in different conditions to observe the performance of patch stacking technique. First case shows the comparison between different thicknesses of h2 while keeping h1 = 2.6 mm and stacked centre (0, 0), as shown in Fig. 3.10. When the value of h2 is changed from 0.4 to 0.9mm iteratively, the overall behaviour of resonance remained same with relatively better frequency bandwidth from 10 to 19GHz approximately. Similarly, the stack centre is changed from previous location to (-1,-1) keeping h1 and other parameters constant. It can been seen that the resonance has partially shifted towards higher frequencies while maintaining the bandwidth from 10 to 19GHz as shown in Fig. 3.11.

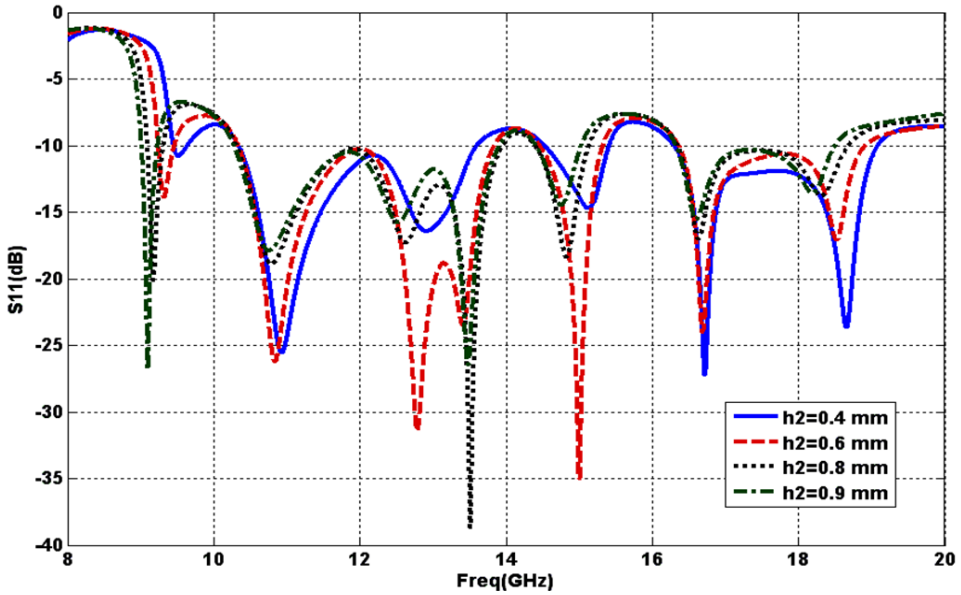

Fig. 3.10 Simulated S11 for h1=2.6 mm, stacked patch center (0, 0)

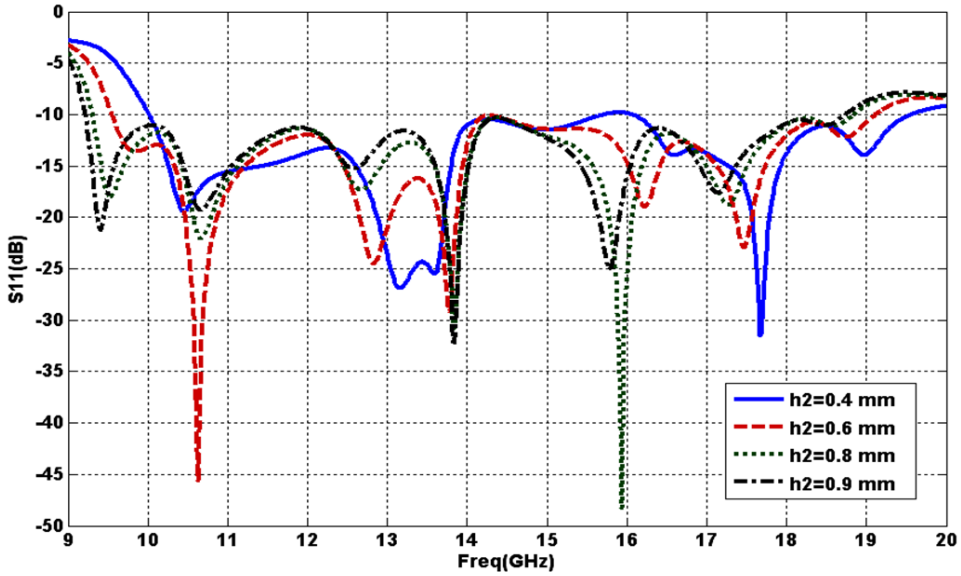

Fig. 3.11 Simulated S11 for h1=2.6 mm, stacked patch center (-1,-1)

In the third case, stack position is shifted to (-1.5, -1.5), the bandwidth is observed as shifting towards the lower frequency band along with irregular resonance at multiple frequencies in the operational band as shown in Fig. 3.12. Decrease in reflection coefficient around 9, 16 and 18GHz is seen which clearly shows the increase in capacitive coupling at these frequencies with change in stack centre location.

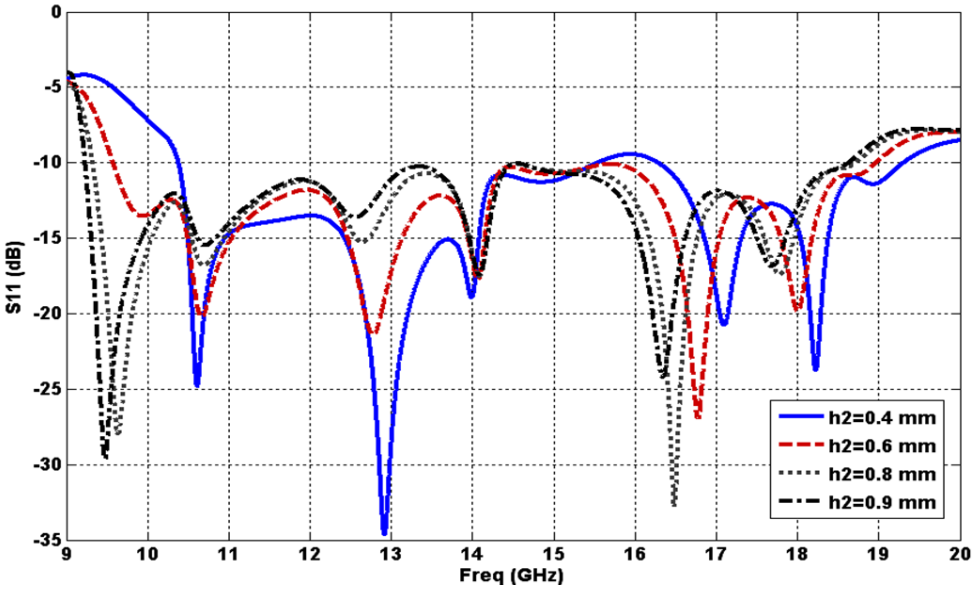

Fig. 3.12 Simulated S11 for h1=2.6 mm, stacked patch center (-1.5, -1.5)

The fourth and last case refer to simulations with stack centre (-2, -2) for h1 = 2.6mm. Fig. 3.13 shows the results for this case and it has been observed that wide bandwidth is now divided in two sub bands one from 10.5 to 13.7GHz and other from 16.8 to 18.5GHz which is not desired.

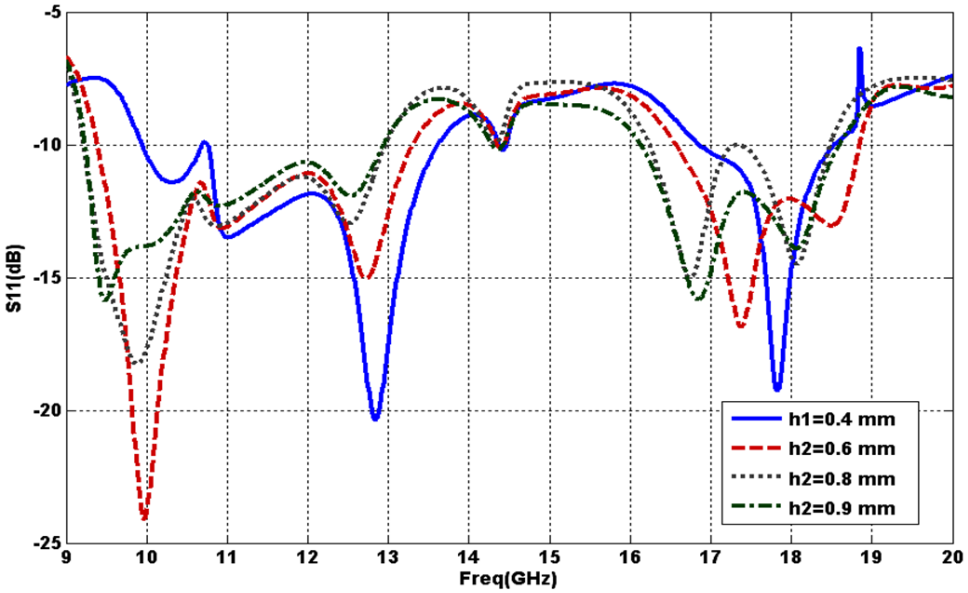

Fig. 3.13 Simulated S11 for h1=2.6 mm, stacked patch center (-2,-2)

From the previous four figures (3.10-3.13), the widest impedance bandwidth is obtained when the stacked patch centre is (-1, -1), and at a distance equal to 0.8mm from the excited patch. Fig. 3.14 shows the comparison between FIT and FEM results for the widest impedance bandwidth case. Convincing agreement between both results has been observed with an impedance bandwidth of 2.04:1 between 9.3-19 GHz.

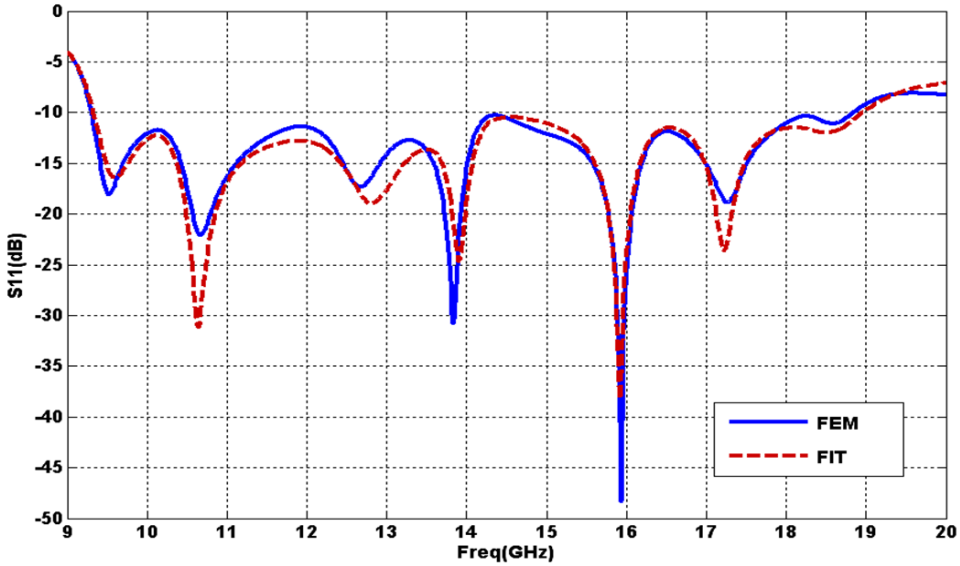

Fig. 3.14 Comparison between FIT and FEM return loss results for widest impedance bandwidth case

Fig. 3.15 (a-b) shows the radiation pattern for presented antenna at 9.5GHz, 13.8GHz, 15.9GHz, and 17.3GHz along X-Y plane and X-Z plane. The results show that the radiation patterns are mostly stable and Omni-directional, and remains unchanged in XY and XZ planes with the frequency variation. The maximum radiation is observed in the broadside direction.

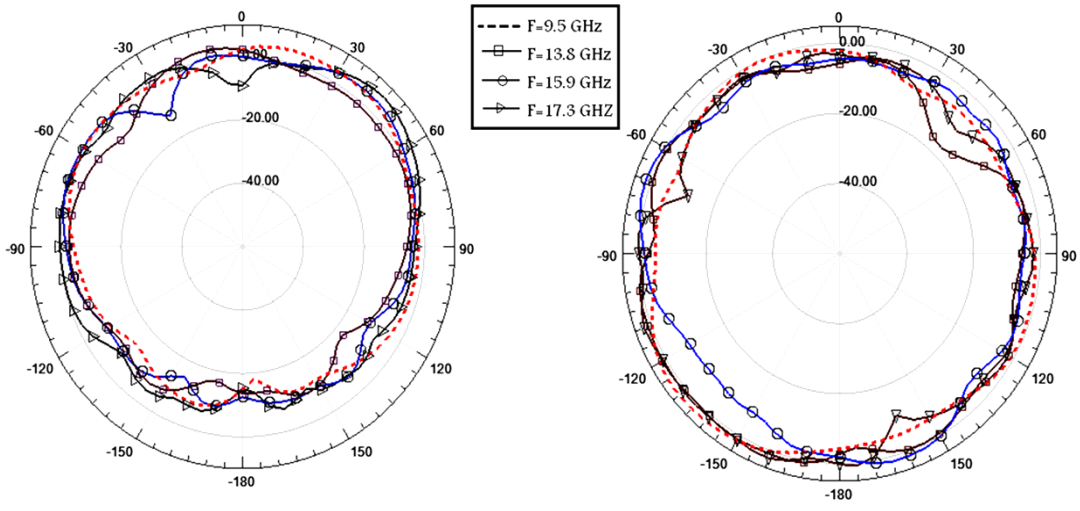

(a) (b)

Fig. 3.15 The simulated radiation pattern of the proposed antenna at different frequencies (a) X-Z plane (b) X-Y plane

The proposed UWB microstrip antennas with presented features can be suitable for applications where wideband resonance with Omni-directional radiation pattern is required such as, microwave imaging of tissues for detection of cancerous cell, for detection of concealed weapons, non-destructive testing of structural defects or quality control and many more applications can utilize with the unique characteristics of designed microstrip antenna. In all these application, the antenna transmits the input

wave through the targeted object and receives back the scattering response which is post processed to extract the dielectric and other electrical properties of the objects.

3.2. Horn Antennas

Microwave, millimetre wave and THz horn antennas with lens corrections [15], dielectric probing [44], photo-Induced coded aperture [45] and many more [46-49] has been used in order to improve the spot focusing for several dielectric material characterization and imaging applications. Particularly the lens-correction techniques has gained our interest where the horn antennas with embedded lens has been reported in measurement setups for material characterization of solid objects [50-52]. However, the lens corrected horns can't measure the scattering response at variable distance due to fixed focusing at focal length of the lens only. For the purpose of study, we have started with conventional pyramidal and conical horn antennas and optimize the structures for desired antenna characteristics, while keeping the best feature of them in position. Later on, we have introduced couple of modified horn profiles for desired focusing and scattering characteristics and compared them with lens corrected horn. The typical horn antenna profile is shown in Fig. 3.16, more discussion on horn profiling can be found in [53-55].

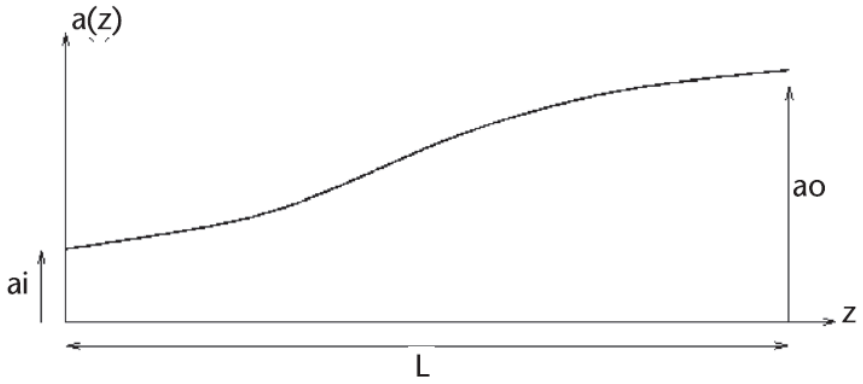

Fig. 3.16 Typical horn antenna profile

The linear horn can be build using eq. 3.1 corresponding to above figure.

$$a(z) = a_i + (a_o - a_i)\frac{z}{L} \qquad (3.1)$$

The custom shaped horn e.g., exponential horn can be built using eq. 3.2.

$$a(z) = a_i \exp[\ln(\frac{a_o}{a_i})\frac{z}{L}] \qquad (3.2)$$

3.2.1. Pyramidal Horn Antenna

The Pyramidal horn served as the starting point for horn antenna analysis and profiling. The Pyramidal horn is built at several desired frequency bands and the performance analysis has been done to identify the problem statement. Initially the pyramidal horn is designed in Ansys HFSS to reduce the model building complexity and computational time. The pyramidal horn model is designed at Ka band is shown in Fig. 3.17.

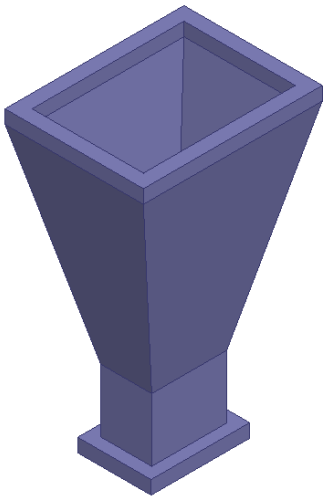

Fig. 3.17 Pyramidal horn model

The Design and dimensions for this pyramidal horn are taken from an available horn antenna model V637 operating at Ka band [55]. The antenna model is built in Ansys HFSS along with the reflective measurement setup for scattering parameters. Fig. 3.18 shows the comparison of simulated and measured reflection coefficient in free space for the modelled pyramidal horn antenna. The results showed good agreement between both results which motivated us to carry forward the horn antenna profiling for material characterization.

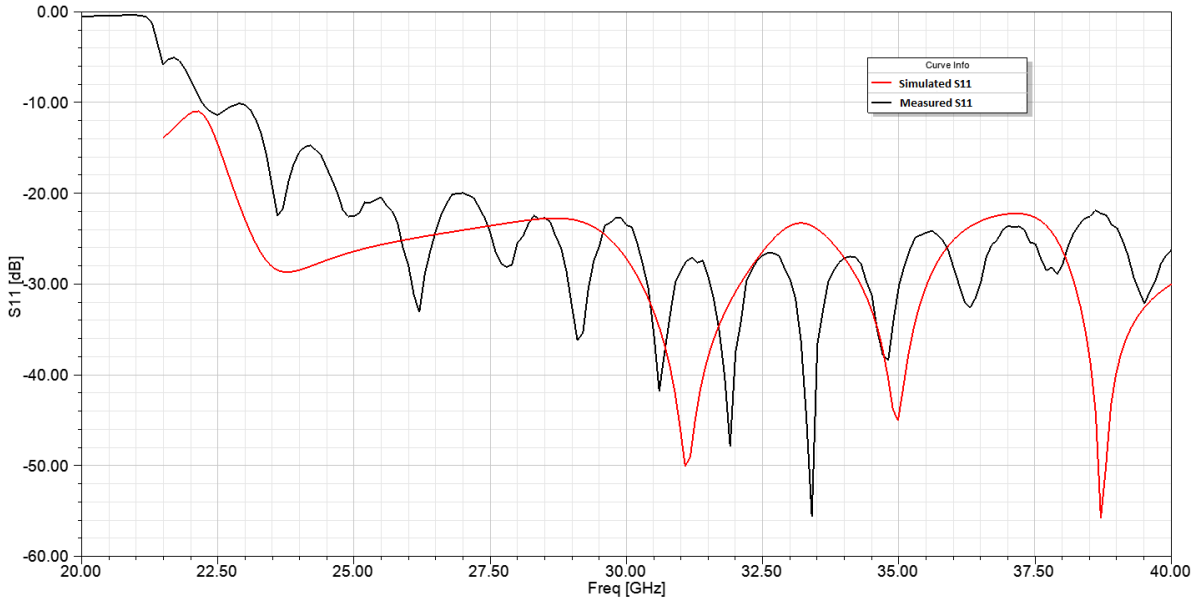

Fig. 3.18 Simulated and measured S11 for pyramidal horn

Fig. 3.19 (a-b) shows the electric field in E-plane and H-plane, which seems to be similar in both planes. The TE_{01} mode is propagating in waveguide of the horn antenna and, provides good spot focusing at a nominal distance range. The sharp edges of horn structure effects the directivity and plane wave generation which is critical in measuring the S11 from the material.

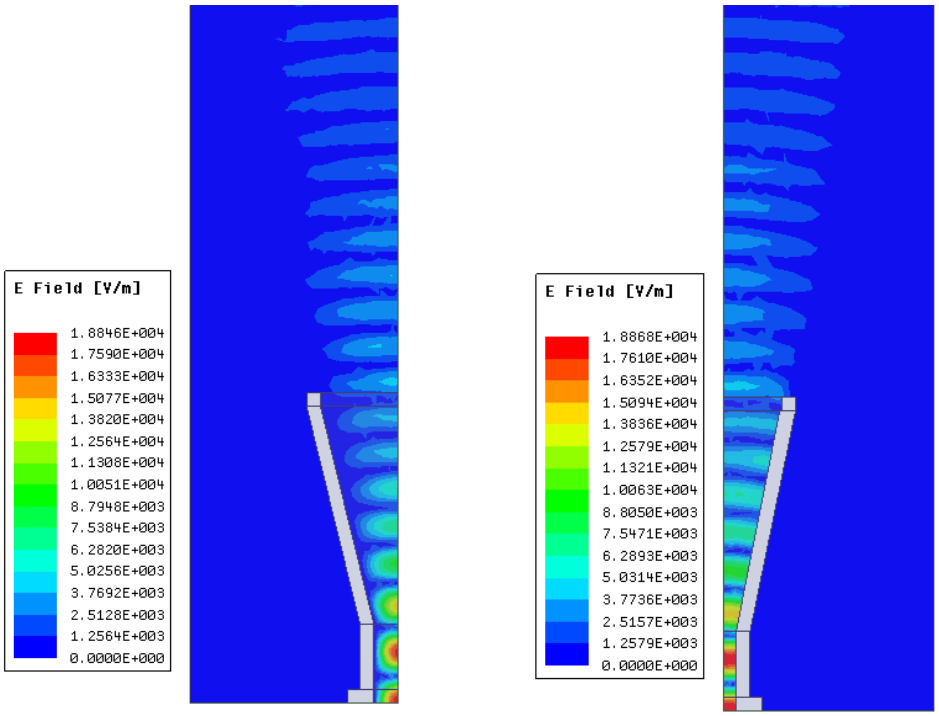

(a) (b)

Fig. 3.19 E-fields for pyramidal horn antenna; (a) E-plane and (b) H-plane

Fig. 3.20 shows the spot focusing magnitude from the top view at two different distance of 6cm and 12cm from the horn aperture. The observed spot focusing is not found suitable for S11 extraction for material characterization becuase the focusing is not centered and its spreading symmetically from the center of the horn aperture. This antenna design analysis realized us to use conical or somewhat exponential horn antenna designs which might provide better spot focusing.

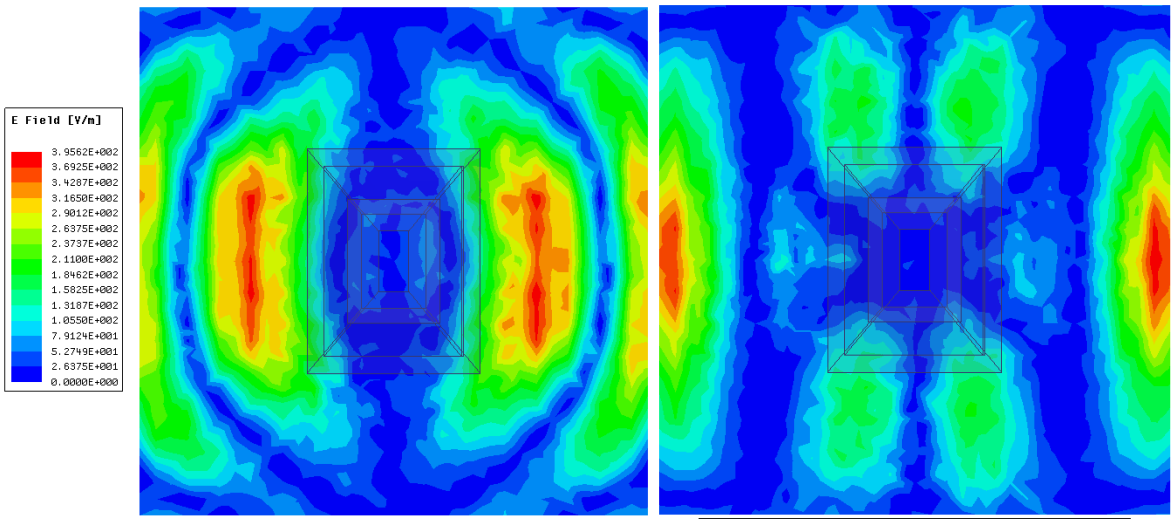

(a) (b)

Fig. 3.20 Spot Focusing at different distances from horn face, (a) 6cm and (b) 12cm

3.2.2. Conical Horn Antenna

After analysis of the pyramidal horn antenna, we have studied the conical horn antenna in same Ka band for the purpose of comparison. The dimensions of the conical horn are taken from the available conical horn available at antenna lab in PoliMI. The length of horn is 53.4mm and aperture radius is 23mm. Fig. 3.21 shows the geometry of conical horn antenna. The conical and exponential horn antennas are simulated in MATLAB 201b using accurate proprietary Body-of-Revolution Finite Element code [43, 54].

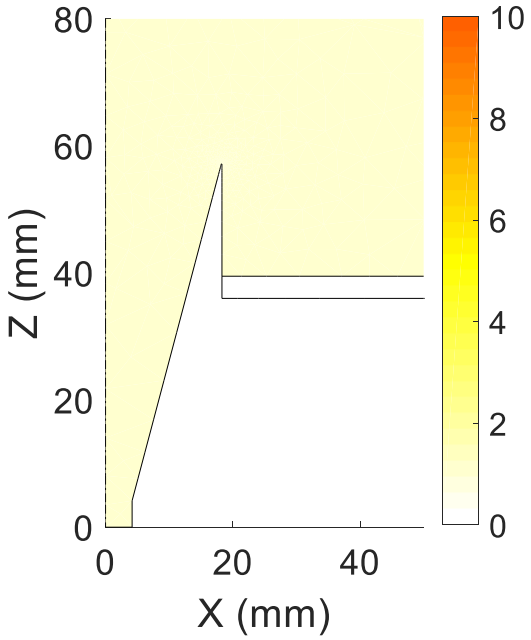

Fig. 3.21 Conical horn antenna geometry

The symmetry boundaries condition is used in simulation to reduce the computational power and time. Fig. 3.22 shows the electric field analysis of conical horn in terms of both magnitude and phase. The operational propagation mode is still TE_{01} but in case of conical horn, the antenna is producing plane waves and better spot focusing in near field. The smooth geometry of the conical structure helped in generating the plane waves. The conical horn provides the spot focusing up to 15cm from the horn aperture but it should be further improved for better estimation of material properties.

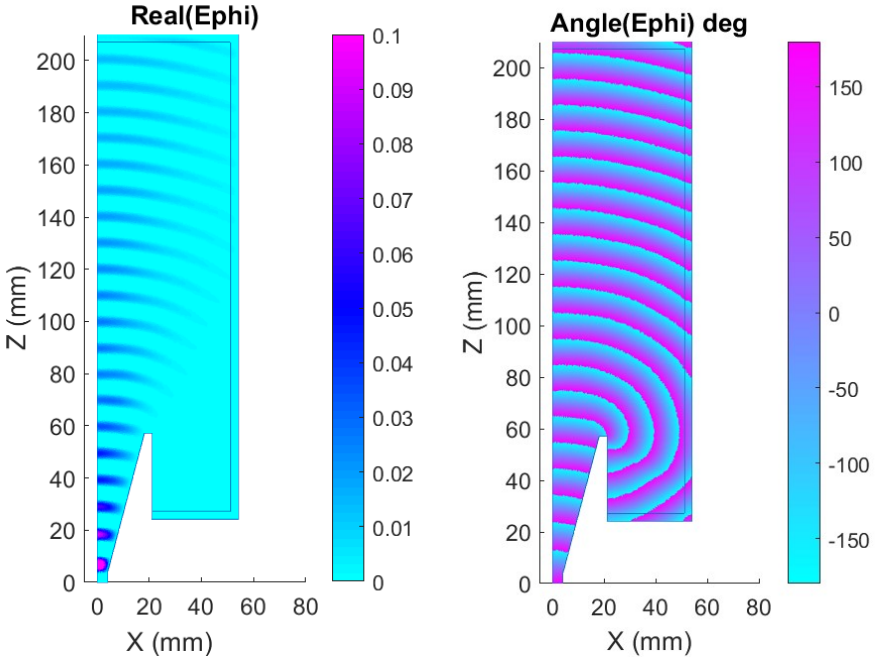

Fig. 3.22 Magnitude and phase of E-fields for conical horn antenna

3.2.3. Exponential Horn Antenna

After the analysis of pyramidal and conical horn antennas at microwave band, we have found that an exponential shape of the horn with custom tuning can provide the best radiation characteristics and spot focusing. The custom structure of exponential horn antenna is shown in Fig. 3.30, antenna is designed in MATLAB 2016b using the symmetry boundaries design approach. The length and horn aperture radius are kept same as the conical horn discussed in section 3.2.2.

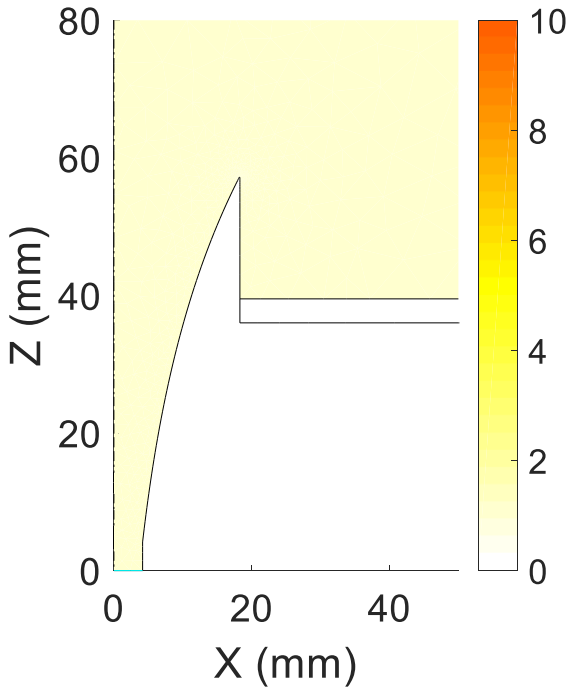

Fig. 3.23 Geometry of the exponential horn antenna

The design of exponential horn antenna is derived through eq. 3.3 where the horizontal dimension increases exponentially with constant increase in vertical dimension.

$$x = 4.2 * \exp(0.0278y) \tag{3.3}$$

The waveguide radius 4.2mm and horn aperture 25mm are kept constant and horn flare is exponentially tunned for optimized and best radiation performance. Fig. 3.31 shows the comparison of S_{11} for conical and exponential horn antennas. The exponential horn antenna is resonating better than conical horn in the desired frequency band.

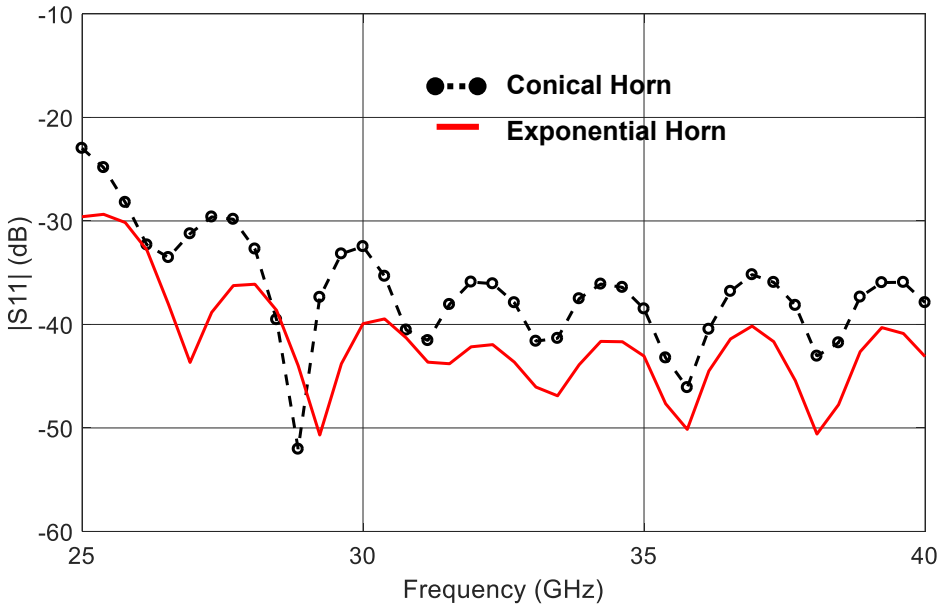

Fig. 3.24 S11 comparison between conical and exponential horn antenna

Fig. 3.32 shows magnitude and phase of the electric field generated from the exponential horn antenna. The antenna provides better plane wave pattern, both in magnitude and phase which helped us to extract the S-parameters from the materials with increased accuracy. Further analysis on material characterization is provided in Chapter 4.

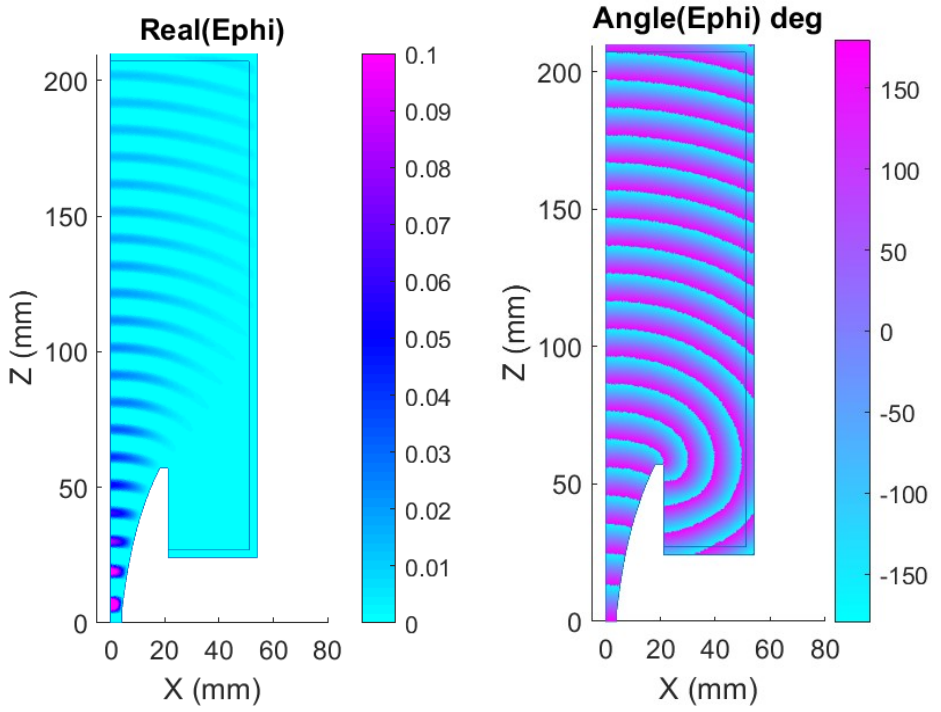

Fig. 3.25 Magnitude and phase of E-fields for exponential horn antenna

3.2.4. Shaped Horn Antenna

In this section, a novel shaped horn antenna is presented for THz frequency spectrum. The THz horn source is designed with an objective to remove lens correction and dielectric materials embedded on horn antenna apertures in order to improve the radiation and focusing performance. The shaped horn antenna is a horn-waveguide-horn design which is modelled to achieve the combined benefits such as plane-wave directive patterns, narrow spot focusing and low cross-polarization. The proposed shape horn antenna is designed for frequency range of 0.9 to 1THz. The performance metrics such as; S11, radiation magnitude and phase, and finite distance spot focusing are analysed at 4 different THz frequencies of 0.92THz, 0.94THz, 0.98THz and 1THz. The shaped horn antenna has circular transverse shape and is fed by a circular waveguide operating in TE_{11} mode. The horn source nearfield patterns confirms the design approach theory.

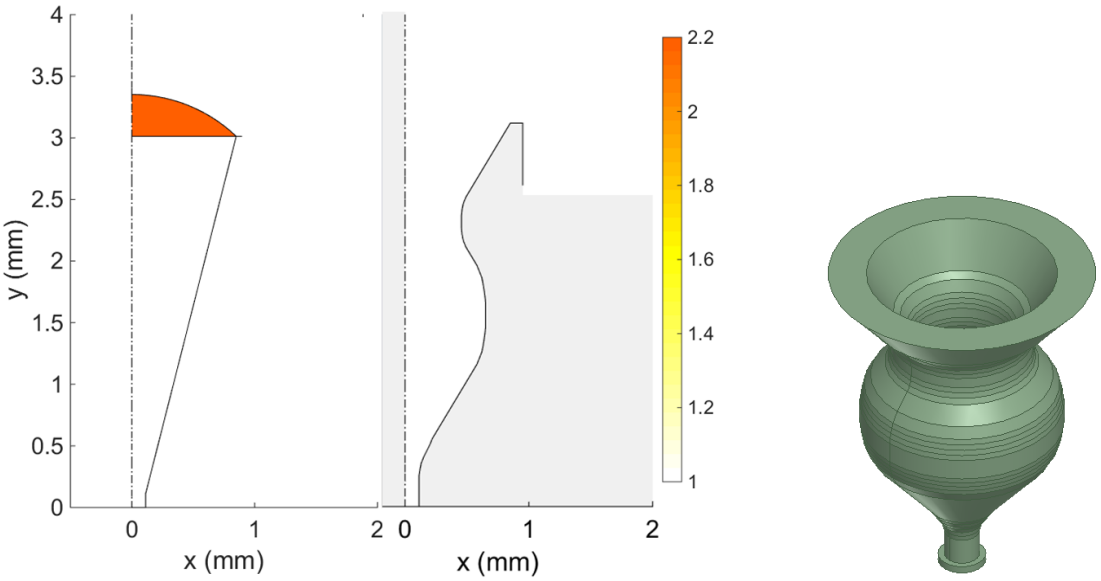

Fig. 3.26 Horn antenna geometry (a) Lens corrected and Shaped horn (b) 3D Shaped horn

A linear conical horn antenna is modified to design a custom shaped horn antenna aimed to provide the spot focusing which is reportedly obtained by lens corrected horn antennas [44]. The lens corrected horn and proposed shaped horn antenna models are shown in Fig. 3.23 (a) and 3D view of the shaped horn in Fig. 3.23(b). The proposed shaped horn antenna is build up with waveguide, radiation diverter and focusing sections in a particular order to create a circular transverse shape as shown in Fig. 3.24. The lens with relative permittivity 2.2 and focal length 2.55mm is used at linear horn aperture whereas the spot focusing point is kept at 2.55mm from horn face of both antennas in order to compare the performance. The horn aperture diameter is kept 1.7mm and length 3.1mm for both type of horn antennas to ease the comparison. Δ is the change in horizontal dimension with respect to vertical dimension of shaped horn antenna.

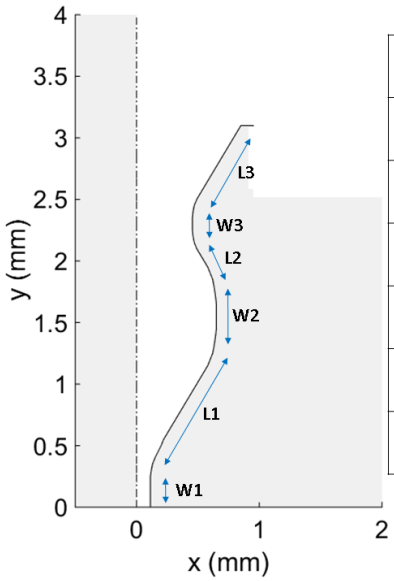

Parameter	Equation
W1	x = constant
L1	Δx = Δy * constant
W2	x = constant
L2	Δx = - Δy * constant
W3	x = constant
L3	Δx = Δy * constant

Fig. 3.27 Shaped horn antenna with geometry and modelling table

Both lens corrected horn and shaped horn antennas are designed and simulated with an accurate proprietary Body-of-revolution Finite-Element code [72]. With the same code, it is possible to analyse the radiation characteristics and spot focusing at finite distances. The commercially available software tools are bypassed in order to reduce the simulation time. The reflection coefficient or S11 curves of lens corrected horn and shaped horn antennas are shown in Fig. 3.25. The small bandwidth is selected for comparison purpose and to avoid frequency dependent changes on lens properties. The S_{11} curve for shaped horn showed better resonance from 0.91 to 0.95THz range than lens corrected horn. Later, two frequencies 0.92 and 0.94THz are picked from high resonance band and 0.98 and 1THz are picked from remaining band to study the radiation and focusing characteristics of both antennas.

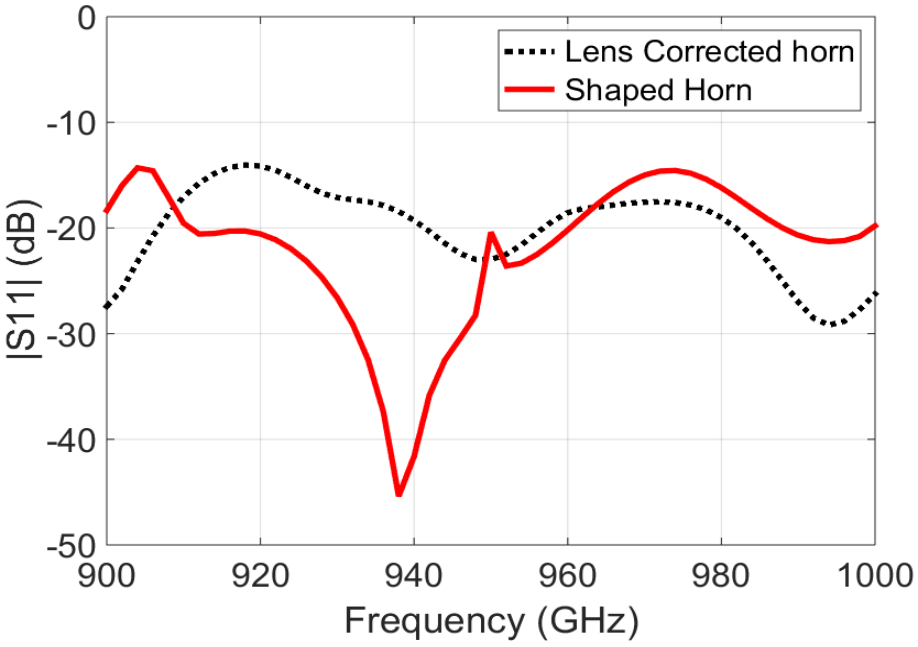

Fig. 3.28 Simulated reflection coefficient of both horn antennas

The magnitude and phase of radiation for lens corrected horn is shown in Fig. 3.26 (a-d) for different frequencies of 0.92, 0.94, 0.98 and 1THz. It has been observed that, the magnitude of radiation is high but plane wave patterns are decreasing with increase in distance. Similarly, phase variations are not smooth at mentioned frequencies. All the radiation figures below are scaled to same unit in order to get better understanding.

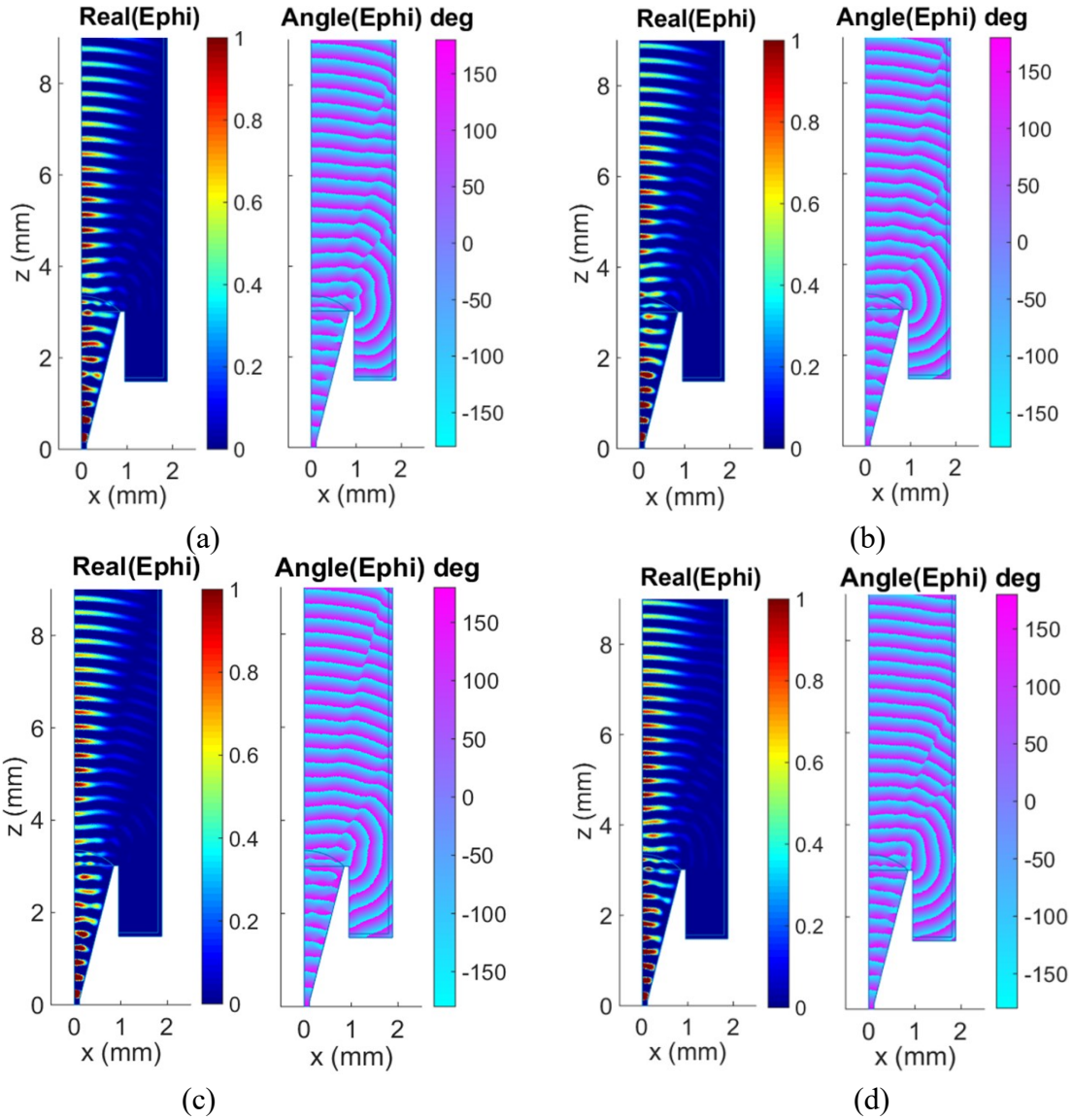

Fig. 3.29 Radiation magnitude and phase of lens corrected horn at different frequencies in dB (a) 920GHz (b) 940GHz (c) 980GHz (d) 1000GHz

The spot focusing of lens corrected horn antenna is shown in Fig. 3.27. The 3dB spot focused beam produced by lens corrected horn at 0.92 THz is 0.98mm (2.97ʎ) at the finite distance of 2.55mm (7.73ʎ). The ratio of focal distance to diameter of the lens F/D was 1.5 where D was approximately 1.7 mm. Similarly, Fig. 3.27 shows the magnitude of spot focused beam at 0.94, 0.98 and 1THz with 3dB focus of 0.99, 0.92 and 0.9mm respectively.

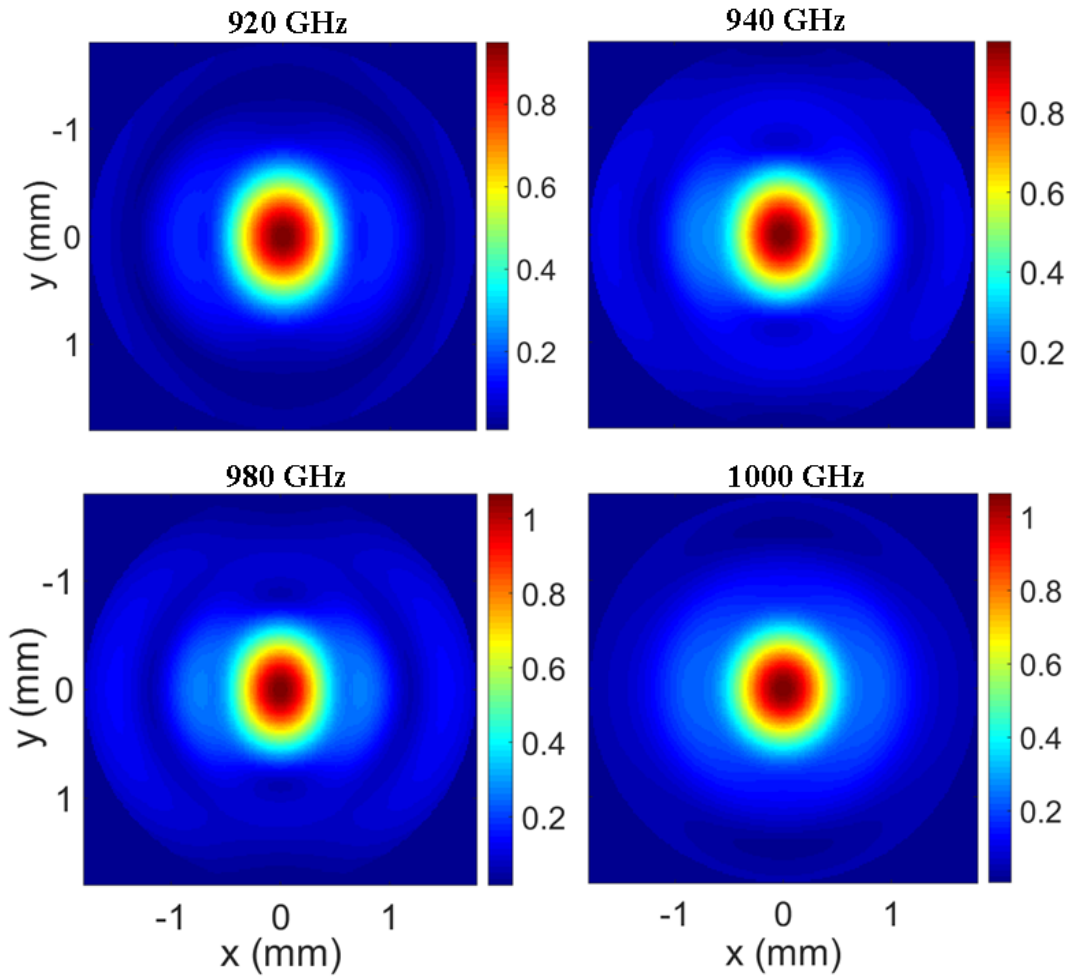

Fig. 3.30 Spot focusing by lens corrected horn at different frequencies in dB

The magnitude and phase of radiation for proposed shaped horn is shown in Fig. 3.28 (a-d) for same set of frequencies 0.92, 0.94, 0.98 and 1THz. Relatively, low magnitude of radiation but smooth plane wave patterns are observed with increase in distance and frequency for shaped horn as compared to lens corrected horn. The flat curved variations in phase has also been seen with increase in frequency. It has been observed that, W3 waveguide is playing major part is reshaping the radiation of shaped horn and improving the focus without using lens.

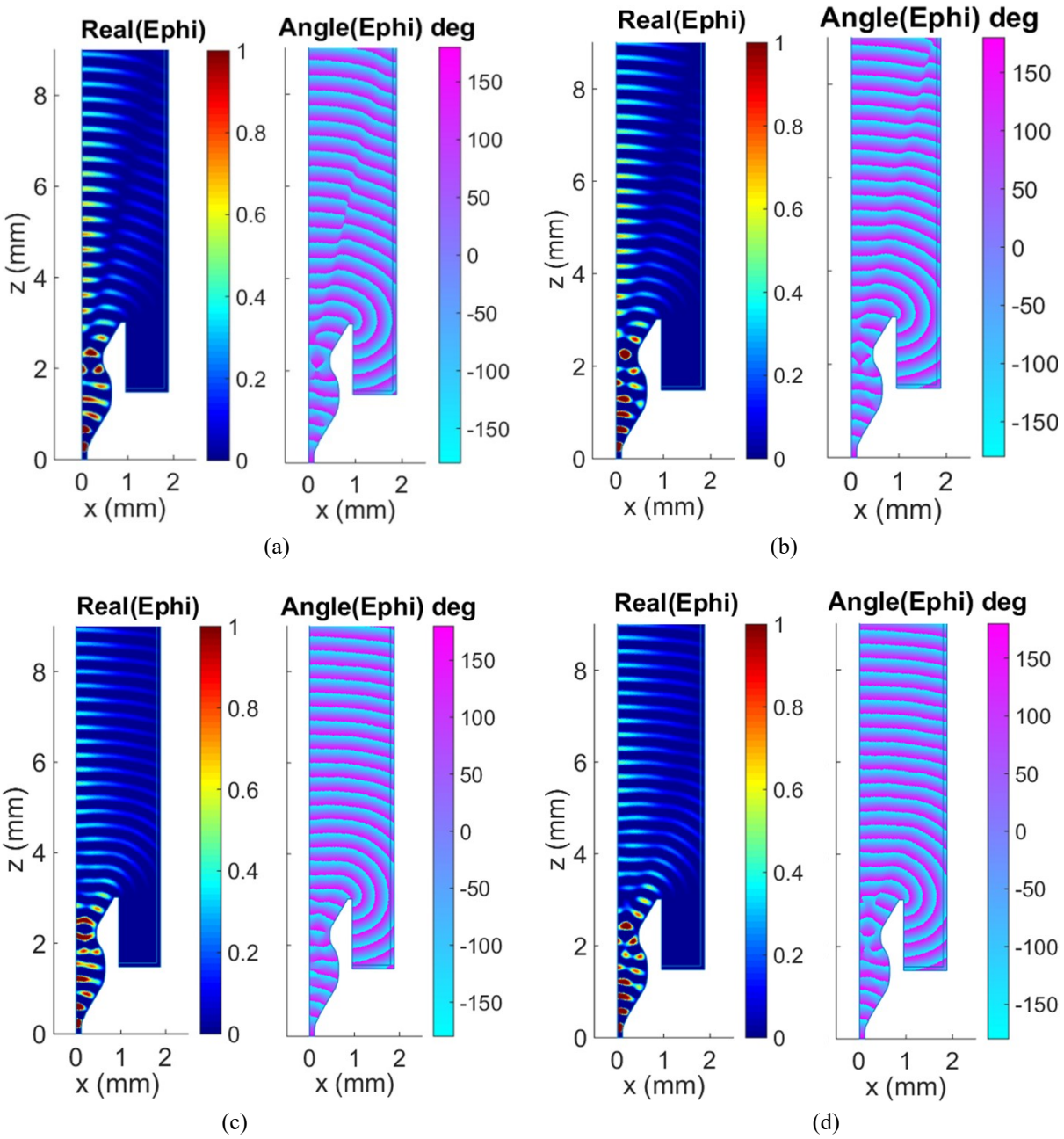

Fig. 3.31 Radiation magnitude and phase of shaped horn at different frequencies in dB (a) 920GHz (b) 940GHz (c) 980GHz (d) 1000GHz

When compared to lens corrected horn, 3-dB spot focused beam generated by shaped horn at 920 GHz is about 0.82 mm (2.48ʎ) at same focused distance of 2.55mm (7.73ʎ). The ratio of F/D is kept same as 1.5 in shaped horn case for better comparison. The spot focused beams of shaped horn at different frequencies are shown in Fig. 3.29. The magnitudes of spot focused beam at 0.92, 0.94, 0.98 and 1THz are calculated as 0.82, 0.84, 0.8 and 0.81mm respectively. These values are better than lens corrected horn and found suitable for terahertz imaging applications.

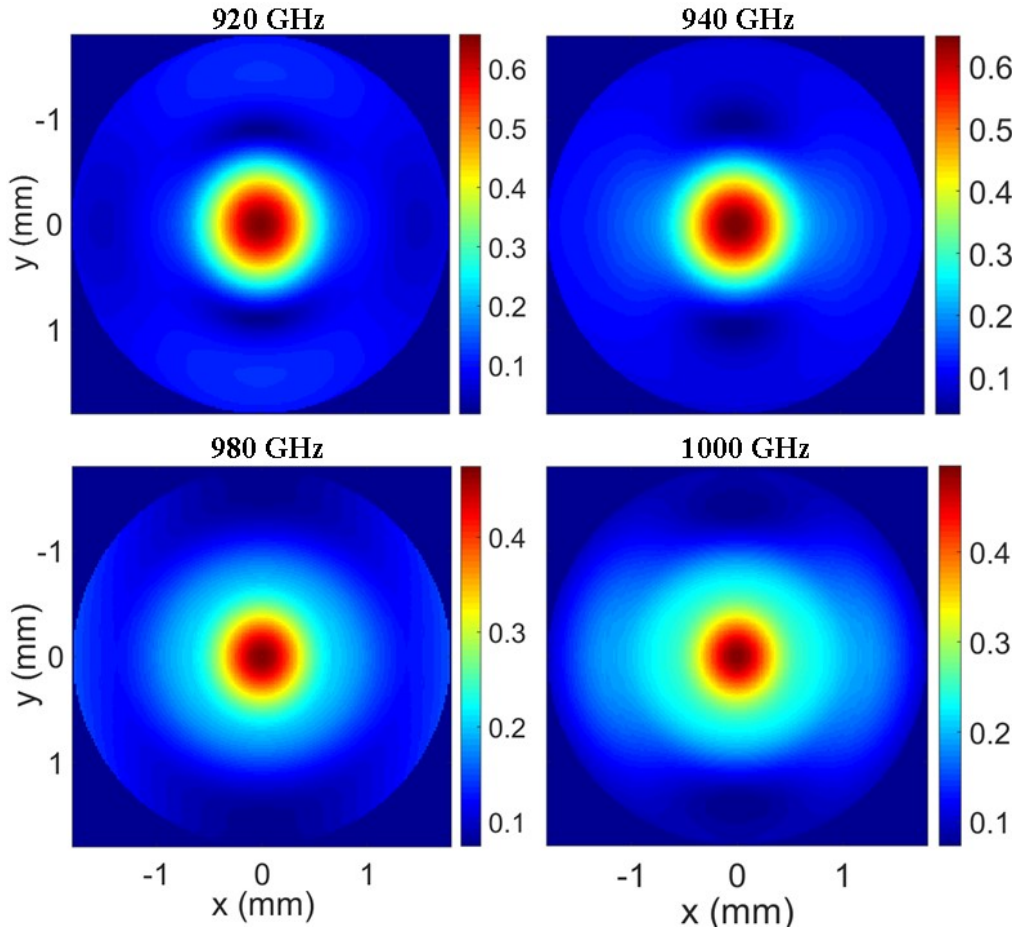

Fig. 3.32 Spot focusing by shaped horn at different frequencies in dB

The summary of comparison between lens corrected horn and presented shaped horn for spot focusing performance is tabulated in Table 3.3. All the values are in mm.

TABLE 3.3: SUMMARY OF SPOT FOCUSING PARAMETRIC STUDY

Spot Focusing			
Frequency	**Lens corrected horn**	**Shaped horn**	**Δ value**
0.92THz	0.98	0.82	0.16
0.94THz	0.99	0.84	0.15
0.98THz	0.91	0.80	0.08
1THz	0.90	0.81	0.09

CHAPTER 4

Data Inversion Methods

The chapter is focused on study and development of novel approaches of material characterization using measured scattering parameters and data inversion methods. The frequency domain technique for estimation of material properties is used at terahertz band whereas time domain technique is used at microwave and millimeter wave bands. The materials with different dielectric constants and thickness are estimated using the measured data in Ka and W bands. The measured are obtained at PoliMi and UPC Barcelona are also presented.

4.1. Frequency Domain Technique

In this section, discussion and results for frequency domain material characterization with no time gating are shown. Avoiding time gating is potentially interesting for very thin layer materials, where time gating may require too large bandwidth for practical use [70-71]. We have presented the results obtained by two type of horns: one uses lens correction for beam focusing, while the other is a newly designed self-focusing horn that does not need lens correction, since focusing is obtained by shaping horn profile. We found rather good estimation of material properties in frequency domain material characterization, although in a narrow bandwidth. The problem of spurious reflections is still present, but reduced, and the shaped horn performs somewhat better than the lens corrected horn.

A measurement setup has been implemented in MATLAB 2016b to extract the simulated scattering parameters from the materials. Two identical shaped horn antennas are placed in front of each other at the 2.55mm symmetrical distance from targeted material. The area of the material is kept large enough to reduce the diffraction effects whereas two different thicknesses of material are studied with varying relative permittivities (dielectic constant). The measurement setup with shaped horns is shown in Fig. 4.1. Similar measurement setup is used for lens corrected linear horn for comparison purpose.

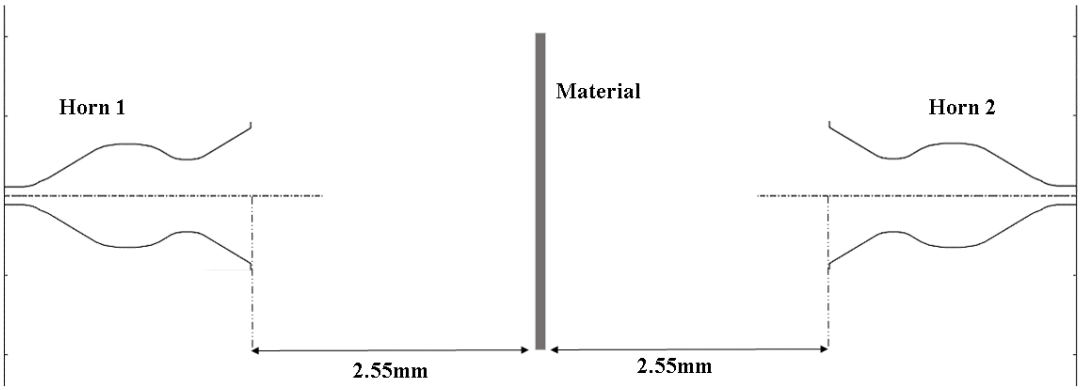

Fig. 4.1 Measurement setup with proposed shaped horn antenna

The shaped horn antenna has been designed and analysed with the above cited code in MATLAB 2016b. Thanks to the use of symmetry of revolution formulation, the code uses 2D FEM which makes it time efficient. A complete measurement setup that uses three TRL standards can be simulated in minutes as compared to one/two days with modern softwares (such as FEKO or Ansys HFSS). Comparison of S11 (reflection coefficient) for lens corrected and shaped horn antenna at THz frequencies is shown in Fig. 4.2. The small bandwidth (915-925GHz) is selected for better scattering response in the measurement setup, which is used later for material characterization.

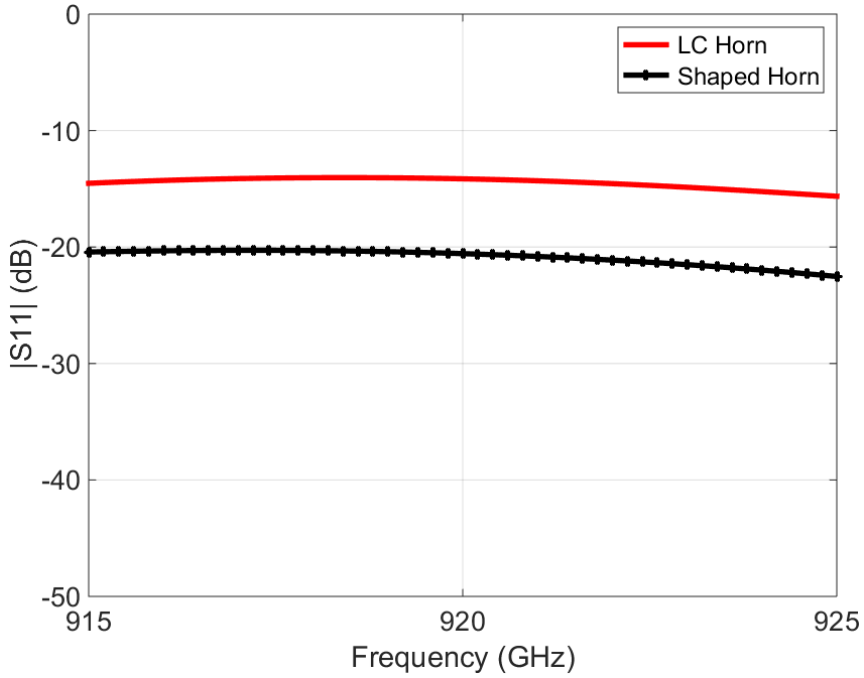

Fig. 4.2 S11 of horn antennas (lens corrected horn and shaped horn)

4.1.1. Spot Focusing Characteristics

The spot focusing of both lens corrected and shaped horn antennas are shown in Fig. 4.3. The 3-dB diameter of focused beam produced by shaped horn at 920 GHz is 0.82 mm (2.48ʎ) at the finite distance of 2.55mm (7.73ʎ) which was found better than focused beam of 0.98mm (2.97ʎ) produced by lens corrected horn at the same distance. The ratio of focal length to diameter of the lens (F/D) was 1.5 with D approximately 1.7 mm. Figure 4.4 (a-b) shows the magnitude and phase of radiation at 920GHz for variable distance.

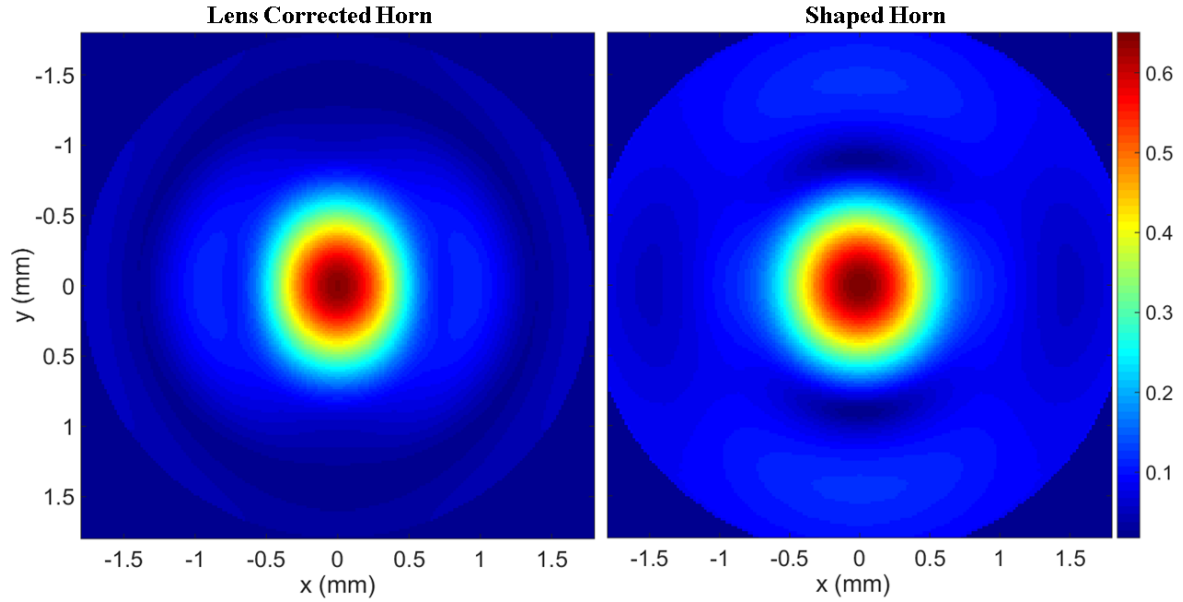

Fig. 4.3 Spot focusing of horn antennas at 2.55mm for 920GHz

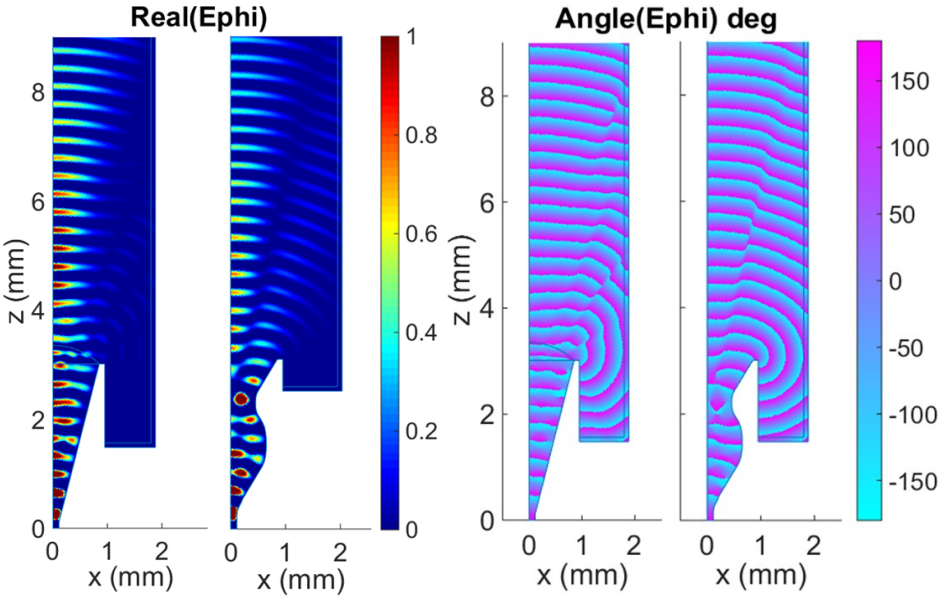

Fig. 4.4 Focusing of horn antennas at 920GHz (a) Magnitude (b) Phase

In the frame of material characterization, lens corrected horns are usually preferred because of the focusing capability of lens, since diffraction effects due to finite size of the sample are greatly reduced [45-47], whereas shaped horn provides focusing at different distances in near field.

4.1.2. TRL Calibration

In the literature, measurement setup is represented by Vector Network Analyzer and a two-horn system, together with a TRL de-embedding procedure to remove reflections caused by the horns themselve [91]. However, after the implementation of complete TRL procedure in the frequency domain, time-gating technique was used in the literature to reduce spurious reflection present after TRL calibration [92]. After time gating, excellent results were obtained in close agreement with waveguide-type measurement setup.

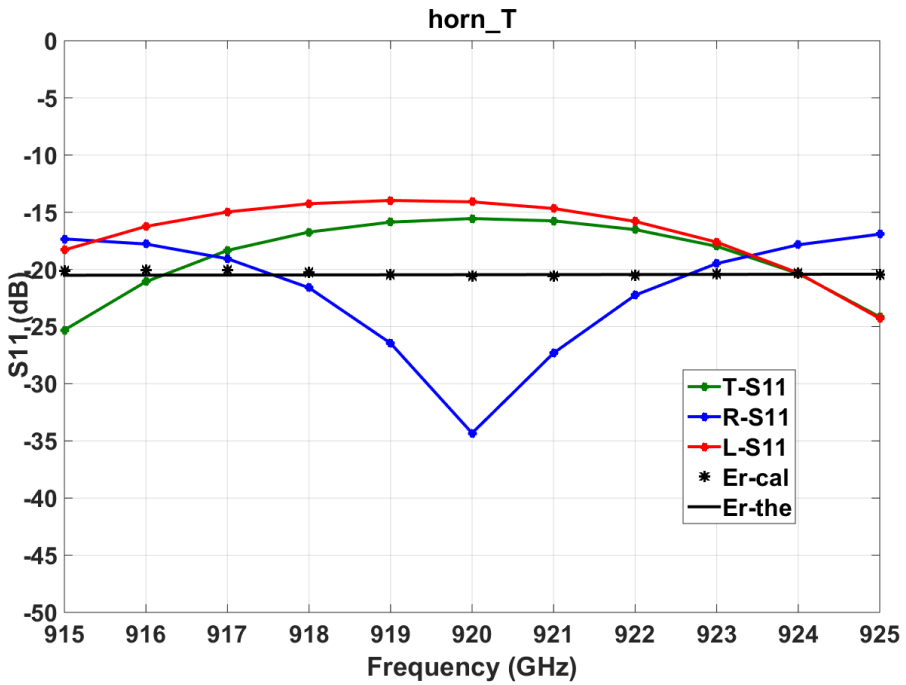

Fig. 4.5 TRL calibration results

A parametric study has been carried out to validate the performance of shaped horn antenna with the measurement setup implemented above. The material samples with three different dielectric constants and two thickness are tested by simulating variety of single and multi-layer cases. The analysis was carried out with dielectric constant values of 2, 4 and 6 for fixed thickness of 0.01 and 0.1mm. The purpose was to infer the material dielectric constant from the scattering parameters using the TRL procedure [88-89]. There are several factors that could affect the correct estimation of the dielectric constant, namely, multiple reflection between antenna and material, curvature of the equiphasic surfaces and the 1/R attenuation with distance. All these factors contribute to divert from the simple plane wave model (or transmission line model) that is employed in the development of TRL equations. The TRL calibration is implemented where, first we simulated the scattering parameters between two horns at a fixed distance and this represent THRU standard [91]. Then, we simulated again the scattering parameter with increased distance between the horns which represents the DELAY standard (typically the difference in length is close to $\lambda/4$). Last, we simulated the reflection from a metal plane at half the distance of the THRU which represents the REFLECT standard. By applying TRL de-embedding procedure, we can obtain the scattering parameters of the material alone and the results can be compared to a simple plane wave model [92].

4.1.3. S-Parameters Extraction

The comparison reflection coeffiecient (S11) after TRL de-embedding for both shaped horn and lens corrected horn are shown in Fig. 4.6, the abbreviations, LCH is lens corrected horn and SH is shaped horn. In general, the agreement is quite good in both cases but the shaped horn performs better. We observed, also previously reported in the literature that, TRL method in larger frequency band suffers from spurious reflection effects that can lead to large errors in the estimation of plane wave scattering parameters, thus, the frequency range must be selected carefully.

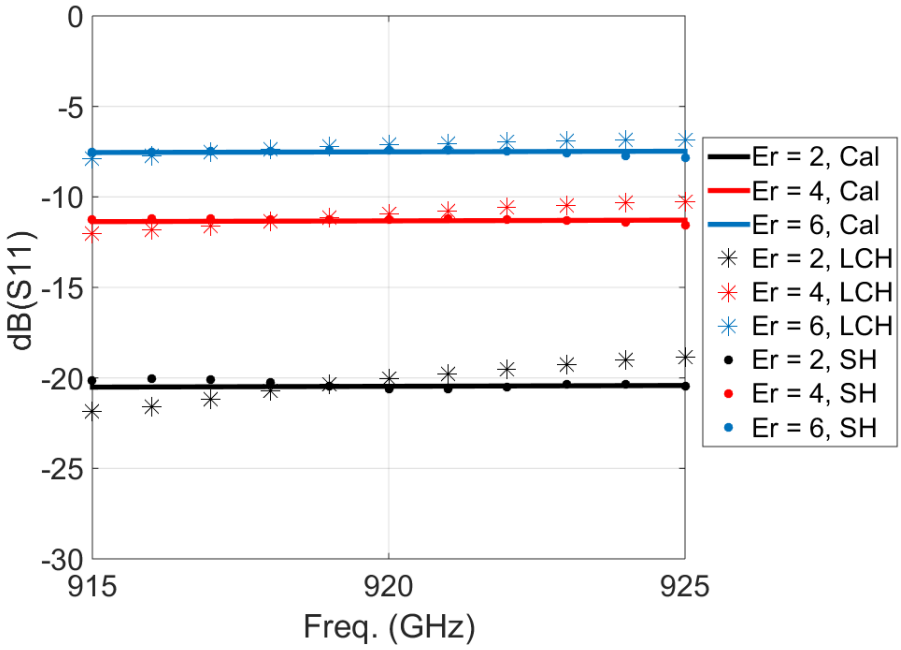

Fig. 4.6 S11 comparison of horn antennas, single layer with thickness = 0.01mm. LCH is lens corrected horn and SH is shaped horn

Using the same dielectric constants at higher thickness of 0.1mm, larger scattering variance is observed due to stronger reflections as shown in Fig. 4.7.

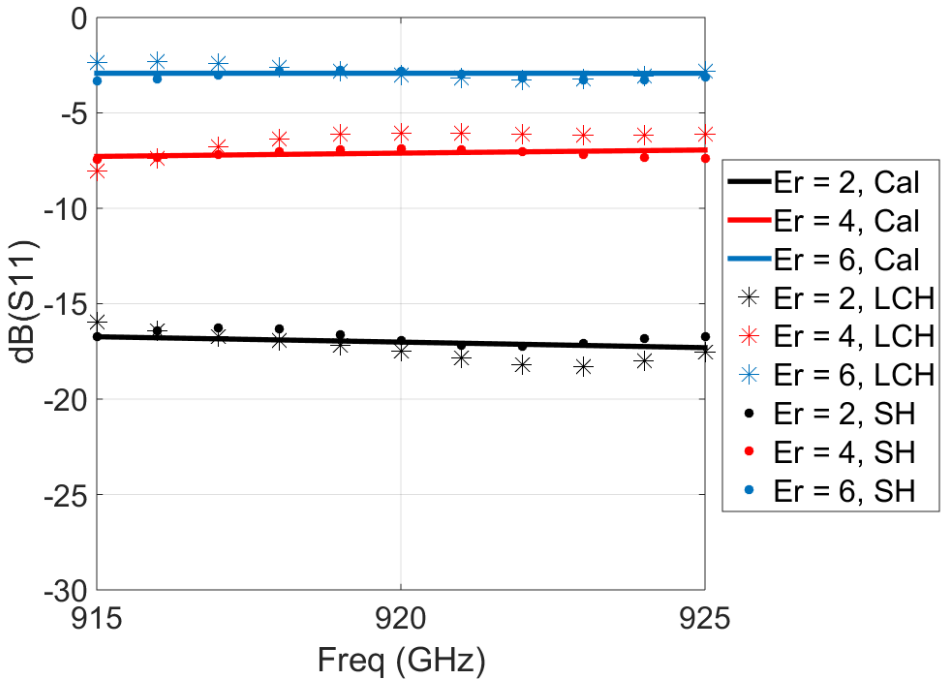

Fig. 4.7 S11 comparison of horn antennas, single layer with thickness = 0.1mm. LCH is lens corrected horn and SH is shaped horn

A multi-layer dielectric materials have also been measured for estimation of dielectric properties. Two layer and three layer mediums with identical thickness of 0.01 and/or 0.1mm are used, along with dielectric constant values 2-4 and 2-4-6 respectively. Fig. 4.8 and 4.9 shows the scattering parameters for multi-layer materials with 0.01 and 0.1mm thickness for each layer.

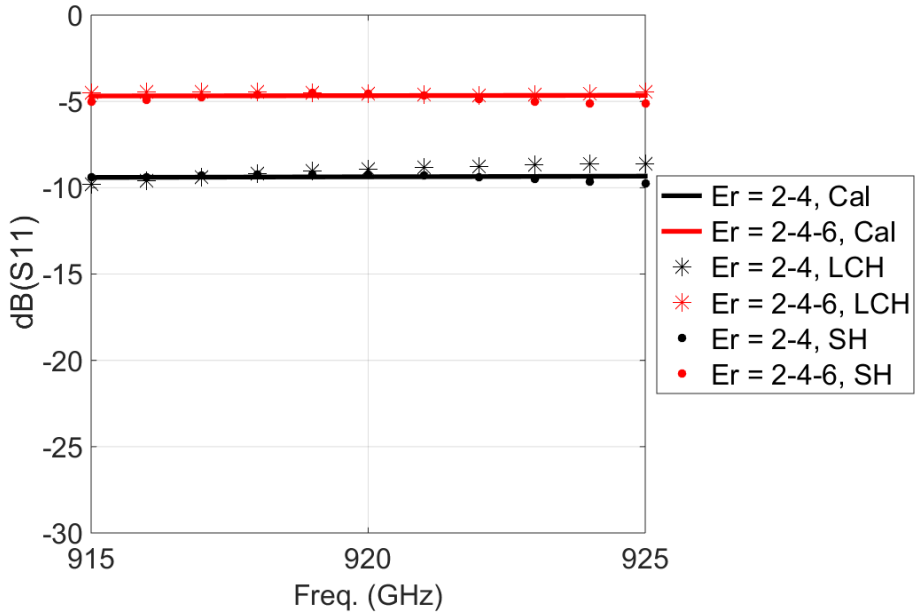

Fig. 4.8 S11 comparison of horn antennas, multi-layer with thickness = 0.01mm per layer. LCH is lens corrected horn and SH is shaped horn

For multi-layer materials, we have observed that the shaped horn antennas provide a good estimate of the plane-wave scattering parameters whereas, larger deviation is observed for the case of lens corrected horn antenna in the implemented measurement setup.

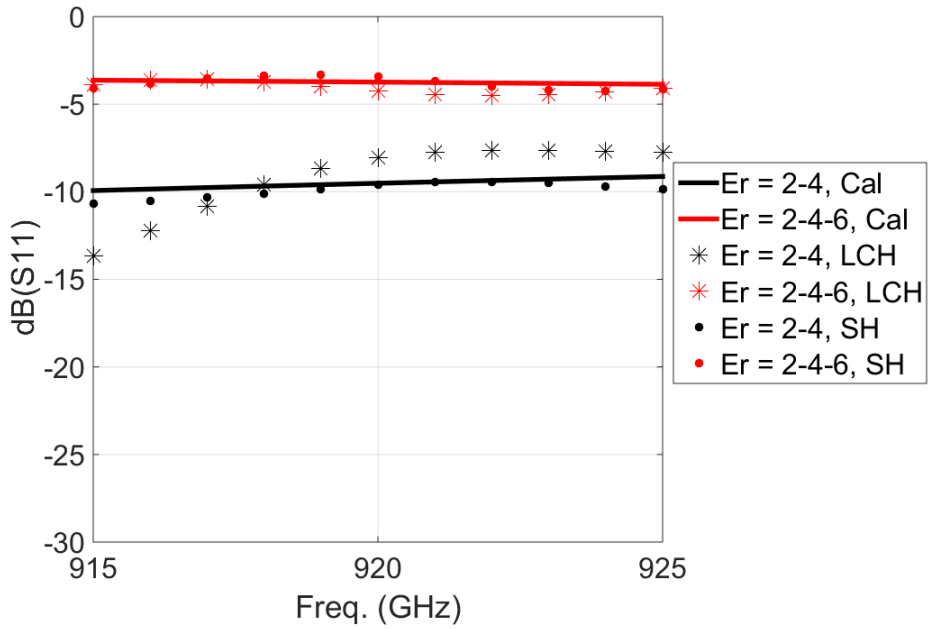

Fig. 4.9 S11 comparison of horn antennas, multi-layer with thickness = 0.1mm per layer. LCH is lens corrected horn and SH is shaped horn

4.1.4. Dielectric Constant Estimation

After extracting the S-parameter of materials using shaped horn and linear horn with lens correction, further analysis is carried out to derive the dielectric constant of material from the knowledge of material thickness and S11 data. Fig. 4.10 shows the estimation of dielectric constant at two different thickness. The curves showed that, less thickness (0.01mm) ensures less variation in the material permittivity (dielectric constant), however increased tolerance is observed with increase in Er values. Similarly, at larger thickness (0.1mm), the variance increased due to increased reflections and it has been observed that, larger thickness of material with higher Er value is not correctly estimated, and time gating is required to reduce the estimation error.

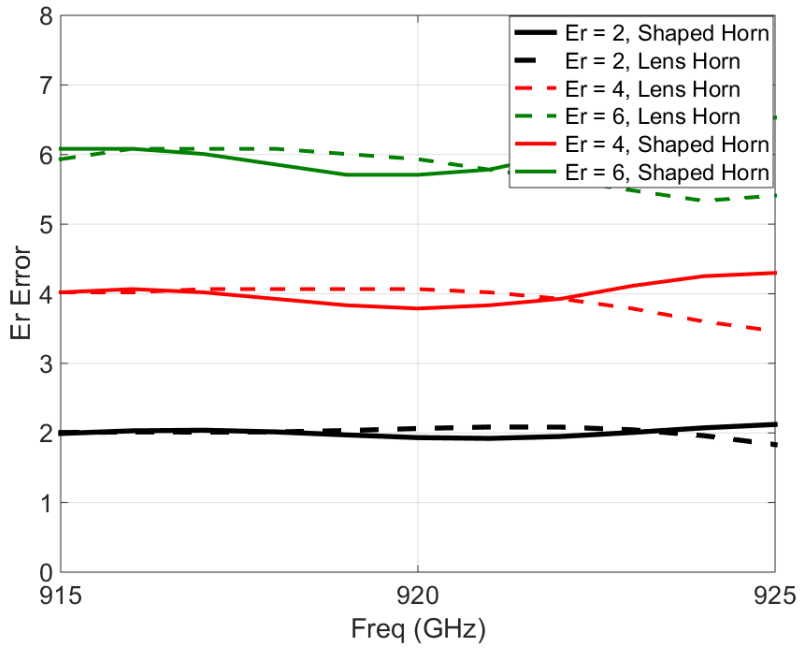

(a)

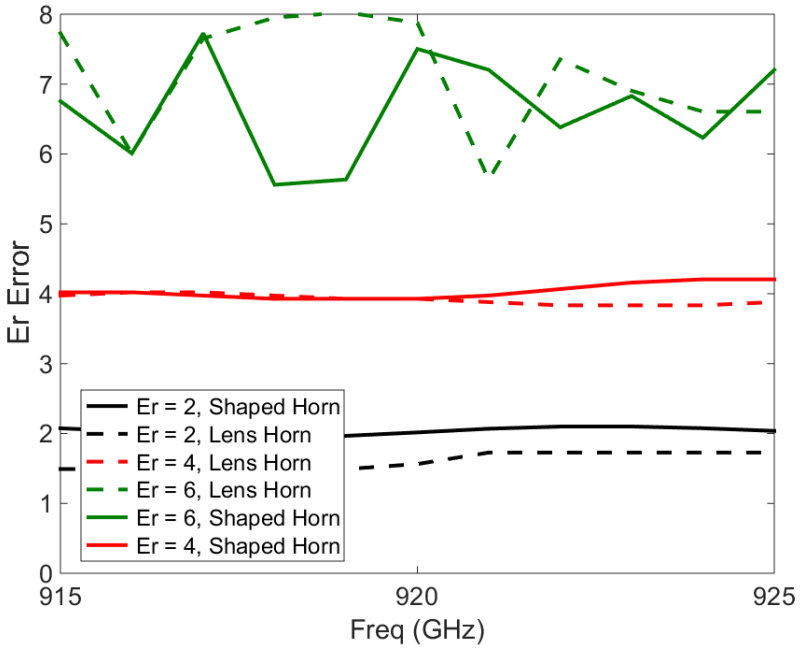

(b)

Fig. 4.10 Er comparison of horn antennas, single-layer with thickness (a) 0.01mm (b) 0.1mm

The results above showed lack of accuracy in the dielectric constant estimation especially when thickness of the sample is increased. To overcome this problem, time domain analysis is introduced and verified at various frequency bands to validate the procedure.

4.2. Time Domain Technique

After frequency domain analysis, the time domain technique is studied and implemented using the same MATLAB code [72]. The reflection only method is used here to extract the scattering parameters (S11) from conical horn and customized exponential horn antenna. The model of horn antenna setup along with material under test (MUT) for microwave measurement of scattering parameters are shown in Fig. 4.11.

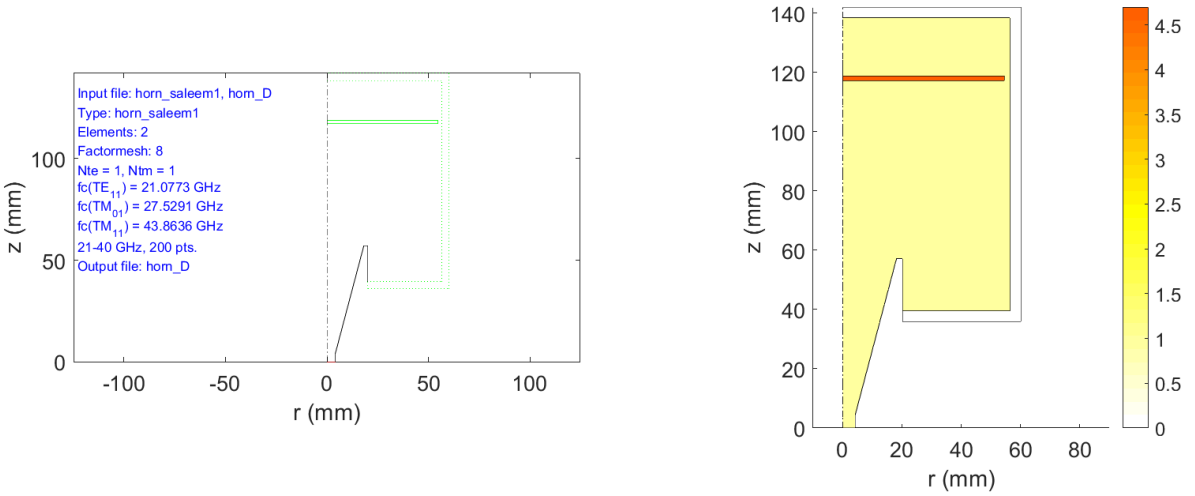

Fig. 4.11 The horn antenna model and setup details

4.2.1. Reflection Method

The reflection method is a non-resonant measurement method, in which only the reflection scattering parameters are measured with the free-space unidirectional measurement system as shown in Fig. 4.12. The incident electromagnetic waves are directed towards the material under test (MUT) and the reflected waves from the MUT are collected with the impedance discontinuity due to the presence of material [6].

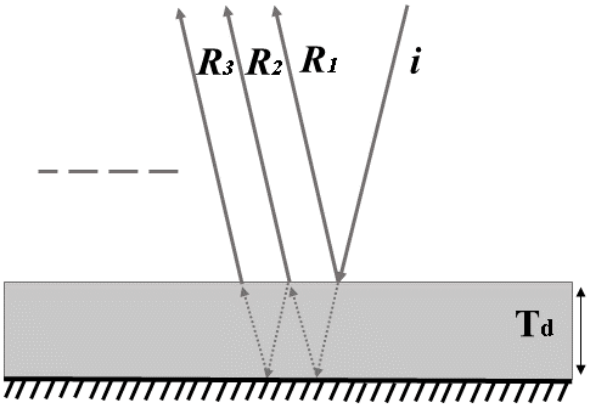

Fig. 4.12 S11 extraction from reflection method

The ground plane measurement is taken first, to be used as the reference response from PEC, the series of five reflections from the MUT are recorded and summed up to increase the quality of received reflective response. The reference curve and the first 5 reflections from the MUT are show in Fig. 4.13. For the second reflection, we added first and second reflective response and named it Vsca2 and similar is done with rest of the reflections, where previous reflection and current reflective response is summed.

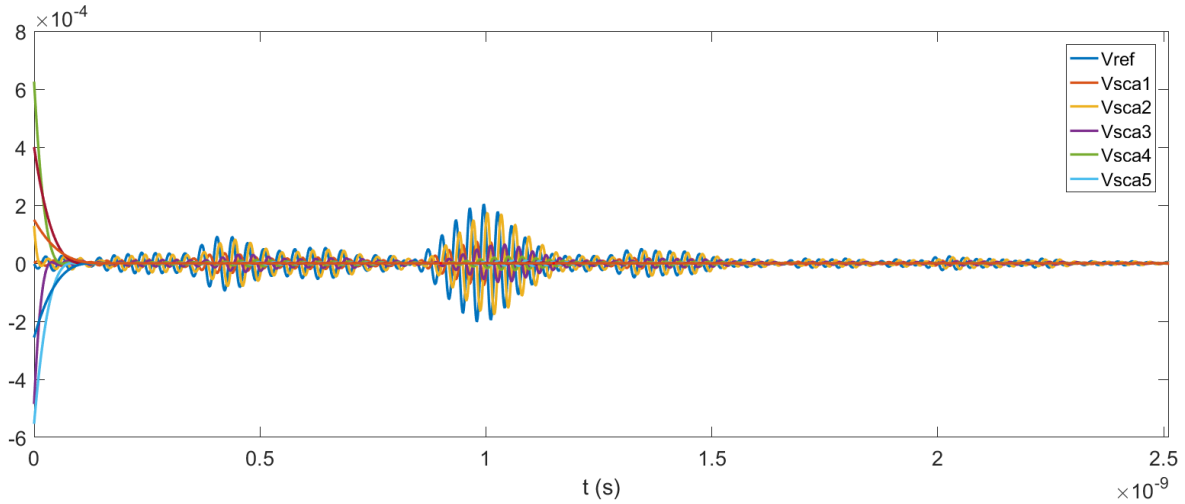

Fig. 4.13 Multiple reflective response from the MUT

After adding the multiple reflections from MUT, the Vsca5 is used to derive the analytical model and compared to the measured scattering response from the MUT. The time domain post-processing is done after getting the scattering data which is explain using the below Fig. 4.14. The time domain methods are well explained in [71].

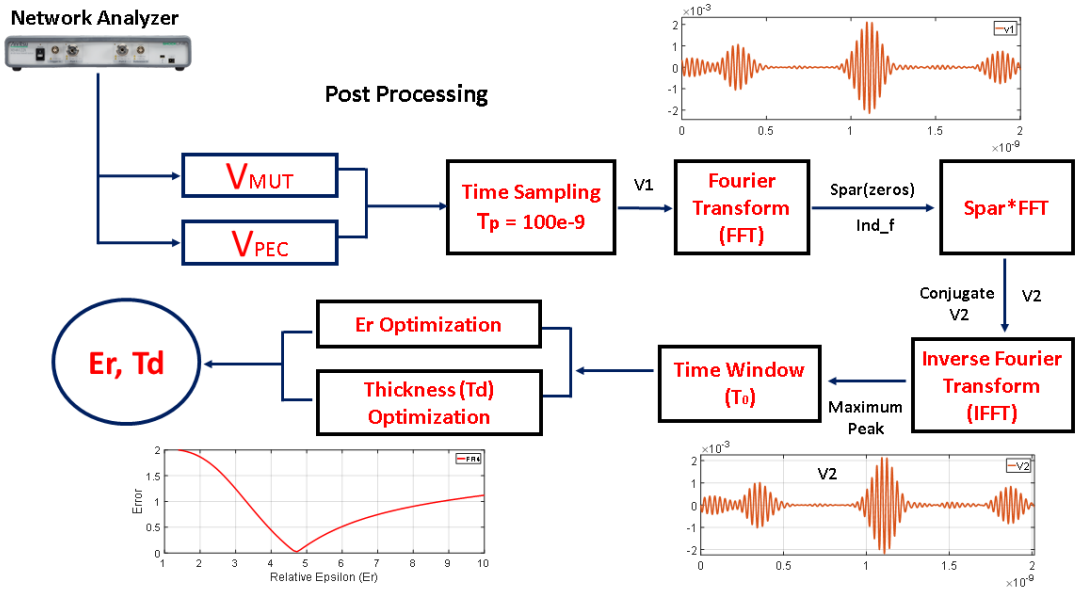

Fig. 4.14 Time domain post-processing method

The V_{MUT} and V_{PEC} are the voltage response in scattering data from MUT and grounded PEC respectively. Initially, we have embedded both data files to the main code and defined the Time sample (Tp) = $100e^{-9}$ and Frequency range (Fp) = $1000e^{9}$. The time sweep N_t is then defined as;

$$N_t = 2 \text{ ^ } \log_2 (T_p * F_p)$$

The conductivity coefficient (δ_{co}) is initially set to the value 0.25 whereas the conductivity of grounded PEC (δ_{pec}) is set as $1x10^4$. The Fourier transform (FFT) of both V_{MUT} and V_{PEC} is taken (which are V1) and divided half in order to multiple with the spar (zeros), and then it's further mirrored on Ind_f as Spar (Ind_F) and stored as V2 for V_{MUT} and V_{PEC}. The conjugate of V2 and V2 is added again and inverse Fourier transfer (IFFT) is taken to get back the scattering data. The response after the inverse Fourier transform and time windowing is shown in Fig. 4.15. The peak response, around $0.7x10^{-9}$ sec, is the reflection from MUT and it has been detected accurately from both derived model and measured S11. The highest peak is determined and time window is applied around the peak response at corresponding peak time value (t_0) and the Δt is defined as;

$$\Delta t = \frac{1.7}{\delta_{co}(f2-f1)}$$

The frequencies f_1 and f_2 are first and last frequencies of the sweep respectively. The limits of time window are defined as;

$$T1 = t_0 - \frac{\Delta t}{3}, \; T2 = t_0 + \frac{\Delta t}{3}$$

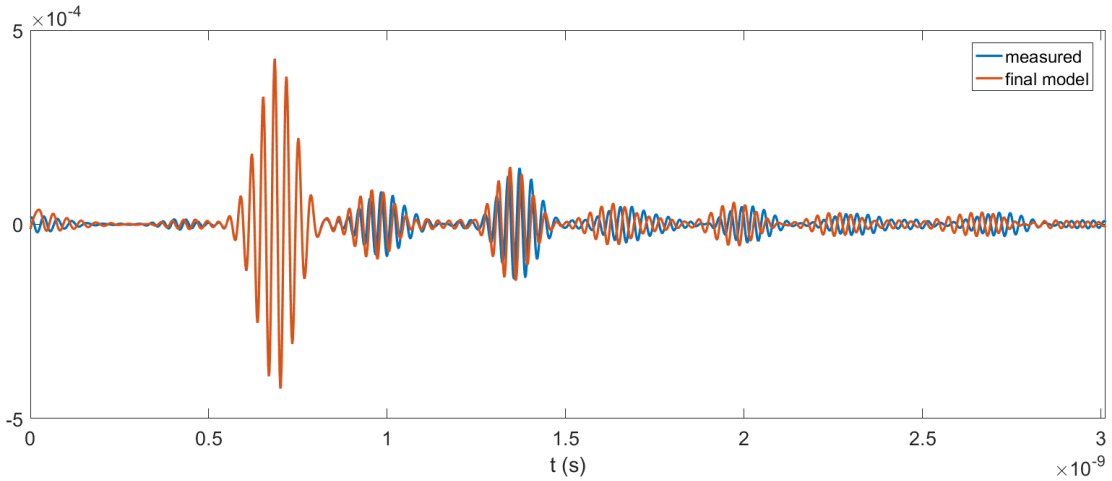

Fig. 4.15 The time response of measured and derived model for dielectric constant estimation

After the comparison of derived model and measured response, the dielectric constant with minimum error is estimated as shown in the graph below, Fig. 4.16. In this particular case, MUT used is FR4 with dielectric constant 4.4 and thickness 1.6mm. This behaved as the starting point of our time domain analysis, the parametric study of different material properties is conducted in next section.

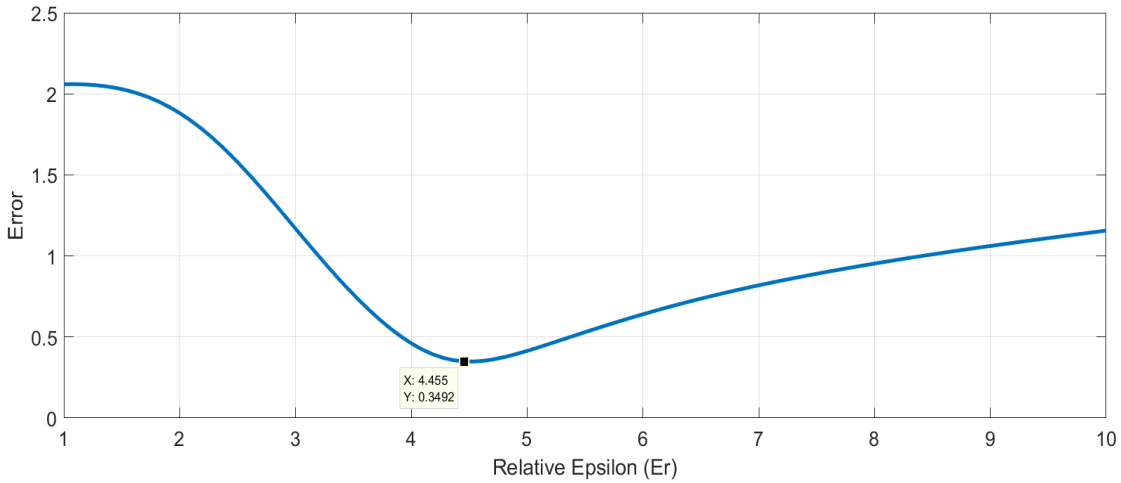

Fig. 4.16 S11 extraction from reflection method

4.2.2. Parametric Study and Discussion

The measurement setup is validated by carrying out the parametric study of different aspects of the setup and physical/electrical properties of MUT. All the simulation are carried out mainly in MATLAB 2016b and partly in Ansys HFSS. First, we have studied out the MUT dimensions analysis where we have changed the area of MUT from 2.5x2.5cm^2 to 10x10cm^2 while keeping the distance between transmitting horn and MUT fixed. The FR4 with dielectric constant 4.7 with thickness 1.6mm is used as MUT. The Fig. 4.17 (a-c) shows the variation of dielectric loss error when the area of MUT is changed from 2.5x2.5cm^2 to 10x10cm^2. It has been observed that, the error decreases with increase in MUT area which is basically effects by the horn antenna beam width. The antenna used in the measurements can allow accurate S11 extraction when the MUT area is 5x5cm^2 or larger.

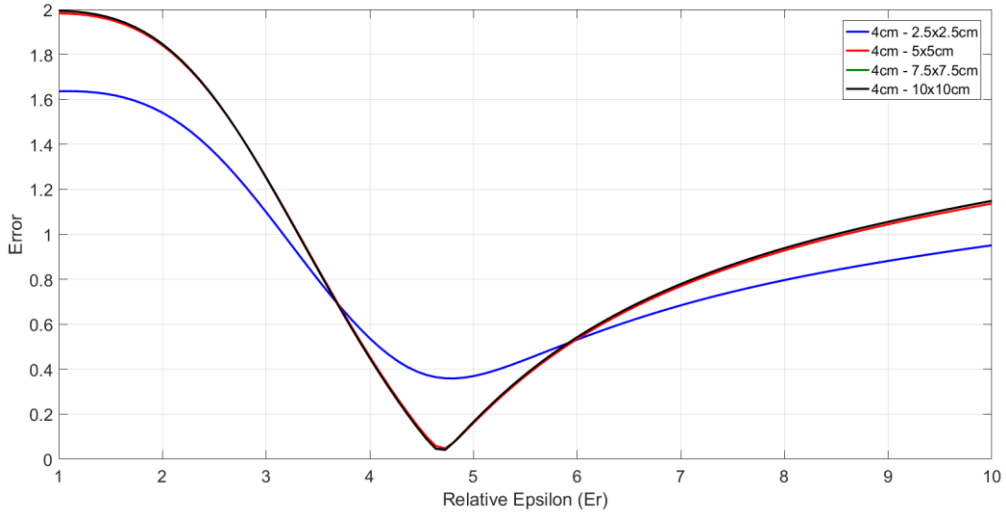

(a)

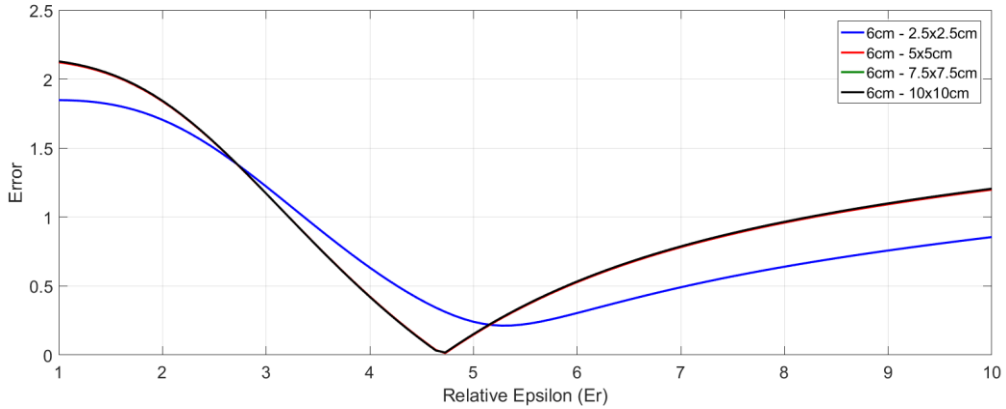

(b)

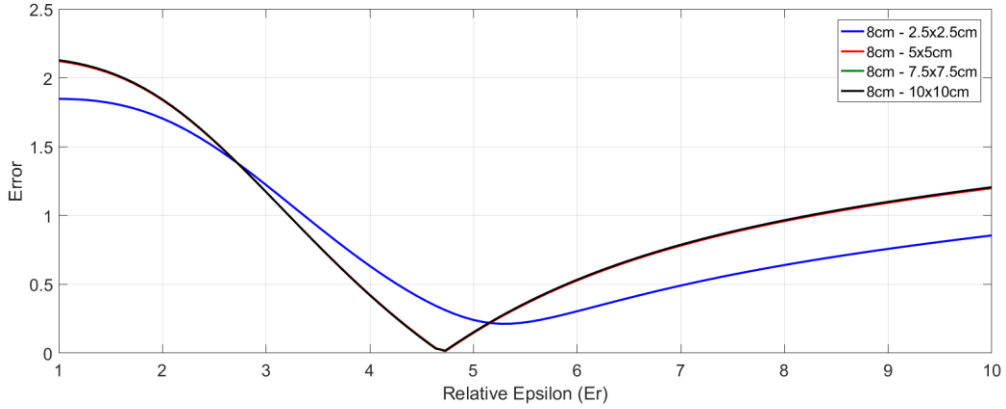

(c)

Fig. 4.17 Effect of MUT area on the dielectric constant estimation (a) 4cm, (b) 6cm, (c) 8cm

The second analysis is carried out to study the behavior of materials with different thickness. The MUT area (Wd) 5x5cm^2 is used for this analysis and FR4, Rogers RT/Duriod 5880 and Silicon with multiple thickness (Td) are examined at 4-10cm distance (Dist) from the transmitter horn antenna. For each material two different thicknesses has been used to verify the performance of method. FR4 with dielectric constant 4.7, Td = 0.8mm and Td = 1.6mm are studied, and dielectric constant estimation in terms of dielectric loss (error) is shown in Fig. 4.18 (a-b). It has been observed that Td = 0.8mm at Dist = 4cm has the higher dielectric loss as compared to other cases. Similarly, the dielectric loss (error) is higher for Td = 1.6mm at Dist = 8 and 10cm. At both distances, the time domain method is unable to reduce the error and accurately estimate the dielectric constant of MUT.

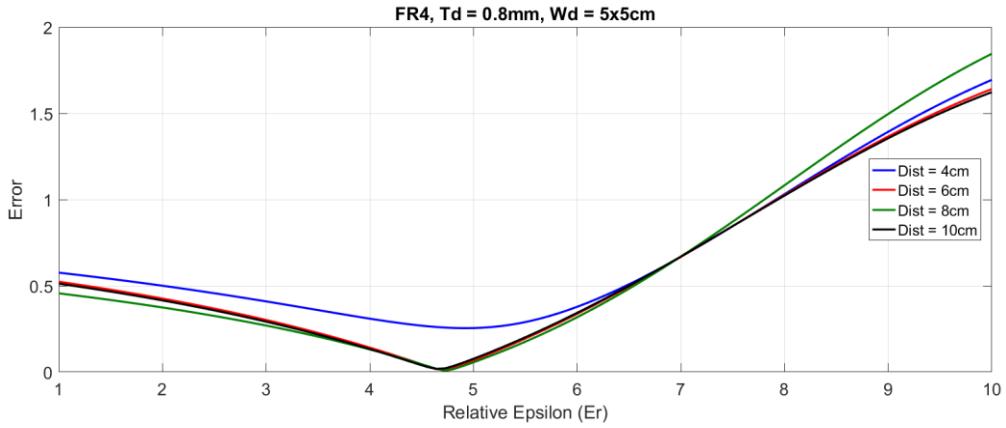

(a)

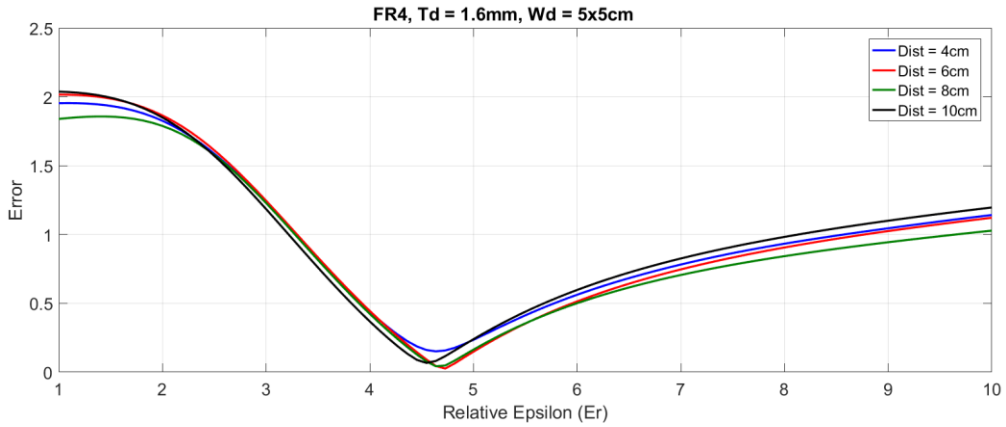

(b)

Fig. 4.18 Effect of FR4 thickness on the dielectric loss tangent (a) 0.8mm, (b) 1.6mm

The second material used in the experimental campaign is Roger RT/Duriod 5880 with dielectric constant 2.2 and, Td = 1mm and Td = 3mm. The dielectric loss (error) response for this case is shown in Fig. 4.19 (a-b). The dielectric loss (error) is higher at Dist = 4cm for the case of Td = 1mm whereas in the other cases, dielectric loss was very low and the dielectric constant was estimated accurately. When we have increased the MUT thickness to Td = 3mm, the dielectric loss was comparatively low

for the predicted dielectric constant, but second harmonic of the dielectric loss has also been seen around Er value 9.5 which is due to the scattering waves being trapped in MUT because of larger thickness Td.

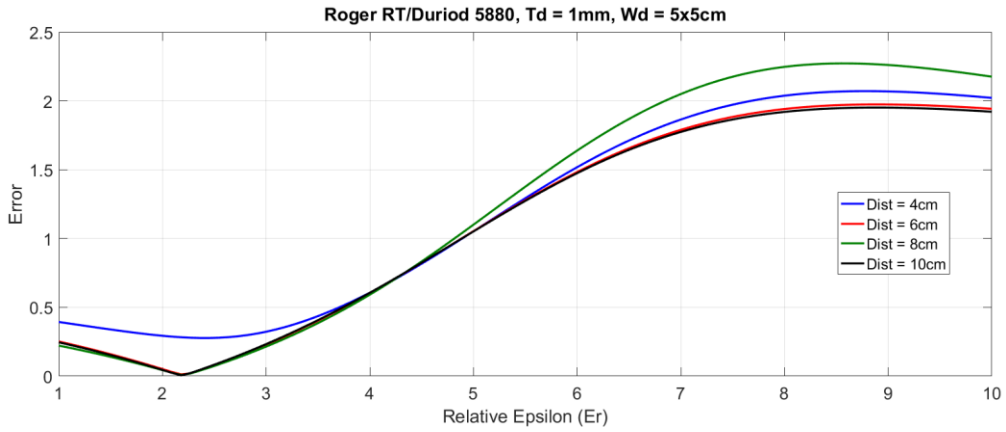

(a)

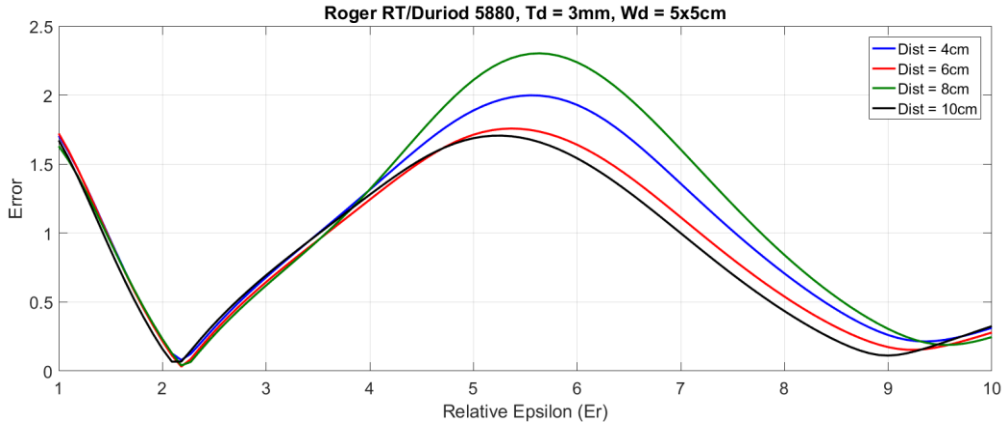

(b)

Fig. 4.19 Effect of Roger RT/Duriod 5880 thickness on the dielectric loss (error) (a) 1mm, (b) 3mm

Third and last material we have used for the estimation is Silicon with dielectric constant 11.9 and, Td = 2mm and Td = 0.5mm. The dielectric loss (error) response for Silicon MUT is shown in Fig. 4.20 (a-b).The material with higher dielectric constant of 11.9 is estimated very well at all the distances from the transmitting horn. The dielectric loss for the Td = 0.5mm, relatively smaller MUT thickness, at Dist = 4cm is not accurately estimated. As compared to the other cases. The analysis showed that smaller Dist and Td values has less accurate estimations for almost all the materials used in this parametric study.

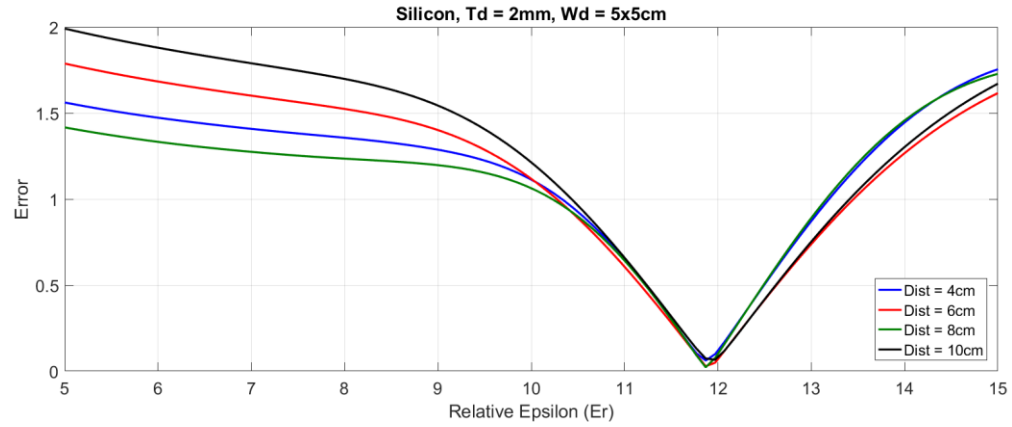

(a)

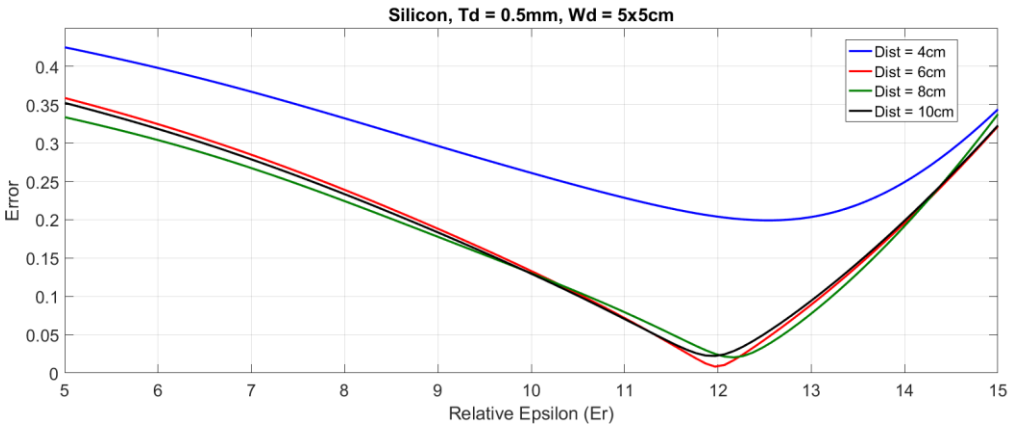

(b)

Fig. 4.20 Effect of Silicon thickness on the dielectric loss tangent (a) 2mm, (b) 0.5mm

The Table 4.1 shows the tabular summary of estimated dielectric constants for three different materials of variable thicknesses. The areas of MUT is also summarized in this table.

TABLE 4.1: SUMMARY OF THE PARAMETRIC STUDY

FR4 - 4.7

Td = 1.6mm

Dist	MATLAB		
	5cm	7.5cm	10cm
4cm	4.694	4.688	4.689
6cm	4.713	4.701	4.702
8cm	4.682	4.699	4.702
10cm	4.559	4.706	4.705

Td = 0.8mm

Dist	MATLAB		
	5cm	7.5cm	10cm
4cm	4.721	4.723	4.723
6cm	4.71	4.715	4.715
8cm	4.719	4.704	4.704
10cm	4.667	4.702	4.7

RT/Duriod - 2.2

Td = 3mm

Dist	MATLAB		
	5cm	7.5cm	10cm
4cm	2.188	2.187	2.187
6cm	2.191	2.191	2.191
8cm	2.201	2.193	2.193
10cm	2.14	2.194	2.193

Td = 1mm

Dist	MATLAB		
	5cm	7.5cm	10cm
4cm	2.204	2.204	2.205
6cm	2.199	2.199	2.198
8cm	2.193	2.189	2.189
10cm	2.184	2.188	2.187

Silicon - 11.9

Td = 2mm

Dist	MATLAB		
	5cm	7.5cm	10cm
4cm	11.885	11.879	11.88
6cm	11.893	11.881	11.881
8cm	11.87	11.883	11.879
10cm	11.925	11.877	11.882

Td = 0.5mm

Dist	MATLAB		
	5cm	7.5cm	10cm
4cm	12.041	12.041	12.04
6cm	11.983	11.997	11.995
8cm	12.03	11.981	11.979
10cm	11.948	11.969	11.963

4.3. Measurement Results

The experimental setup has been developed in Politecnico di Milano (PoliMI) and Universitat Politècnica de Catalunya (UPC) Barcelona to validate the simulated results of the material properties estimation and time domain procedure. The reflective measurement setup at PoliMI is shown in Fig. 4.21, where D = Dist, and h = Td. The transmitting horn antenna is placed on top facing downwards and grounded MUT is placed on the test bench table. Anritsu VNA is used for measurement of scattering parameters whereas, the manual positioning is done for variable 'Dist'.

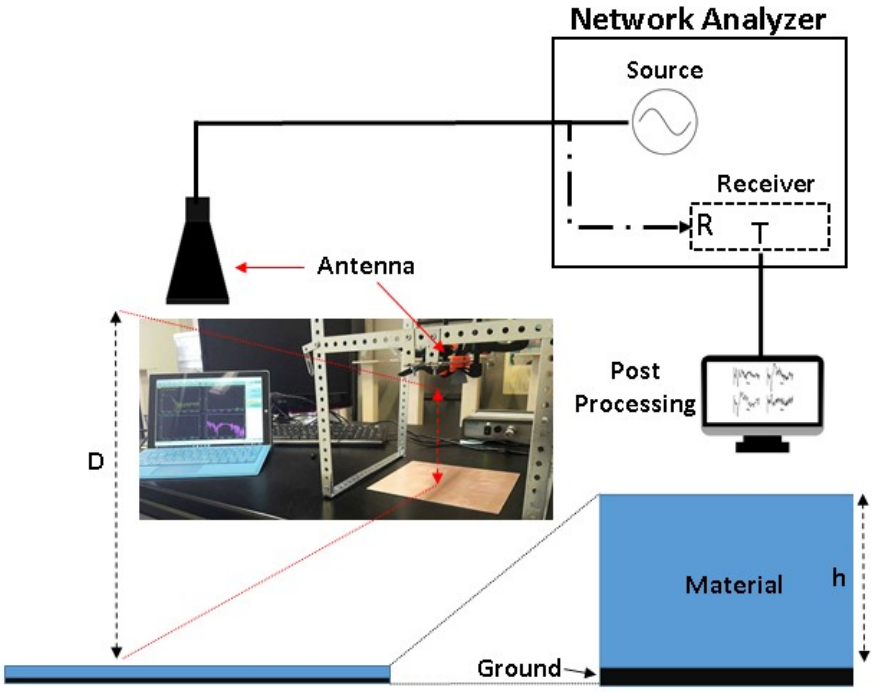

Fig. 4.21 Experimental setup at PoliMI

In order to validate the results, we have also measured the results at more specialized facility of UPC Barcelona. The experimental setup is horizontally developed on test bench, where the transmitter was fixed in a customized mechanical support to make sure the correct alignment between antenna and MUT as shown in the Fig. 4.22. The absorbers has also been placed around the MUT to reduce the diffracting and scattering from MUT support and surroundings. The experimental setup at UPC Barcelona has been used to extract scattering parameters at Ka and W frequency bands.

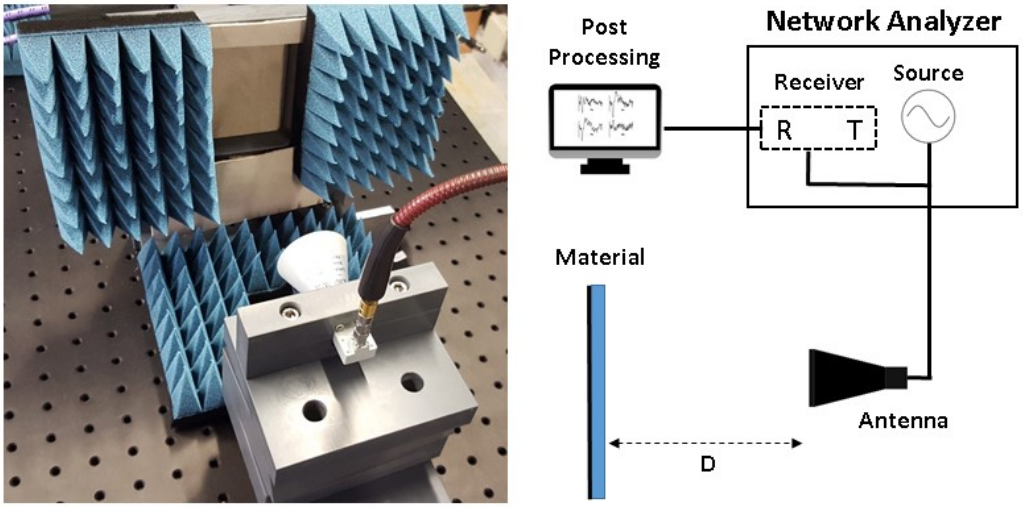

Fig. 4.22 Experimental setup at UPC Barcelona

4.3.1. Frequency Dispersion Analysis

The measured scattering data has been sampled on the time scale T_p and post-processed to get the comparison between initial model, final model after evaluation and experimental data as shown in Fig. 4.23. The same time domain data inversion method and time window approach is used for processing the measured data. The response curves showed delay between V_{MUT} and V_{PEC} due to positioning error which has been removed by adding the delay factor of $-1x10^{-8}$.

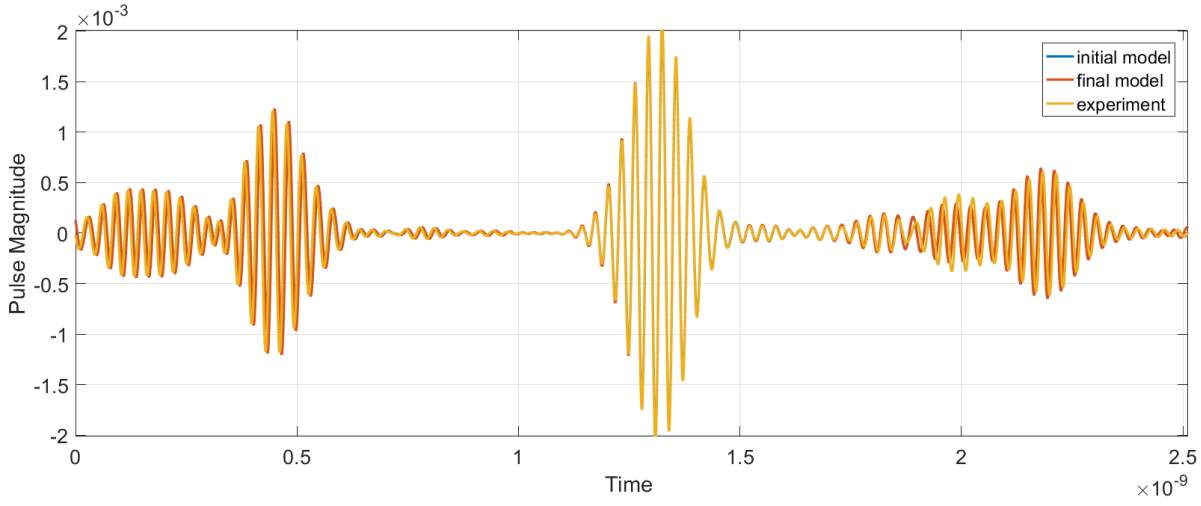

Fig. 4.23 Derived models and measured time response from MUT

The magnitude and phase of measured curves for both grounded PEC and MUT are shown in Fig. 4.24 (a-b), for the case of Dist = 8cm, Td = 1.6mm, and material FR4. VSIM0 and VSIM1 are grounded PEC and MUT data curves respectively. The plotted data showed good agreement between both curves in magnitude and phase in general whereas the magnitude remained higher between 28 and 35GHz in the Ka band. The phase agreement is considered very important in accurate material properties estimation as it testifies that both curves has been transmitted and received at same time instance.

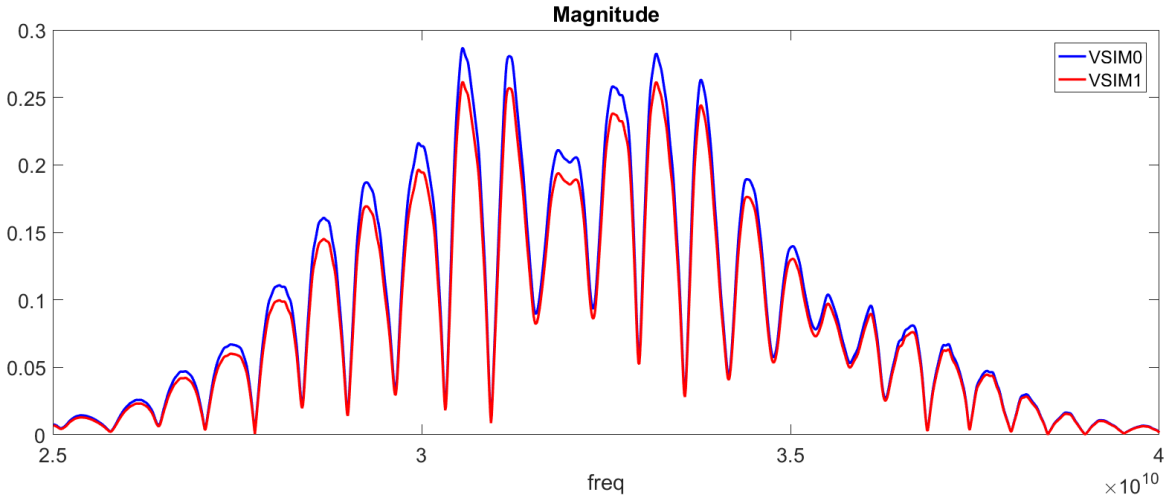

(a)

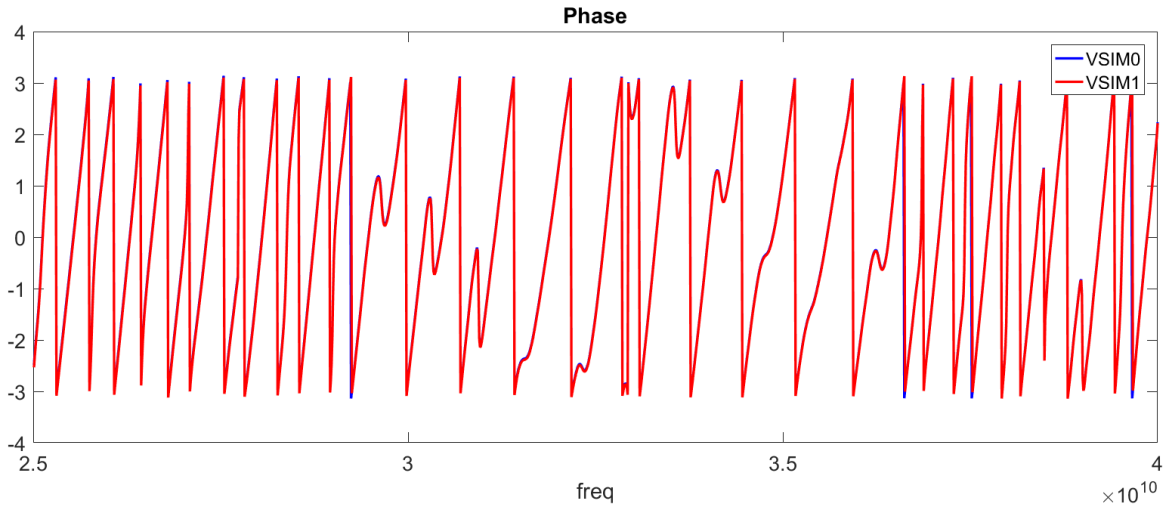

(b)

Fig. 4.24 Magnitude and phase of measured data for grounded PEC and MUT

The experimental parametric study is done for the Dist = 6, 8, 10, 13 and 18cm while the MUT area is kept fixed to 10x10cm^2. The dielectric constant and loss tangent are computed separately from measured results for the Ka band. Fig. 4.25(a-b) show the relative epsilon (Er) and loss tangent estimation for FR4 with Td = 0.8mm, however the result are not convincing as far as the predicted Er value (4.4) is concerned. Similarly, the loss tangent was also not estimated correctly as it has negative values for some

frequency points. To ensure the stability of results, we have recorded 10 measurement of the same case on 3 different days with new VNA calibration all the time.

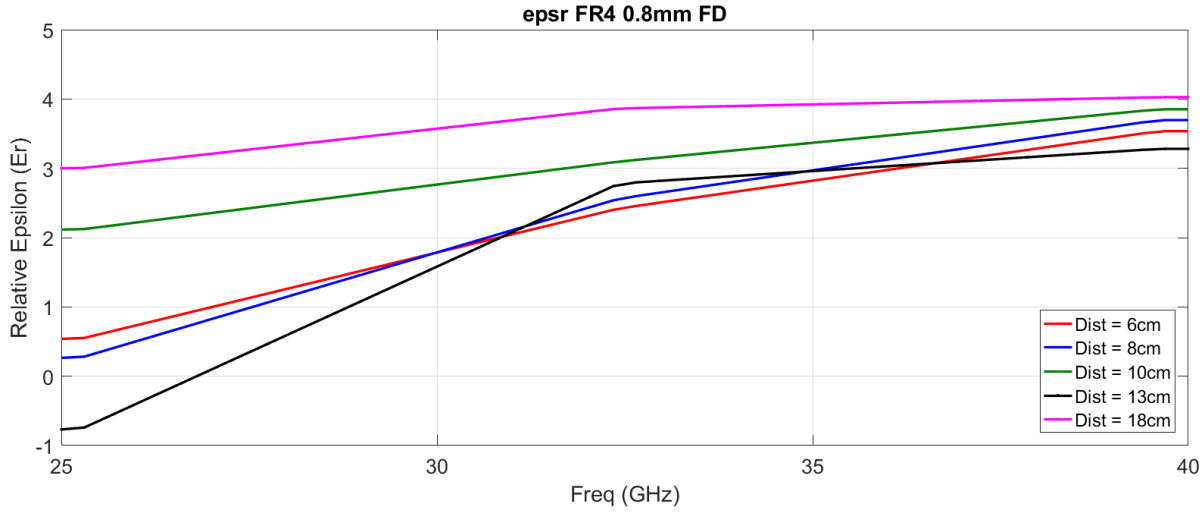

(a)

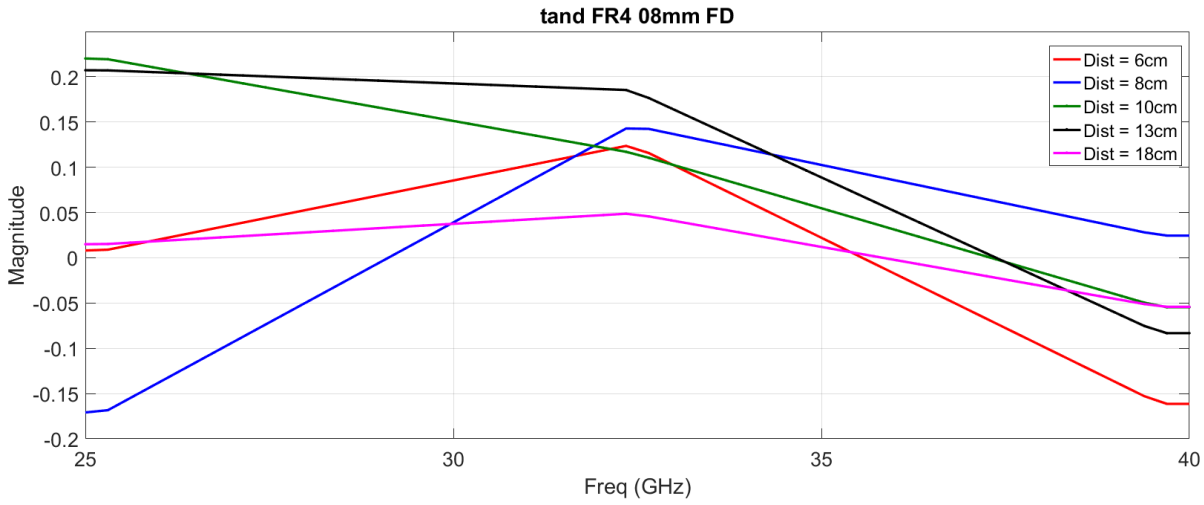

(b)

Fig. 4.25 Material properties estimation for FR4 at Td = 0.8mm (a) relative epsilon (Er) (b) loss tangent

The second case which has been studied through measured results is FR4 with Td = 1.6mm using the same 10x10cm^2 MUT sample. The FR4 estimation for Td = 1.6mm is much better than estimation at Td = 0.8mm. The best results are found when Dist = 10cm as Er value remained between 4.62 and 4.22. For other cases of Dist = 6, 8, 13 and 18cm, the variation in Er value is higher and it went as low as 3.83. The thickness of the MUT has lot to do with the scattering parameters and the materials with lower thickness were not correctly estimated with the developed time domain data inversion method. Therefore, we have explored on other approaches to estimate the material properties with better accuracy. The Bayesian inversion method has been developed for dielectric constant and material thickness estimation and it has been discussed in detail in next chapter.

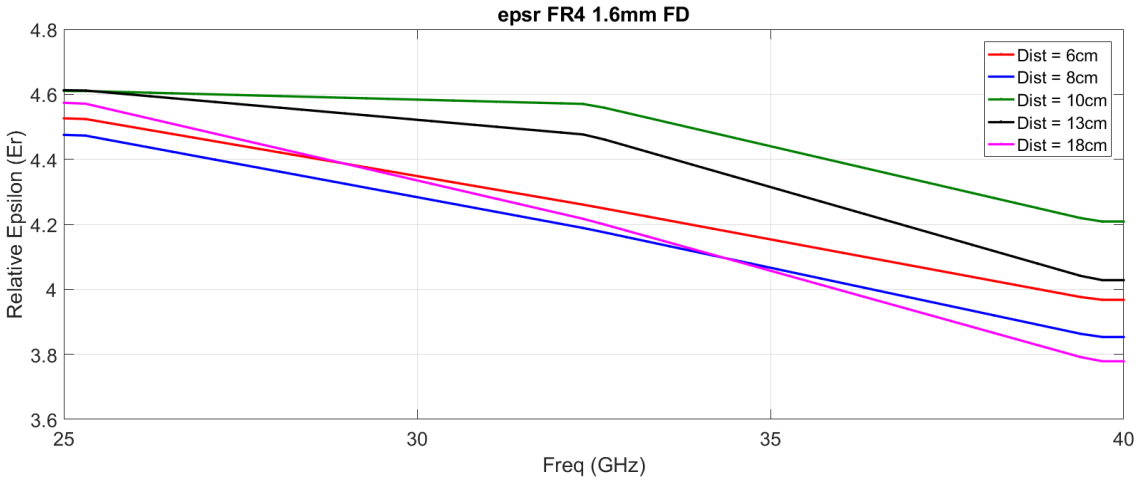

(a)

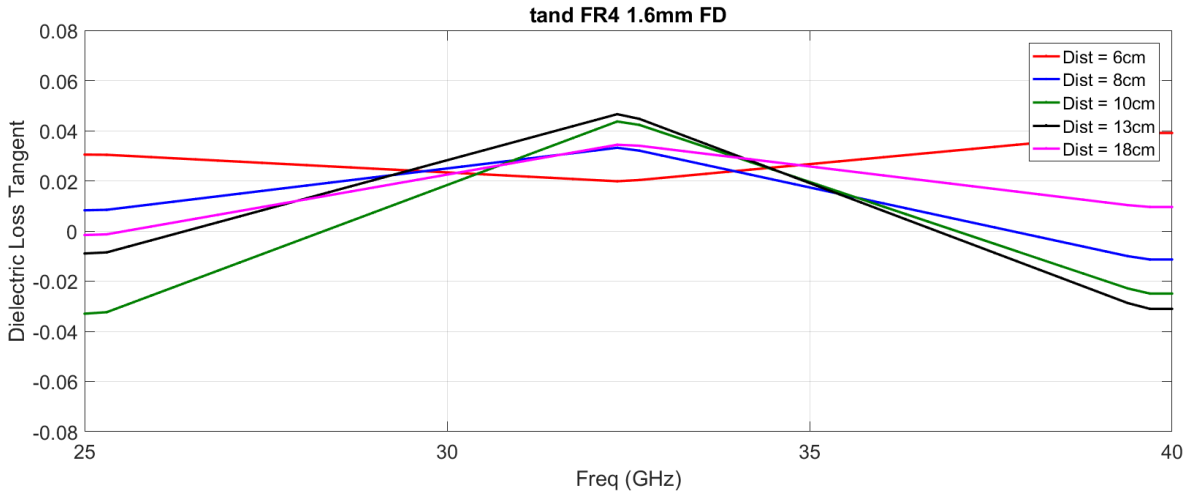

(b)

Fig. 4.26 Material properties estimation for FR4 material at Td = 1.6mm (a) relative epsilon (Er) (b) loss tangent

4.3.2. W-band Measured Results

We have also measured the scattering parameters of some material at W band from 70 to 110GHz. The setup for W-band is available at Antenna Lab, UPC Barcelona and it is shown in Fig. 4.27. For W-band measurement setup, the concave lens has been used between the transmitter horn and MUT. The distance between horn and lens (D1), and lens to MUT (D2) is fixed due to mechanical limitations and it is 20cm for both D1 and D2 separately. Measurements were carried out using the R&S VNA capable of scattering measurement from 10MHz to 110GHz.

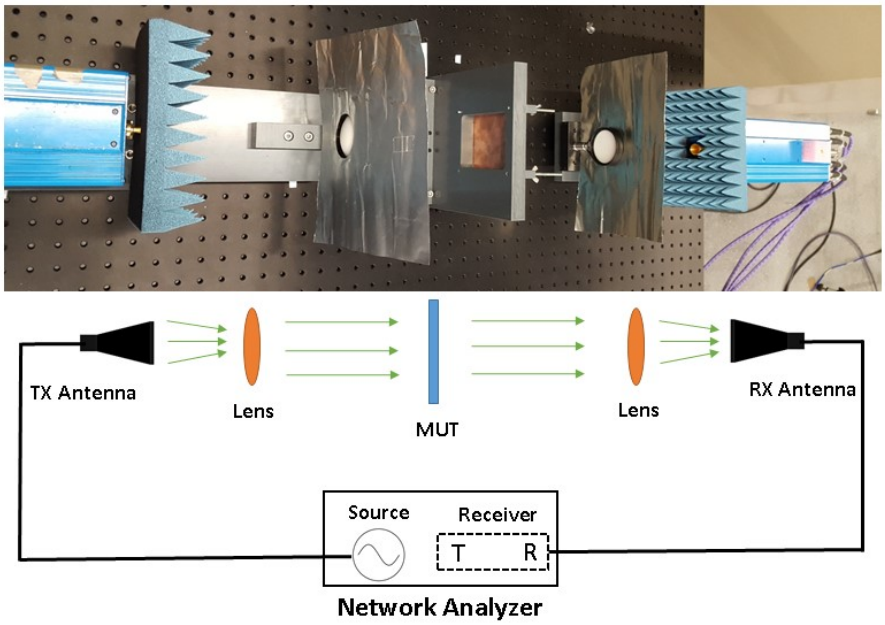

Fig. 4.27 Experimental setup for W-band at UPC Barcelona

The scattering response of different materials have been measured for wide range of material thickness in order to validate our conclusion that presented time domain method doesn't work well for thinner MUT's. The materials used in this study are FR4 (Er = 4.4. Td = 1.6mm), AD600 (Er = 6.15, Td = 0.65mm), Bayblend white (Er = 2.73, Td = 3.3mm), Bayblend black (Er = 2.76, Td = 3.3mm) and MK2447 (Er = 2.72, Td = 10mm). The estimation results of dielectric constant for these materials are shown in Fig. 4.28 and it has been observed that Er estimation for the materials with larger thickness (MK2447) is more accurate than the estimation of thinner materials (AD600).

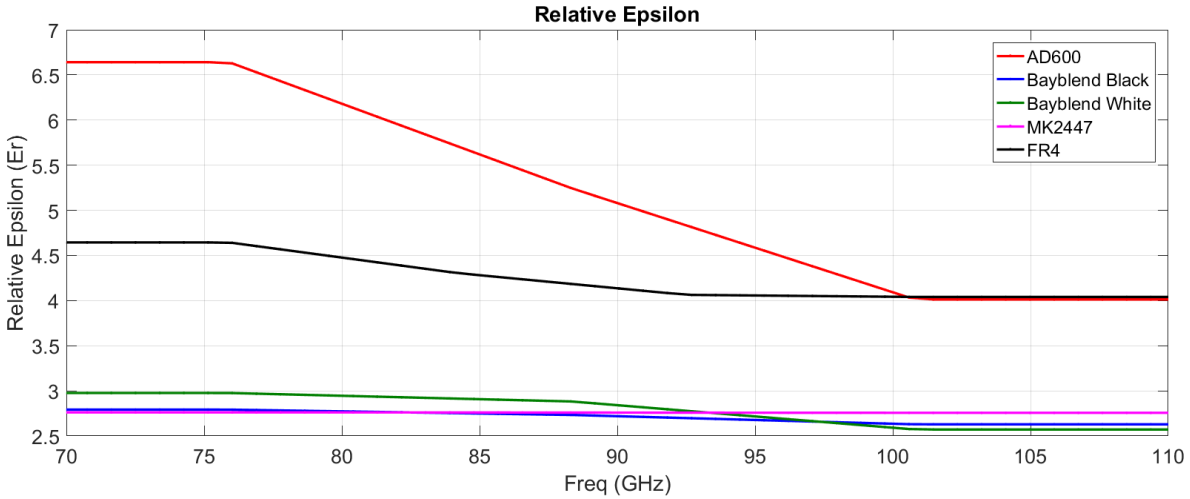

Fig. 4.28 Estimation of dielectric constant at W-band

CHAPTER 5

Bayesian Inversion Method

This chapter demonstrates the Bayesian inversion method and its implementation for material characterization of different materials, it is usually used for characterization of underground rock properties. In this chapter, we have presented the estimation of dielectric constant, dielectric thickness and MUT positioning error factor. The same measured data used in chapter 4 is considered here and evaluated for the extraction of material properties but using more efficient approach.

5.1 Theoretical Approach

The time domain Bayesian inversion method is reported as one of the accurate and time efficient inversion methods especially for reducing the uncertainties in estimation of electrical and magnetic parameters of various materials. This method is used in quantitative characterization of desired material properties from the measured scattering parameters, particularly the thickness of material and positioning error and dielectric constant properties. The set of constitutive equations are derived to develop the relation between the measured scattering parameters and prior material properties [70-72]. The interpretation of the material parameters can be done separately as well as jointly, here we have used the joint interpretation approach to estimation the dielectric constant (Er), material thickness (Td_2) and positioning error (Td_1) from the measured data. We have developed the measurement setup to extract the free space scattering parameters from the material under test (MUT). In this method, an MUT is placed at a finite distance (Dist) from the transmitting horn antenna (Tx) and the reflection scattering data is recorded both from the reference grounded PEC and the MUT. We have started the process of estimation by analysis of the various solid physics models [73], which could possibly develop the relation between the MUT properties and measured scattering variables, to be able to extract the cross properties; Er, Td_1 and Td_2. The material characterization is considered as the inverse problem and the parameter uncertainties are accounted in the inversion method through the concept of solid physics [74-75]. The investigation on the observed data is carried out using the reflection scattering data, which is sub categorized as the reflection coefficient, time instant of reflection and distance between Tx and MUT. The echo response of both computed and observed data is compared and the ambiguities has been reduced between the MUT thickness and positioning error. Initially, the value of positioning error is set to 0. We have exploited the cross relationship between the different models while doing the join inversion of scattering measurements, thus allowing us to get a better estimate of the uncertainty of dielectric material parameters and accuracy of the solution. We have used the iterative identification procedure to find the inversion convergence of the residual between the computed data and measured data. At the end, we have carried out the inversion on the real observed data with the constitutive equations that best fits the logged data. This approach can be useful for any measured data set with tunable constitutive equations to check the reliability of interpretation of the data.

5.1.1 Inversion Procedure and Dielectric Properties

The Bayesian inversion method is used to get the information about model parameters in terms of probability density [73]. Later, this probability density is used to find uncertainties in the assumed model parameters in order to build the confidence on measured results. We have been able to reduce the uncertainties in material properties like dielectric constant, MUT thickness and its positioning. We have derived the constitutive equations which are used to develop the link between the material properties and the observed data as shown in Fig. 5.1. We have used the free space measurements for the estimation

of material properties. The scenario is taken into account where the MUT with grounded surface is placed at a fixed distance (Dist) from the transmitter antenna, the area of MUT is also fixed for similar set of measured data whereas the following measured parameters and MUT properties are used in the constitutive equations;

- Reflection coefficient of scattering wave from the MUT in time domain, (R_{mut})
- Time response of the reflected wave (Ts)
- Distance between Tx and MUT (Dist)
- Dielectric constant (Er) and Thickness (T_{d2}) of the MUT
- MUT positioning error (T_{d1})

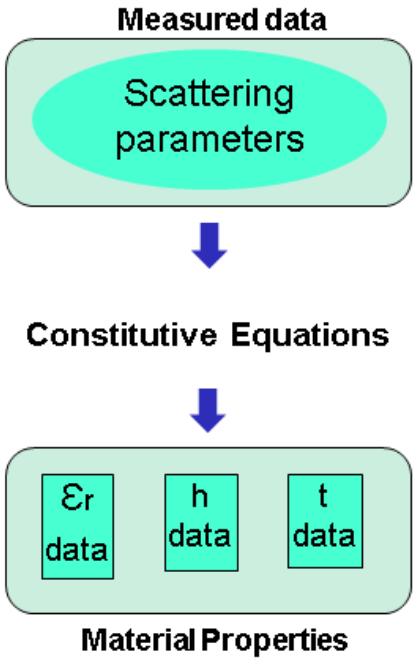

Fig. 5.1 Inversion iterative procedure

Dielectric and physical properties are parameters related to heterogeneous well-log observations: they are fundamental in the integration of measurements, in order to enhance the characterization of material [83-87]. Constitutive equations relate the equivalent medium of observed data (D_{obs}) to the dielectric constant and the vector $T_d = [T_{d1}, T_{d2}]^T$ of physical thickness of the MUT

$$D_{obs} = g(Er, T_{\mathbf{d}}) \qquad (5.1)$$

The above mentioned 1-Dimensional relation is simple and it can be used for different cases by using the appropriate set of constitutive equations, which depends on the material properties or/and the measured results. It has been seen that, the cross property relations are useful in estimating one property of material from another e.g., the thickness of MUT can be estimated easily which can be further used to estimate the MUT positioning error. The probabilistic approach is used for implementation of the

solution [84], where we have found the probability densities, solid materials model and data uncertainties, and the prior model for set of desired material properties.

5.1.2 Model and Data Space

Using Tarantola's notation [87], we have defined a vector of Z_m for the unknown model parameters of MUT which are included in the model space M_1,

$$m = [E_r, T_{d1}, T_{d2}]^T \tag{5.2}$$

Here, $T_d = T_{d1} + T_{d2}$. The set of desired model parameters are represented by the priori model M_{priori} and by a convergence matrix C_M in order to record the uncertainties in the M_{priori}. We have defined another vector of Z_d for the logged observed data from the scattering measurements, which is included in the model space M_2,

$$d = [D_{obs}]^T \tag{5.3}$$

The observed data in composed of different parameters such as; time domain reflection coefficient, time instant and the distance between Tx and MUT. Similarly, the prior data of measurements is given in the convergence matrix C_D which store the uncertainties in the measured data. The forward model is used as relation between the model parameters and the observed data parameters, and its given as;

$$d = g(m) \tag{5.4}$$

Here, g is a non-linear vectorial function which is used to predict, for a given set of model parameters $m \in M_1$, the values of the observable parameters $d \in M_2$. The forward model then calculate the approximations in the modelling uncertainties and stores them in convergence matrix Cg.

The solution to the inverse problem is hidden in the probabilistic framework and it can be derived through the iterative procedure in which the forward model linearizes around the current model (M_k) and it gives a new model (M_{k+1}) by using the Jacobian matrix J_k which comprise of the derivatives of the forward model equation and the current model parameters;

$$M_{k+1} = M_{priori} - [G_k^T C_d^{-1} G_k + C_M^{-1}]^{-1} G_k^T C_d^{-1} \text{ x } [(g(M_k) - d) - G_k(M_k - M_{priori})] \tag{5.5}$$

Here, the convergence matrix Cd store the uncertainties of both observed data and modelling data, with the Gaussian assumption, Cd = CD + Cg [86-88]. After first iteration, the current estimated model M_1 is set to a priori model M_{priori}. The calculated data is compared with the observed data and the solution is obtained by upgrading the current model until the posterior probability density of the model is maximized [gp-print]. The iterative algorithm stops when

$$M_{i,k+1} - M_{i,k} < \varepsilon, \forall i = 1, \ldots, Zm \tag{5.6}$$

The uncertainty of the solution is stored in the convergence matrix C_{Mpost} which also computed the final uncertainty values of the solutions as;

$$C_{M,post} = [G_k^T C_d^{-1} G_k + C_M^{-1}]^{-1} \quad (5.7)$$

The Figure 5.2 is block diagram of the inversion procedure.

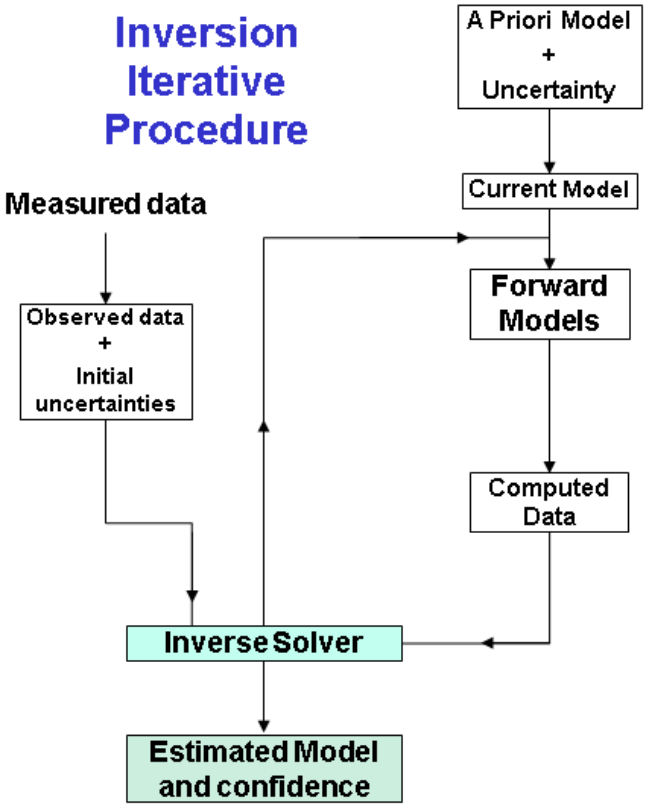

Fig. 5.2 Steps involved in the inversion procedure

5.1.3 Analysis of Uncertainties and Sensitivities

The uncertainties in the solution are calculated and reduced in section 5.1.2. The singular value decomposition analysis [89] is performed on the uncertainty of observed data by using the same constitutive equations around the reference M_{priori} model;

$$m_0 = [E_{r,0}, T_{d1,0}, T_{d2,0}]^T \quad (5.8)$$

$$d - d_0 = G(m - m_0) \quad (5.9)$$

Here, d_0 is the data vector which is generated by the data of reference M_{priori} model using the constitutive equations whereas G is the Jacobian matrix which contains all the first order partial derivatives of forward model [51], with respect to the material parameters;

$$G = \left[\frac{\partial D_{obs}}{\partial E_r} \quad \frac{\partial D_{obs}}{\partial T_{d1}} \quad \frac{\partial D_{obs}}{\partial T_{d2}}\right] \quad (5.10)$$

The singular value decomposition of G is [11-12];

$$G = A\Lambda B^T \quad (5.11)$$

Here, the matrix A contains the Eigen vectors of data space while the Λ is diagonal matrix of all the singular values. The purpose of Λ matrix is to represent the magnitude of data due to the normalized variation along Eigen vectors axis in the model space. The matrix B contains the Eigen vectors of the model space, where linear pairs of the unknown model parameters Er, Td_1, Td_2 are made by forming the orthogonal basis in the model space [90]. The real values of model parameters in the form of eigenvectors can be represented in the model space as in Fig. 5.3: eigenvectors are ordered (left to right) with decreasing singular values.

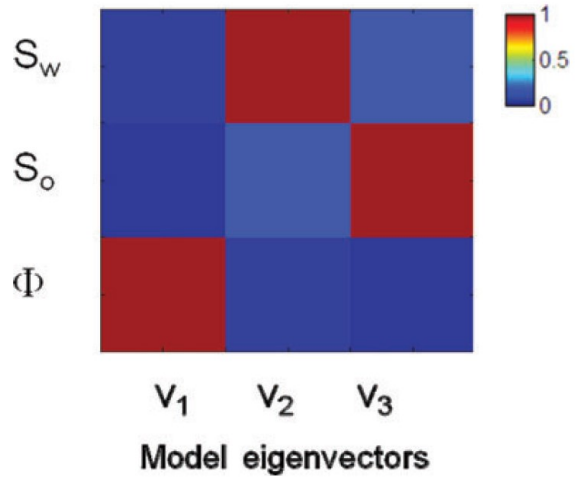

Fig. 5.3 Matrix G: absolute value of eigenvectors in the model space [51]

5.2 Bayesian Inversion Results

The MATLAB 2016b is used to formulate and simulate the Bayesian inversion method. The software interface in MATLAB is shown in Fig. 5.4(a-b). The software is design to include all the necessary assignments before the simulation run, Fig. 5.4(a) shows the model assignment wizard for the Bayesian inversion where the options such as, parameter scaling, C_M constant, standard deviation of Er and Td as well as the 4 point ranges of Er and Td are included. It's important to mention that, in this software, we can add as much as layers of Er and Td to find the individual values. Similarly, Fig. 5.4(b) shows the inversion parameters assignment such as, the number of iterations, residual type and threshold %, line search type and delta % to compute the derivatives. After assignment of above parameters, we select the model index, save file name and run the simulation which give us 3 different result wizards, the tabular values of Er and Td, the Er vs Td curves, residual % curves, the time echoed pulse comparison, and the Eigen vector data for the given case of MUT.

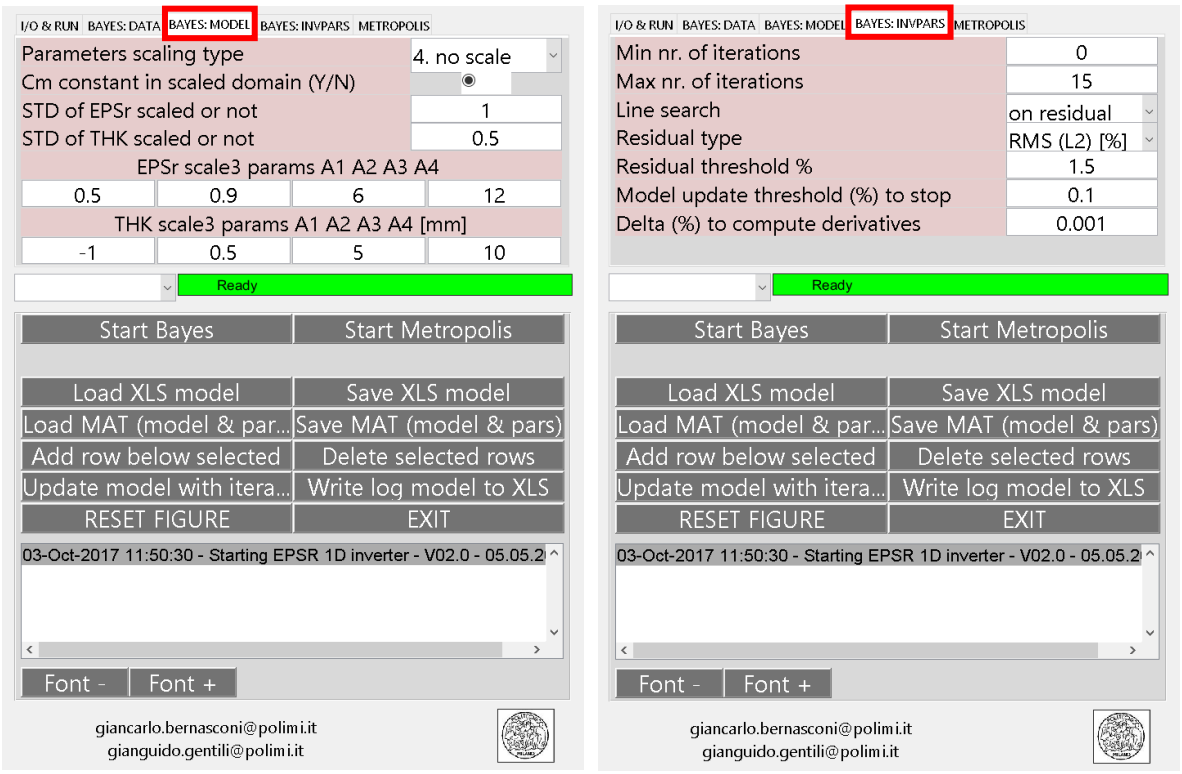

(a) (b)

Fig. 5.4 Bayesian inversion software (a) Model parameters (b) Inversion parameters

5.2.1 Single Layer Materials

The first analysis is carried out on scattering data of the single layer materials. In single layer, we have two sub catagories, i-e; MUT with grounded PEC surface and MUT without grounded PEC. The PEC surface at the back of MUT helps to reflect the transmitted waves in order to receive better scattering response.

a) MUT with Grounded PEC

In case of grounded MUT measurements, one sided copper (PEC) coated materials are used. The layer of PEC was 0.035mm approximately and 10x10cm^2 area of MUT for all the measurements. Different single layer materials are discussed in detail. The MUT is placed at five different distances from the transmitter antenna (Tx) at 6, 8, 10, 13 and 18cm.

i. Rogers AD600

The first material presented is Rogers AD600 with given Er = 6.15 and Td = 0.52mm. The scattering data is converted into the time domain echoed data and compared with computed echo curve. The Fig. 5.5 shows the comparison of echo curves for both observed and computed data. The full time scale is from 0-9ns but the time window function is applied on the scattering response to process only the reflection response of MUT for further analysis. It can be seen that the curves are in good agreement and sampled over each other for time specific values. The reflected peak-to-peak values in the echo

curves are identical for all the Dist values but only shifted in time at, 1.18ns, 1.31ns, 1.45ns, 1.62ns and 1.91ns for 6cm, 8cm, 10cm, 13cm and 18cm respectively.

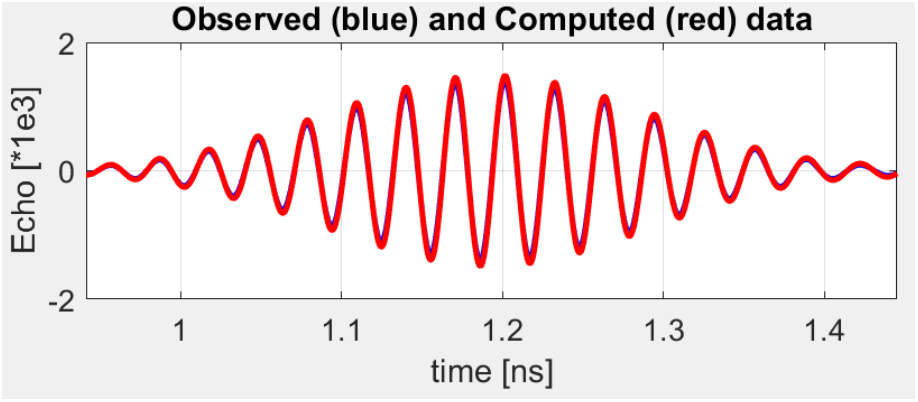

Fig. 5.5 Echo comparison for the case of single layer Rogers AD600

The residual is also calculated for Rogers AD600 at all the distances from Tx. In these cases, the maximum probability density is achieved with maximum three model iterations (M_3) from the prior model (M_{priori}). The minimum residual percentage of 6.8% is found at Dist = 6cm for the 2nd model iteration (M_2), but the estimation wasn't good enough. The residual % is very high at Dist = 13cm but the inversion method was still able to estimate the correct Er value. Fig. 5.6 shows the % residual curves for all the single layer cases of Rogers AD600.

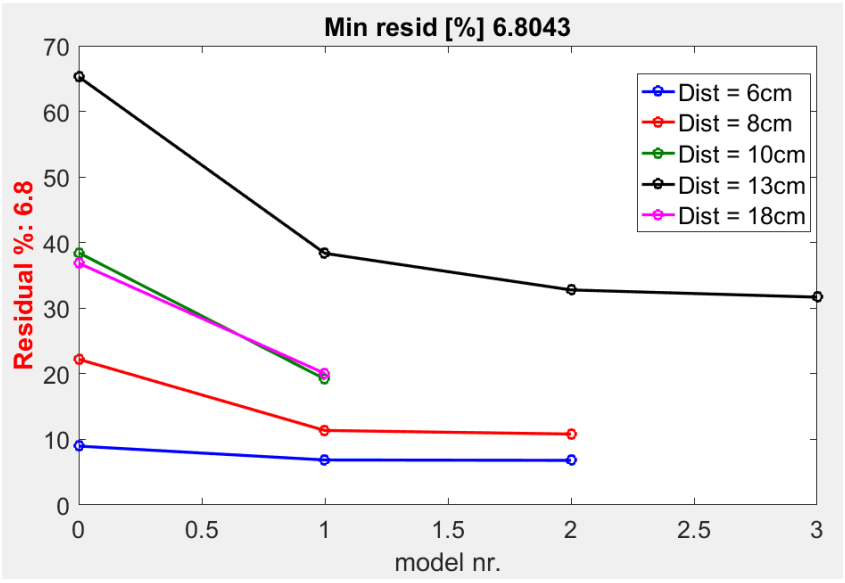

Fig. 5.6 Residual analysis for the cases of single layer Rogers AD600

The estimated parameter are Er, Td_1 and Td_2 where Td_1 is positioning error in the placement of MUT and Td_2 is the thickness of MUT. Fig. 5.7 shows the Er vs Td_2 graph where Er value of corresponding thickness is plotted for each case of Dist. The positioning error was more than 0.1mm for the case of 6cm and 8cm whereas the thickness of Roger AD600 is estimated between 0.414 and 0.473mm, and

when we add the corresponding positioning error, the estimation at 10cm and 18cm were found in good agreement with the given values. TABLE 5.1 summarize the analysis of Rogers AD600 in terms of Er and Td estimations.

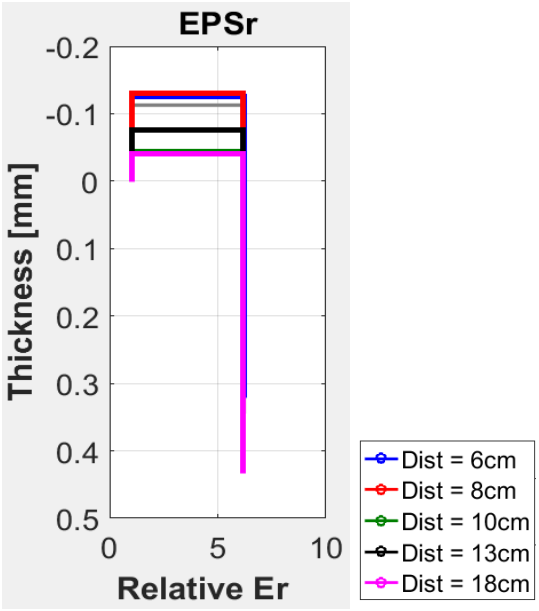

Fig. 5.7 Dielectric constant (Er) vs thickness (Td) for the cases of single layer Rogers AD600

TABLE 5.1 SUMMARY OF ANALYSIS – SINGLE LAYER ROGERS AD600

Parameter	**Relative Er**	**Thickness Td_2 (mm)**	**Positioning Error Td_1 (mm)**
6cm	6.213	0.447	-0.127
8cm	6.154	0.414	-0.138
10cm	6.149	0.466	-0.044
13cm	6.147	0.419	-0.077
18cm	6.149	0.473	-0.041

The probability density is presented with respect to the eigenvectors in model space. The Rogers AD600 material with all five Dist experiments has been discussed and the confidence on model parameters has been predicted from the given model space. The absolute values of eigenvectors in model space behave the same way as shown in Fig. 5.8, where eigenvectors are stacked on the horizontal axis (left to right) with decreasing singular values whereas the model parameters are stacked on the vertical axis (bottom to top). From the legend bar, it can be understood that the blue colour shows the lowest confidence on model parameter and yellow colour shows the highest confidence on the model parameter. From Fig.

5.8, Td_2 was the parameter with highest confidence (associated to the first eigenvector), then Td_1 (second eigenvector) and finally Er (third eigenvector). In the free space measurements, the inversion problem is able to find higher confidence in thickness of MUT as compared to dielectric constant (Er).

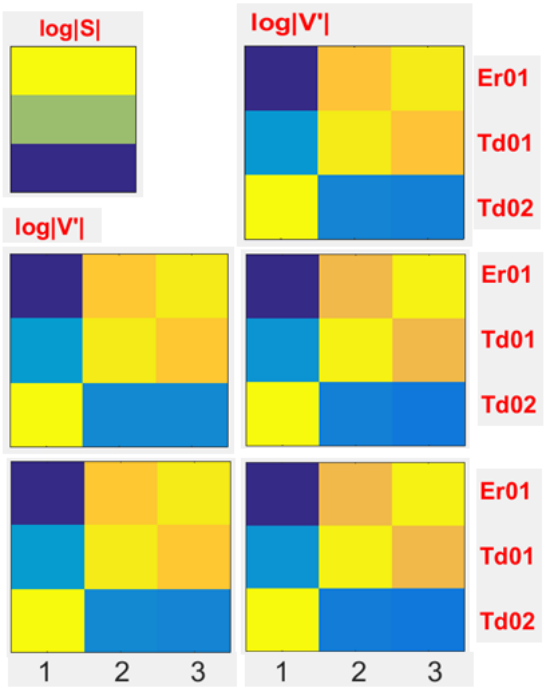

Fig. 5.8 Matrix G: eigenvectors in the model space for all the cases of single layer Rogers AD600

ii. FR4 Epoxy

The second single layer material presented is FR4 Epoxy with given Er = 4.4 and Td = 1.52mm. Same as before, the observed data is converted into the time domain echoed pulse and compared with computed echo curve as shown in Fig. 5.9. The full time scale is from 0-9ns but the time window function is applied on the scattering data to filter the reflection response of MUT for further analysis. The curves showed a good matching for both observed and computed data for MUT reflected echoes. The behaviour of reflected peak-to-peak echo curves are same in presentation for all the Dist values, but only time shifted at, 1.21ns, 1.33ns, 1.48ns, 1.66ns and 1.98ns for 6cm, 8cm, 10cm, 13cm and 18cm respectively.

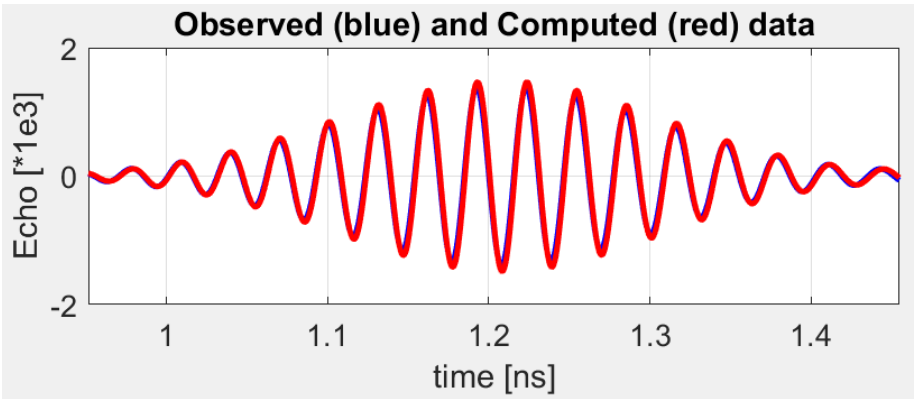

Fig. 5.9 Echo comparison for the cases of single layer FR4 Epoxy

The residual response is also calculated for FR4 Epoxy and compared at all the distances from Tx. The maximum probability density is achieved at third model (M_3) iteration starting from the M_{priori}. The minimum residual percentage of 12.7% is observed at Dist = 10cm for the 2nd model iteration (M_2), with most accurate estimation among the cases and minimum positioning error. The higher residual % were observed at Dist = 8cm and 18cm, and both cases tend to behave similar as far as estimation of model parameters are concerned. Fig. 5.10 shows the % residual curves for all the single layer cases of FR4 Epoxy.

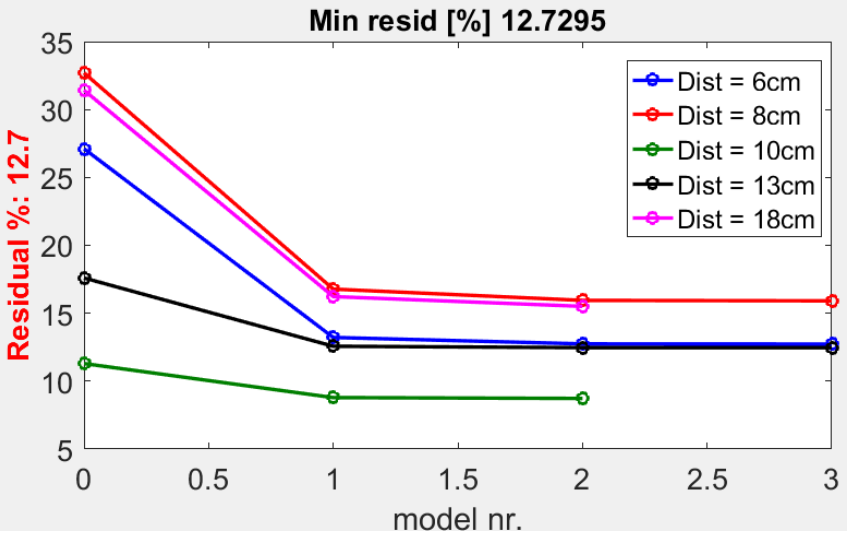

Fig. 5.10 Residual analysis for the case of single layer FR4 Epoxy

The estimated model parameter are Er, Td_1 and Td_2 where Td_1 is positioning error in the placement of MUT and Td_2 is the thickness of MUT. Fig. 5.11 shows the Er vs Td_2 graph where Er value of corresponding thickness is plotted for each case of Dist. The positioning error remained less than 0.1mm for all the case whereas the thickness of FR4 Epoxy is estimated between 1.504 and 1.54mm, and after adding the corresponding positioning error, the estimation at 10cm was found in good agreement with the given Er and Td_2 values. Generally, the higher positioning error leads to lower estimation accuracy. TABLE 5.2 summarize the analysis of FR4 Epoxy in terms of Er and Td estimations.

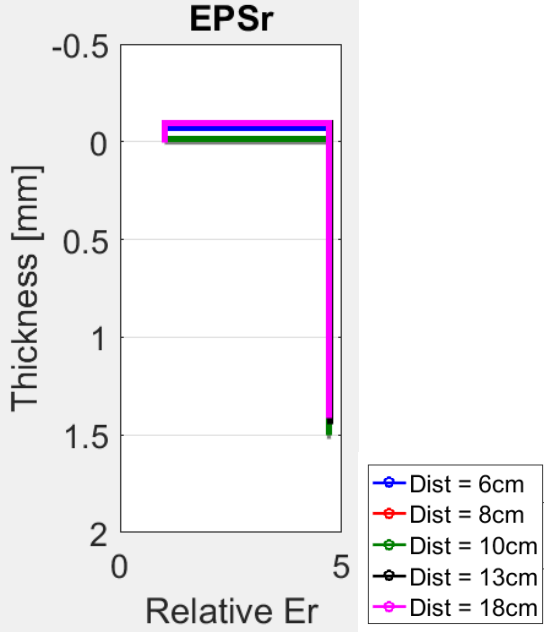

Fig. 5.11 Dielectric constant (Er) vs thickness (Td) for the case of single layer FR4 Epoxy

TABLE 5.2 SUMMARY OF ANALYSIS – SINGLE LAYER FR4 EPOXY

Parameter	**Relative Er**	**Thickness Td_2 (mm)**	**Positioning Error Td_1 (mm)**
6cm	4.685	1.504	-0.073
8cm	4.689	1.508	-0.082
10cm	4.696	1.511	-0.014
13cm	4.721	1.540	-0.091
18cm	4.688	1.508	-0.096

The probability density is presented with respect to the eigenvectors in the model space. The FR4 Epoxy material with all five Dist experiments has been discussed and the confidence on model parameters has been predicted from the given model space. The absolute values of eigenvectors in the model space behave the same way as shown in Fig. 5.12, where the eigenvectors are stacked on the horizontal axis (left to right) with decreasing singular values whereas the model parameters are stacked on the vertical axis (bottom to top). Td_2 was the parameter with highest confidence (associated to the first eigenvector), then Td_1 (second eigenvector) and finally Er (third eigenvector). Same as the case of Rogers AD600, the inversion problem is able to find higher confidence in the thickness of MUT as compared to dielectric constant (Er).

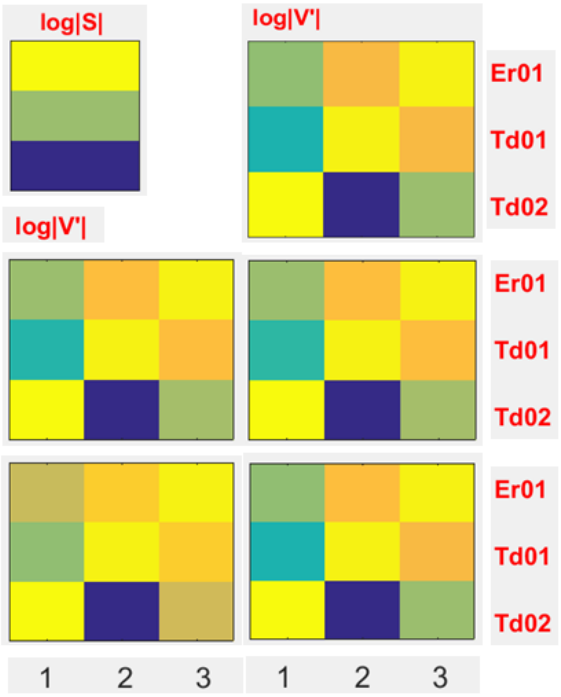

Fig. 5.12 Matrix G: eigenvectors in the model space for all the cases of single layer FR4 Epoxy

iii. Rogers RT/Duriod 5880

The third single layered material discussed is Rogers RT/Duriod 5880 with given Er = 2.2 and Td = 0.65mm. The scattering data (S_{11}) is converted into the time domain echoed data and compared with computed echo curve of the reference model. The Fig. 5.13 shows the comparison of echo curves of both observed and computed data. It can be seen that the curves are showing almost similar behaviour on the time scale, and delay factor is not needed yet. The reflected peak-to-peak values in the echo curves looks identical in presentation for all the Dist values but only shifted in time at, 1.85ns, 1.29ns, 1.44ns, 1.61ns and 1.87ns for 6cm, 8cm, 10cm, 13cm and 18cm respectively.

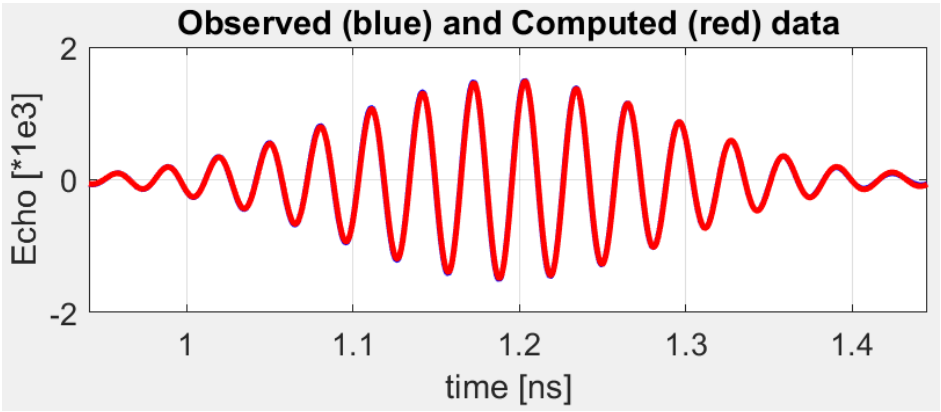

Fig. 5.13 Echo comparison for the case of single layer Rogers RT/Duriod 5880

The residual is also calculated for Rogers RT/Duriod 5880 at all the distances from Tx. The residual is calculated using the RMS % approach which allowed us to get the maximum probability density with

maximum third model iteration (M_3). The minimum residual percentage of 2.9% is found at Dist = 6cm and 8cm over the 2nd model iteration (M_2), and the minimum positioning was also found in these cases. Despite increase in the residual % with increase in Dist values, the inversion method has estimated the correct Er value for all the cases with less than 5% tolerance. Fig. 5.14 shows the % residual curves for all the single layer cases of Rogers RT/Duriod 5880.

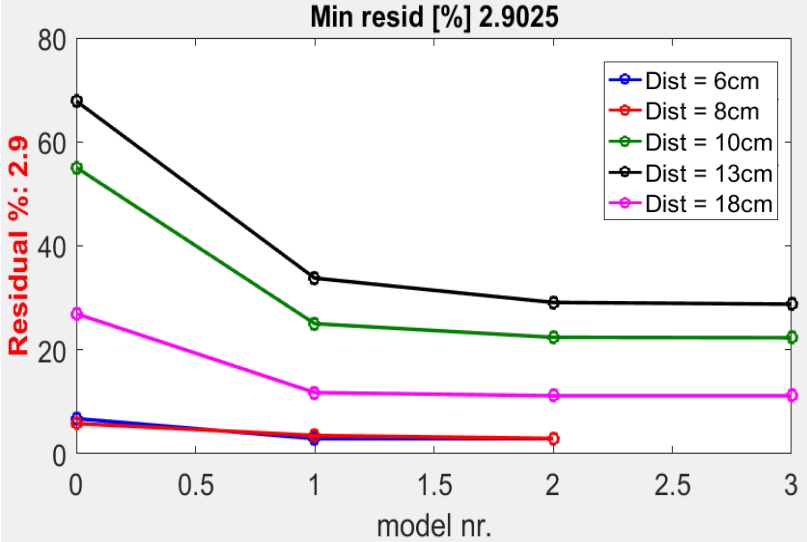

Fig. 5.14 Residual analysis for the case of single layer Rogers RT/Duriod 5880

Fig. 5.15 shows the Er vs Td_2 graph for each case of Dist value and model iteration. The negative value on thickness axis represent the positioning error of MUT in the setup. The positioning error was very less (-0.007mm) for the case of 6cm whereas it was more than 0.1mm for the case of 13cm, the thickness of Roger RT/Duriod 5880 is estimated between 0.508 and 0.640mm, where Td_1 = 0.508mm was for the case of Dist = 13cm. It has been concluded that the estimation at lower Dist values were found in good agreement with the given parameter values. TABLE 5.1 summarize the analysis of the Roger RT/Duriod 5880 in terms of Er and Td estimations.

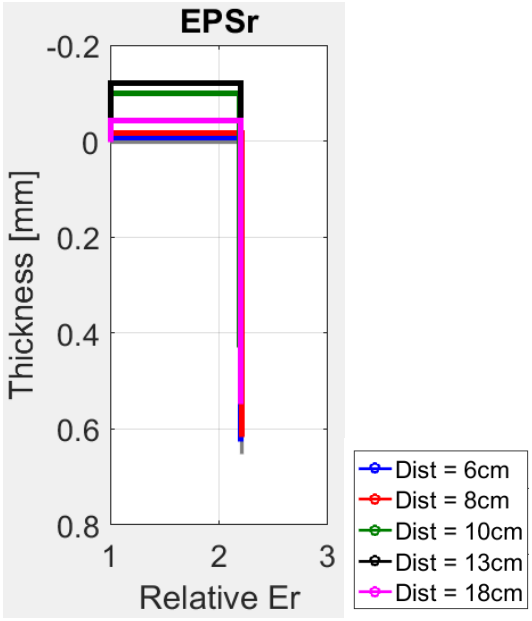

Fig. 5.15 Dielectric constant (Er) vs thickness (Td) for the cases of single layer Rogers RT/Duriod 5880

TABLE 5.3 SUMMARY OF ANALYSIS – SINGLE LAYER ROGERS RT/DURIOD 5880

Parameter	**Relative Er**	**Thickness Td_2 (mm)**	**Positioning Error Td_1 (mm)**
6cm	2.192	0.632	-0.007
8cm	2.201	0.640	-0.011
10cm	2.187	0.592	-0.099
13cm	2.188	0.508	-0.121
18cm	2.189	0.592	-0.044

The probability density is presented with respect to the eigenvectors in the model space. The absolute values of eigenvectors in model space behaved the same way as shown in Fig. 5.16. From the legend bar, it can be understood that the blue colour shows the lowest confidence on the model parameter and the yellow colour shows the highest confidence on the model parameter. From the Fig. 5.16, Td_2 was the parameter with highest confidence (associated to the first eigenvector), then Td_1 (second eigenvector) and finally Er (third eigenvector). The inversion problem still showed higher confidence in the thickness of MUT as compared to dielectric constant (Er) for all the single layer cases of MUT with grounded PEC.

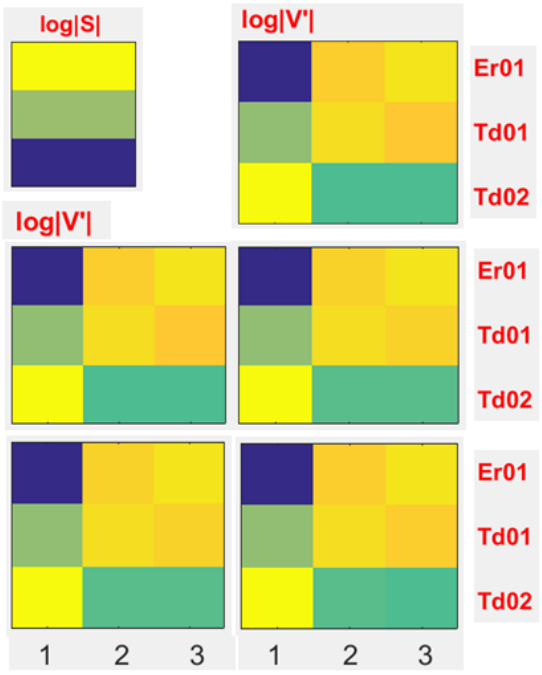

Fig. 5.16 Matrix G: eigenvectors in the model space for all the cases of single layer Rogers RT/Duriod 5880

b) MUT without Grounded PEC

In this case, scenario of measurements without PEC layer on the back of MUT is experimented. The 10x10cm^2 area of MUT is used for all the measurements whereas the free space propagation was assumed on both sides of the MUT. Different single layer materials without grounded PEC are discussed in detail. Similar measurement setup is used where the MUT is placed at five different distances from the transmitter antenna (Tx) at 6, 8, 10, 13 and 18cm.

i. FR4 Epoxy

The FR4 Epoxy with given Er = 4.4 and Td = 1.52mm is used, this time without copper (PEC) layer on the back side. Similar measurement campaign is carried out where the scattering data is extracted and later used to transform into the time domain echoed data and compared with computed echo curve as shown in Fig. 5.17. It can be seen that the curves are in good agreement and sampled over each at the same time instants. The reflected peak-to-peak response in the echo curves is identical for all the Dist values but only shifted in time at, 1.2ns, 1.32ns, 1.49ns, 1.65ns and 1.96ns for 6cm, 8cm, 10cm, 13cm and 18cm respectively.

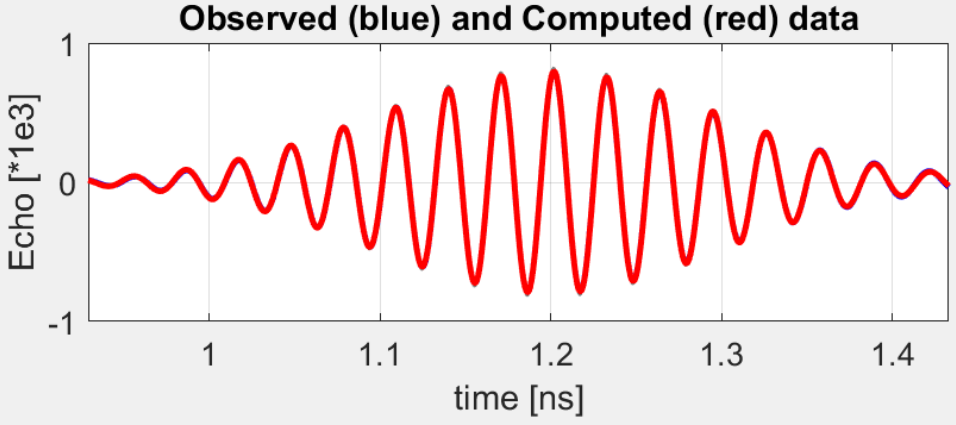

Fig. 5.17 Echo comparison for the case of single layer FR4 Epoxy (WO)

The residual response is different for MUT without ground plane, FR4 Epoxy, at all the distances from Tx. The maximum probability density is achieved with higher model iterations up to M_8 but the residual % is very less as compared to the residual response for the grounded PEC cases. The minimum residual percentage of 0.8% is found at Dist = 6cm at the 2nd model iteration (M_2). It has been seen that increasing the Dist value increases the residual % and thus decreasing the estimation accuracy of both Er and Td. The residual % is very high at Dist = 13cm leading to poor estimation of model parameters. Fig. 5.18 shows the % residual curves for all the MUT without PEC back, single layer cases of of FR4 Epoxy.

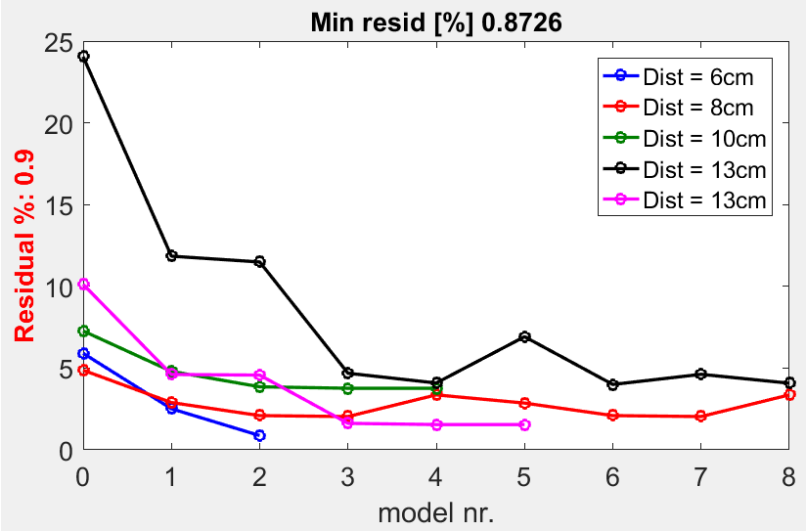

Fig. 5.18 Residual analysis for the case of single layer FR4 Epoxy (WO)

The estimated model parameter are Er, Td_1 and Td_2 where Td_1 is positioning error usually arises due to the manual placement of MUT in the measurement setup and Td_2 is the thickness of MUT. Fig. 5.19 shows the Er vs Td_2 graph where Er value of corresponding thickness and positioning error is plotted for each case of Dist values. The positioning error was more than 0.1mm for the case of Dist = 13cm whereas the least Td_1 is observed at Dist = 6cm (Td_1 = 0.004mm). The thickness of FR4 Epoxy remained between 1.533 and 1.646mm, and after adding the corresponding positioning error, the estimation at

6cm was found in good agreement with the given model parameters. TABLE 5.4 summarize the analysis of the FR4 Epoxy in terms of Er and Td estimations.

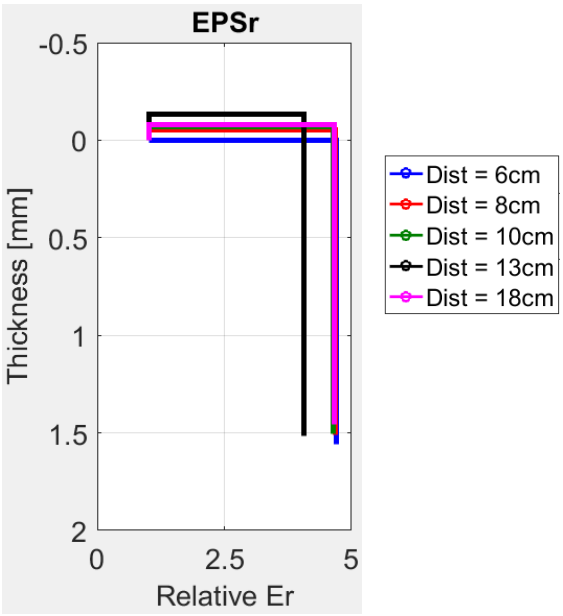

Fig. 5.19 Dielectric constant (Er) vs thickness (Td) for the case of single layer FR4 Epoxy (WO)

TABLE 5.4 SUMMARY OF ANALYSIS – SINGLE LAYER FR4 EPOXY (WO)

Parameter	**Relative Er**	**Thickness Td_2 (mm)**	**Positioning Error Td_1 (mm)**
6cm	4.695	1.558	-0.004
8cm	4.665	1.559	-0.054
10cm	4.632	1.575	-0.073
13cm	4.055	1.646	-0.134
18cm	4.653	1.533	-0.079

The probability density is presented with respect to the eigenvectors in the model space. The absolute values of eigenvectors in the model space behave the same way as shown in Fig. 5.20, where the eigenvectors are stacked on the horizontal axis (left to right) with decreasing singular values whereas the model parameters are stacked on the vertical axis (bottom to top). From the Fig. 5.20, for the case of Dist = 6, 8, 10 and 18cm, Td_2 was the parameter with highest confidence (associated to the first eigenvector), then Td_1 (second eigenvector) and finally, Er (third eigenvector), whereas, for Dis = 13cm, the confidence matrix is changed as, the Td_2 was the parameter with highest confidence (associated to

the first eigenvector) but then, no confidence on any parameter is found on the second eigenvector (v2), and Td_1 has a confidence at the third eigenvector (v3). In the free space measurements, the inversion problem is able to find higher confidence again, in the thickness of MUT as compared to dielectric constant (Er).

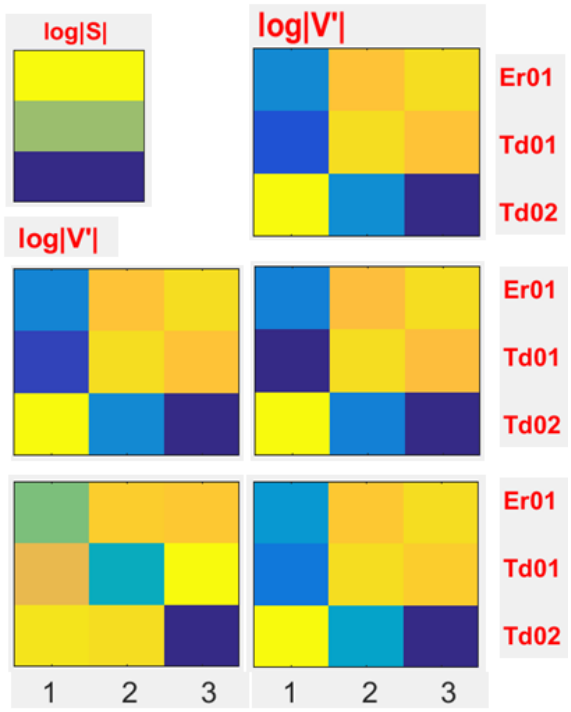

Fig. 5.20 Matrix G: eigenvectors in the model space for all the cases of single layer FR4 Epoxy (WO)

ii. Rogers RT/Duriod 5880

The second material discussed without grounded PEC is Roger RT/Duriod 5880 with given Er = 2.2 and Td = 0.65mm. The scattering response data is extracted without PEC back and converted into the time domain echoed data and compared with computed echo curve as shown in Fig. 5.21. The full time scale is from 0-9ns but the time windowing is applied on the observed data to filter out the reflection response of MUT for further in data inversion analysis. It can be seen that the curves aren't exactly in good agreement and a small time delay, magnitude difference is observed, which has effected the estimation of model parameters. The reflected peak-to-peak response in the echo curves is identical for all the Dist values and only shifted in time axis at, 1.18ns, 1.31ns, 1.46ns, 1.69ns and 1.94ns for 6cm, 8cm, 10cm, 13cm and 18cm respectively.

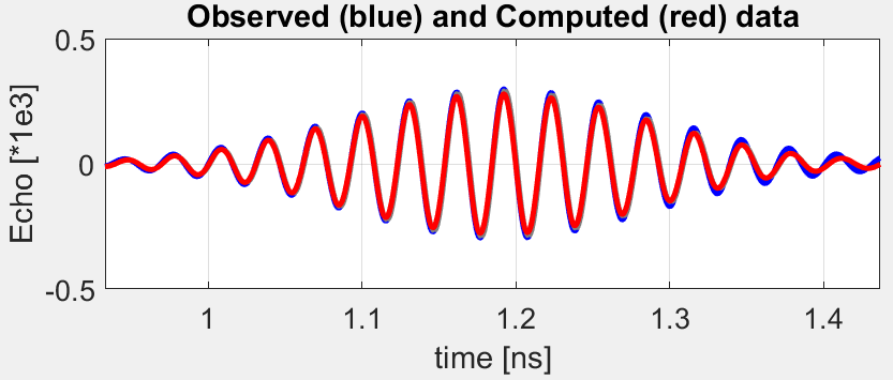

Fig. 5.21 Echo comparison for the case of single layer Rogers RT/Duriod 5880 (WO)

The residual response % for without grounded MUT, Rogers RT/Duriod 5880, was less than 25% except the response at Dist = 18cm from the Tx. The maximum probability density is achieved with higher model iterations up to M_8, the irregular residual response is observed for case of Dist = 13cm. The minimum residual percentage of 6.6% is found at Dist = 6cm at the 3rd model iteration (M_3). The unusual residual response has been observed for Rogers RT/Duriod 5880 and the accuracy in estimation of the model parameters can't be formulated e.g., the residual % is very high at Dist = 18cm leading to poor estimation of model parameters. The observation showed that the MUT without grounded PEC needs the MUT thickness to be higher. Fig. 5.22 shows the % residual curves for all the MUT without PEC back, single layer cases of Rogers RT/Duriod 5880.

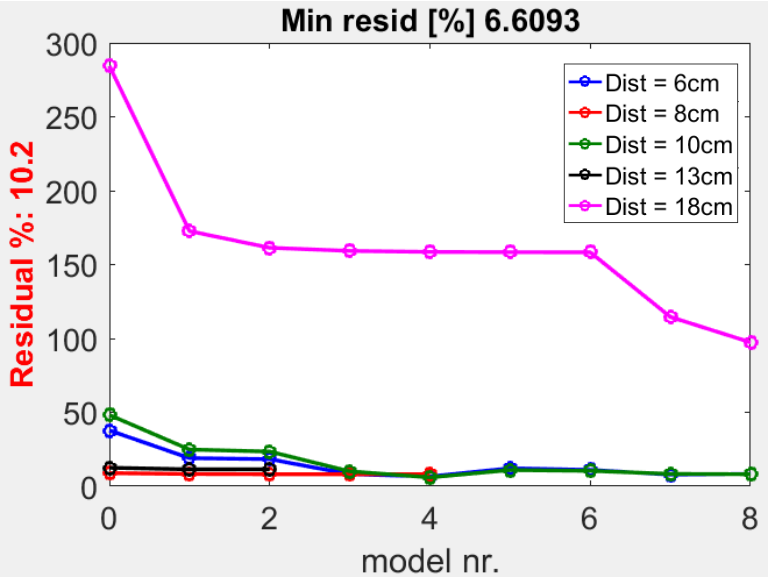

Fig. 5.22 Residual analysis for the case of single layer Rogers RT/Duriod 5880 (WO)

Fig. 5.23 shows the Er vs Td_2 graph for each case of Dist value and model iteration. The negative value on thickness axis represent the positioning error of MUT in the setup. The least positioning error (-0.017mm) was found for the case of 8cm whereas it was more than 0.1mm for the case of 6cm, the thickness of Roger RT/Duriod 5880 is estimated between 0.337 and 0.5260mm, where Td_1 = 0.337mm

was for the case of Dist = 18cm. It has been concluded that at lower Td_2 value with increasing Dist values, the model parameters weren't estimated accurately. TABLE 5.5 summarize the analysis of the Roger RT/Duriod 5880 in terms of Er and Td estimations for the MUT without PEC back scenario.

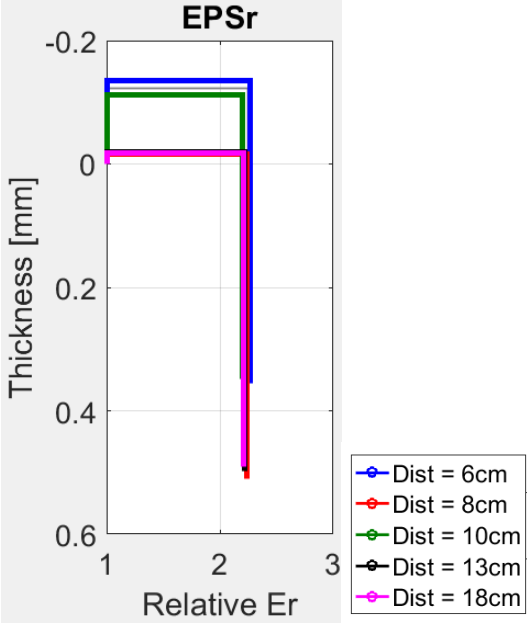

Fig. 5.23 Dielectric constant (Er) vs thickness (Td) for the case of single layer Rogers RT/Duriod 5880 (WO)

TABLE 5.5 SUMMARY OF ANALYSIS – SINGLE LAYER ROGERS RT/DURIOD 5880 (WO)

Parameter	**Relative Er**	**Thickness Td_2 (mm)**	**Positioning Error Td_1 (mm)**
6cm	2.264	0.489	-0.136
8cm	2.231	0.526	-0.017
10cm	2.046	0.512	-0.073
13cm	2.214	0.518	-0.020
18cm	1.767	0.337	0.094

The probability density is presented with respect to the eigenvectors in the model space. The absolute values of eigenvectors in the model space behave the same way as shown in Fig. 5.24, where the eigenvectors are stacked on the horizontal axis (left to right) with decreasing singular values whereas the model parameters are stacked on the vertical axis (bottom to top). From the Fig. 5.24, Td_2 was the parameter with highest confidence (associated to the first eigenvector), then Td_1 (second eigenvector) and finally, Er (third eigenvector). The confidence on the Td_2 and Er parameter was not good enough

at the Dist = 18cm case. In the free space measurements, the inversion problem is able to find higher confidence in the thickness of MUT as compared to dielectric constant (Er).

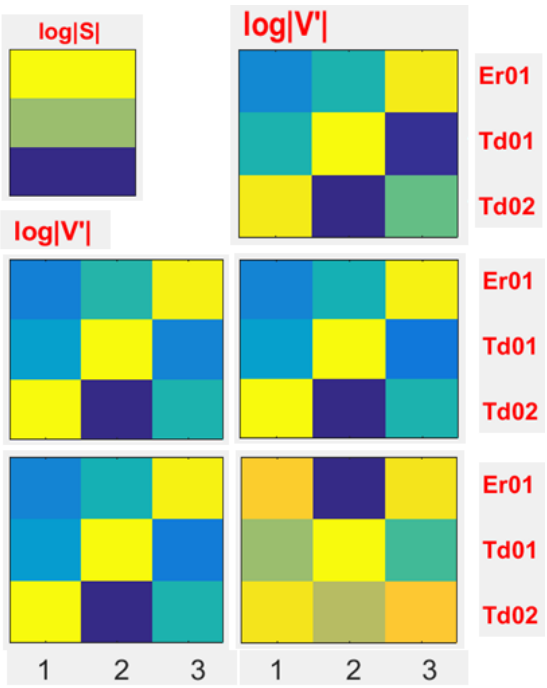

Fig. 5.24 Matrix G: eigenvectors in the model space for all the cases of single layer Rogers RT/Duriod 5880 (WO)

c) Measurements at W band (70 -110GHz)

Another set of measurements has been conducted at UPC Barcelona for W band (70-110GHz). Different material with wide range of MUT thickness (Td_2) has been used in the measurements such as Rogers AD600 (Er = 6.15, Td_2 = 0.52mm), Rogers RT/Duriod 5880 (Er = 2.2, Td_2 = 0.65mm), FR4 Epoxy (Er = 4.7, Td_2 = 1.52mm), Bayblend White (Er = 2.76, Td_2 = 3.3mm) and MK2447 (Er = 2.74, Td_2 = 10mm). The scattering data measurements has been done using the focusing lens between Tx and MUT, and the distance between Tx-Lens and Lens-MUT was fixed at 20cm. The similar Ka band approach is applied here, the scattering response is converted into the time domain echoed data and compared computed echo curve as shown in the Fig. 5.25. The time delay has been observed in the measured and computed echo curves and a delay factor of $1x10^{-8}$sec is added in the observed echo curve before the inversion process.

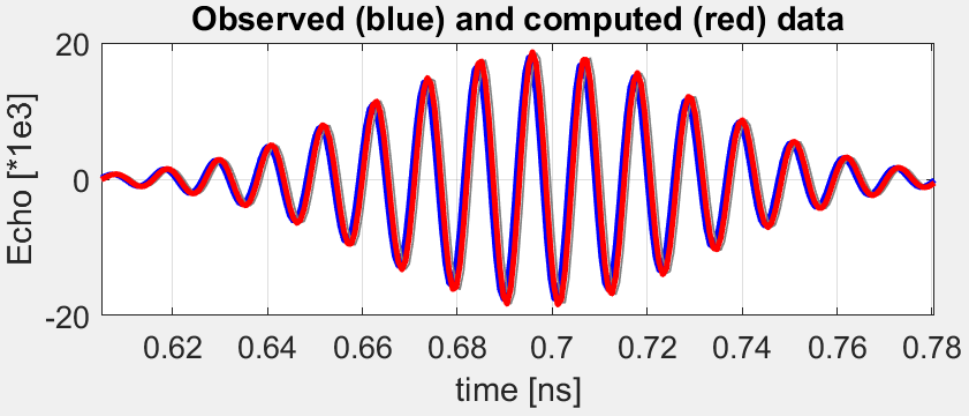

Fig. 5.25 Echo comparison for the case of single layer materials – W band

The residual response for different materials is calculated at the W band for a fixed distance from the Tx. Each material behaved differently and lowest residual was observed for the material with less thickness whereas FR4 Epoxy, Rogers RT/Duriod and MK2447 showed the similar residual response, with the maximum probability density achieved at 4th model iteration (M_4). The minimum residual % of 2.6 was found for Rogers AD600 at the 6th model iteration (M_6). The highest residual % was observed for Bayblend white but the inversion method was still able to estimate the accurate model parameters with less than 5% tolerance. Fig. 5.26 shows the % residual curves for all the single layer cases at W band.

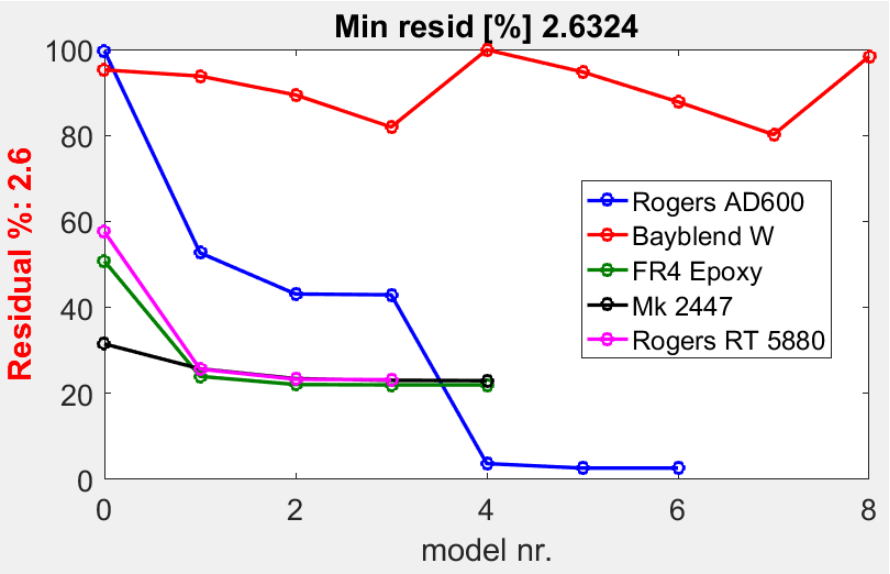

Fig. 5.26 Residual analysis for the cases of single layer materials – W band

The estimated model parameter are Er, Td_1 and Td_2 where Td_1 is positioning error in the placement of MUT after the lens and Td_2 is the thickness of MUT. Fig. 5.27 shows the Er vs Td_2 graph where Er value against the corresponding thickness (Td_2) is plotted for each material. The positioning error was very high for the case of Rogers AD600 i-e; 0.65mm which is more than the thickness of the MUT.

Similarly, positioning error was also high for Rogers RT/Duriod 5880 i-e, 0.27mm which effected the estimation of Er too. For the cases of FR4 Epoxy, Bayblend and MK2447, we have found good estimation of the model parameters with lesser positioning error. It has been concluded that, at higher frequency measurements, the model parameters for the materials with larger thickness are easy to estimation as compared to the materials with less thickness. TABLE 5.6 summarize the analysis of different materials at W band in terms of Er and Td estimations.

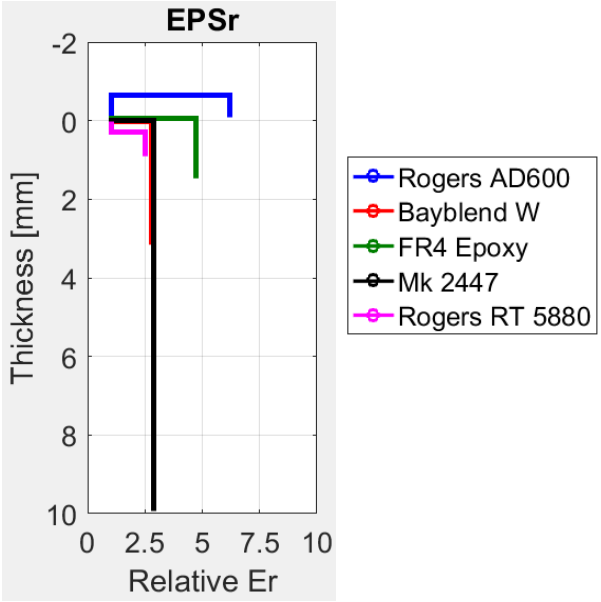

Fig. 5.27 Dielectric constant (Er) vs thickness (Td) for the cases of single layer materials – W band

TABLE 5.6 SUMMARY OF ANALYSIS – SINGLE LAYER MATERIALS

Material	**Relative Er**	**Thickness Td_2 (mm)**	**Positioning Error Td_1 (mm)**
Rogers AD600	6.180	0.556	-0.652
Bayblend W	2.753	3.132	0.013
FR4 Epoxy	4.701	1.520	-0.076
MK2447	2.877	9.921	-0.006
Rogers RT/Duriod 5800	2.487	0.621	0.279

The probability density is presented with respect to the eigenvectors in the model space. The five different materials at a fixed Dist = 18cm are discussed and the confidence on the model parameters has been found from the given model space. The absolute values of eigenvectors in the model space behave the same way as shown in Fig. 5.28, where the eigenvectors are stacked on the horizontal axis (left to right) with decreasing singular values whereas the model parameters are stacked on the vertical axis (bottom to top). From the Fig. 5.28, it is observed that for the case of Rogers AD600, FR4 Epoxy and Rogers RT/Duriod 5880, Td_2 was the parameter with highest confidence (associated to the first eigenvector), then Td_1 (second eigenvector) and finally, Er (third eigenvector), whereas, for the case of Bayblend white, Td_1 was the parameter with highest confidence (associated to the first and second eigenvector), and finally, Td_2 (third eigenvector). In case of MK2447, Er was the parameter with highest confidence (associated to the first eigenvector), then Td_1 (second eigenvector) and finally, Td_2 (third eigenvector). In the free space measurements, the inversion problem is able to find higher confidence in the thickness of MUT or positioning error as compared to dielectric constant (Er), expect in case of Dist = 13cm.

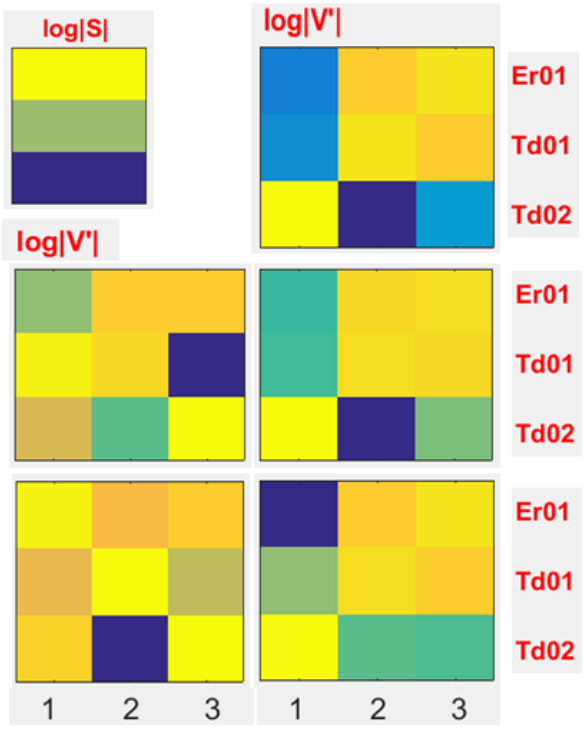

Fig. 5.28 Matrix G: eigenvectors in the model space for all the cases of single layer materials – W band

5.2.2 Multiple Layer Materials

After the detailed single layer analysis of various materials, we have studied the multi-layer materials with given Er and thickness. We have carried out measurements at Ka band for three multi-layer cases which include two dual-layer cases and one tri-layer case. The multi-layer cases along with the estimated model parameters are tabulated in Table. 5.7. The dual-layer cases show good estimation of model parameters with low positioning error, similarly, the tri-layer case also showed relatively higher positioning error but still good estimation of model parameters are obtained. We have studied many other multi-layer cases but only knowledgeable results and cases are presented here.

TABLE 5.7 SUMMARY OF ANALYSIS – MULTI-LAYER MATERIALS

Cases	Material	Relative Er	Thickness (mm)	Positioning Error (mm)
Case 1	Rogers RT/Duriod 5800	2.177	0.538	0.012
	FR4 Epoxy	4.668	0.759	
Case 2	Rogers AD600	6.152	0.504	-0.018
	FR4 Epoxy	4.687	1.503	
Case 3	Rogers RT/Duriod 5800	2.487	0.621	0.279
	FR4 Epoxy	4.690	0.776	
	Rogers AD600	6.147	0.501	

The residual response is also calculated for all the three cases of multi-layer. All the multi-layer case presented above are measured at Dist = 18cm. In these cases, the maximum probability density is achieved with maximum 3rd model iterations (M_3) from the prior model (M_{priori}). The minimum residual percentage of 6.2% is found for case 2 at the 2nd model iteration (M_2), but the estimation of model parameters were also in good agreement with assumed parameters. The residual response for tri-layer materials was also 15% at maximum 3rd model iteration (M_3). Fig. 5.29 shows the % residual curves for all the multi-layer cases at Ka band.

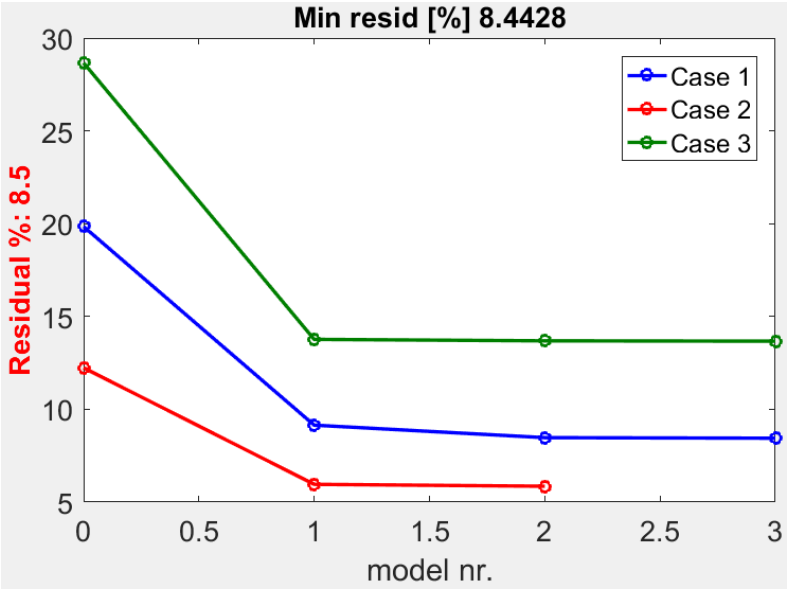

Fig. 5.29 Residual analysis for the cases of multi-layer materials

The estimated model parameter are Er, Td_1 and Td_2 where Td_1 is positioning error in the placement of multi-layer MUT and Td_2 is the thickness of MUT. Fig. 5.30 shows the Er vs Td_2 graph where Er value of each layer with respect to corresponding thickness is plotted for all the multi-layer cases. The positioning error was more than 0.2mm for tri-layer case but it didn't effected the estimation of model parameters. For both dual layer cases, the positioning error remained below 0.01mm and the model parameters were estimated with less than 5% tolerance.

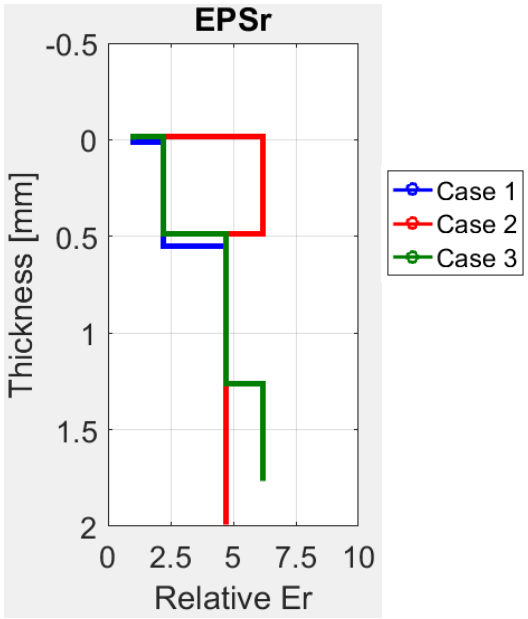

Fig. 5.30 Dielectric constant (Er) vs thickness (Td) for the cases of multi-layer materials

The three different cases of multi-layer has been discussed and confidence on the model parameters has been found from the given model space. The absolute values of eigenvectors in the model space behave the same way as shown in Fig. 5.31(a-b). From the Fig. 5.31(a), it is observed that, for the first dual layer case (left side), Td_2 was the parameter with highest confidence (associated to the first eigenvector), then Td_3 (second eigenvector), Td_1 (third eigenvector), Er_2 (fourth eigenvector) and finally, Er_1 (fifth eigenvector), whereas, for the second dual layer case (right side), Td_3 was the parameter with highest confidence (associated to the first eigenvector), then Td_2 (second eigenvector), Er_2 (third and fourth eigenvector) and finally, Td_1 (fifth eigenvector). From the Fig. 5.31(b), for the case of tri-layer materials, Td_3 was the parameter with highest confidence (associated to the first eigenvector), then Td_2 (second eigenvector), Td_4 (third eigenvector), Er_3 (fourth eigenvector), Er_4 (fifth eigenvector) and finally, Er_1 (sixth and seventh eigenvector). In the free space measurements, the inversion problem has found higher confidence in all the thicknesses of MUT as compared to different dielectric constants (Er) of multi layers.

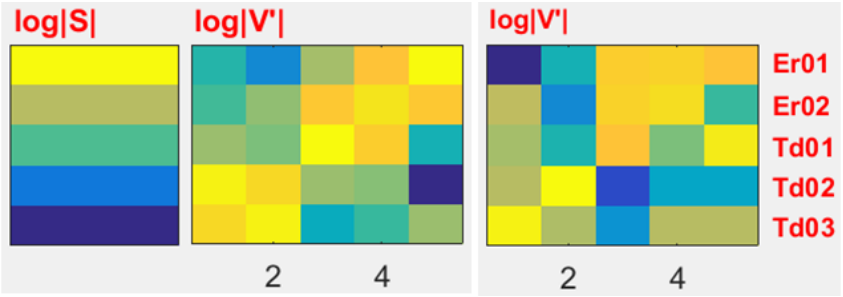

(a)

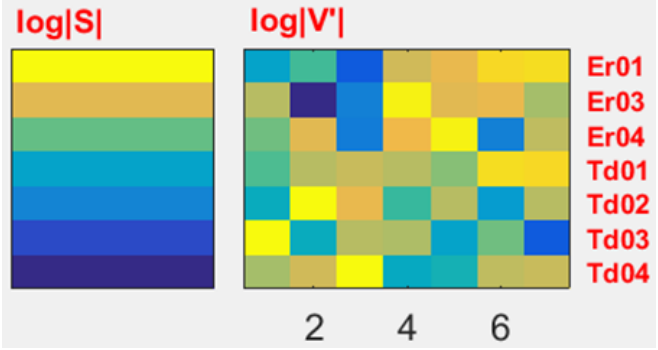

(b)

Fig. 5.31 Matrix G: eigenvectors in the model space for all the cases of multi-layer materials (a) 2 layers (b) 3 layers

CHAPTER 6

Conclusion and Future Work

This chapter summarizes my research work with all the important results of studies and contributions to the knowledge made during the course of this doctoral thesis. All the work done is briefly recalled to provide the reader with full overview of research contributions, possible applications and future work sugesstions.

6.1 Conclusion

The doctoral thesis is summarized in terms of all the contributions made to the knowledge during this research work. Initially, the study on conventional microstrip and horn antenna designs has been conducted, especially for radiation characteristics and spot-focusing enhancement. We have designed stacked patch antennas to achieve UWB with good radiation characteristics and horn antennas with novel idea, to improve the horn antenna profile rather than including the lens correction. The horn antenna profiling allowed us to measure the scattering reflection parameters of MUT at variable distances from the horn antenna source which was not possible with lens corrected horns. We have designed two different spot focused horn antennas; shaped horn for frequency domain analysis and exponential horn for time domain analysis. In the second part of thesis, the research work is focused on the characterization of electrical and physical properties of the materials such as dielectric constant, loss tangent and thickness for single and multi-layered materials at different frequency bands i-e; 26-40GHz, 75-110GHz and 915-925GHz. The free space reflection measurement technique is used for data acquisition using commercially available Anritsu VNA. The dielectric measurements are carried out at PoliMI and UPC Barcelona to validate the results in multiple environments and test benches. The frequency domain analysis is done at 915-925GHz band which was a simulation based research. Although, different data inversion techniques in time domain analysis are used at Ka (26-40GHz) and W band (75-110GHz) bands. The time domain Fourier inversion and time domain Bayesian inversion methods are implemented and improvement in this thesis with the focus on betterment of results accuracy as well as reduction of computational power and time. We have successfully achieved relatively improved estimation of dielectric properties as compared to the reported techniques whereas the computation power and time is significantly reduced when compared to commercial softwares like Ansys HFSS and CAD FEKO. Eventually, the novel horn antenna designs and improved time domain data inversion methods made this research, a very useful contribution in the development of latest dielectric measurement and imaging systems.

The major contributions done in this doctoral research work are highlighted in following points;

1. **Antenna Profiling:** The different antenna are designed for improved performance in dielectric measurements where, the novel design UWB microstrip antennas with stacked patch configuration has been proposed. Furthermore, the shaped horn and exponential horn antenna structures has been presented with customized profiles especially tuned to enhance the spot focusing performance which is helpful in improvement of image resolution in dielectric measurements. All the simulation work is carried out in MATLAB 2016b and Ansys HFSS; both for antenna design as well as antenna integration in measurement setup.
2. **Dielectric Measurements:** The reflection based dielectric measurement system has been implemented as discussed in chapter 3. The experiments are conducted both in simulations and

measurements using MATLAB 2016b and Ansys HFSS, and experimental setups at PoliMI and UPC, respectively. The scattering responses are extracted for multiple distances between Tx and MUT, different materials, thicknesses and areas of MUT. The scattering parameters (S_{11} and S_{21}) are obtained at terahertz band (915-925GHz) using both transmission and reflection methods for frequency domain dielectric properties estimation. Later, scattering parameters (S_{11}) for the microwave and millimetre wave bands (26-40GHz and 75-110GHz) has also been obtained by only reflection method to be used for time domain data inversion.

3. **Time Domain Inversion:** The scattering results obtained by measurements has been used to estimation the material parameters using different data inversion methods. The custom built MATLAB post processing code with Fourier inversion and Bayesian inversion methods has been used for material characterization. The variety of dielectric substrates e.g., FR4, Roger AD600, RT/Duriod5880, Bay-blend, MK2447 etc. has been measured and their dielectric properties are estimated over frequency dispersion. Using MATLAB was found time efficient as compared to commercially available softwares.
4. **Bayesian Inversion:** The Bayesian data inversion method is found one of the accurate and time efficient inversion methods especially for reducing the uncertainties in estimation of electrical and magnetic parameters of various materials. This method is used in quantitative characterization of desired material properties from the measured scattering parameters, particularly the thickness of material (Td_2) and positioning error (Td_1) and dielectric constant (Er). The estimations were in good agreement with the prior model parameters having less than 5% tolerance.
5. **Multi-Layer Estimation:** The multi-layer materials with given Er and thickness parameters are also estimated using the Bayesian inversion method. We have carried out measurements for three multi-layer cases which include two dual-layer cases and one tri-layer case. The multi-layer analysis is done at Ka band and the scattering data is obtained and converted into the time domain echoed data and compared with corresponding computed echo curve. The dual-layer cases showed good estimation of model parameters with low positioning error, whereas, the tri-layer case showed relatively higher positioning error but still good estimation of model parameters are obtained with lower confidence on Er values. There are many other multi-layer cases which has been studied to validate the inversion method.

6.2 Future Work

To the best of our knowledge, still plenty of work can be done in dielectric measurements and material characterization. The time domain inversion provide more scope of improvement in the parameter estimation accuracy as compared to frequency domain analysis. There are many innovative ideas that can be suggested for future work in order to solve several problems that still need to be addressed for better results, such as:

1. Designing a microstrip and horn antennas with more directive radiation characteristics and spot focused beam, to get better scattering results for MUT area lesser than $5x5cm^2$.
2. The extraction of scattering parameters by using more accurate positioning system which can help reducing the challenge of positioning error in the measurements.
3. The expansion of dielectric measurement to other form of materials apart from solid materials such as flexible materials, liquids etc.
4. The improvement of data inversion methods for the estimation of lower material thicknesses and higher dielectric constants.
5. The extension of analysis on multi-layer materials with possibly four or higher layers stacked without air gaps.

LIST OF PUBLICATIONS

1. **Saleem Shahid,** G. Guido Gentili, “Material Properties Estimation for Microwave Imaging using Body of Revolution Technique”, *submitting in IEEE Transactions on Microwave Theory and Techniques*, 2017, IF: 2.897
2. **Saleem Shahid,** G. Guido Gentili, “Material Characterization at W-band using Bayesian Inversion Technique”, *submitting in IEEE Microwave and Wireless Components Letters*, 2017, IF: 1.887
3. **Saleem Shahid**, Hamza Nawaz, G. Guido Gentili, "Wideband Dielectric Resonator Antenna using CPW Fed Segments", *Wiley Microwave and Optical Technology Letters*, vol. 58 pp.441-445, October 2015, IF: 0.731 [link]
4. **Saleem Shahid**, G. Guido Gentili, “Terahertz Horn Antenna for Frequency Domain Material Properties Estimation”, *2017 IEEE AP-S Symposium on Antennas and Propagation and USNC-URSI Radio Science Meeting*, San Diego, USA, July 9–14, 2017 [link]
5. **Saleem Shahid**, G. Guido Gentili, “Shaped Horn Antenna for Spot Focusing THz Imaging Application”, *2016 Loughborough Antennas & Propagation Conference*, Loughborough, UK, 14-15 November 2016 [link]
6. A. Radawan, **Saleem Shahid**, M. D’Amico, G. Guido Gentili, “Design of Stacked Segmented Ultra-Wide Band Antenna”, *2016 Loughborough Antennas & Propagation Conference*, Loughborough, UK, 14-15 November 2016 [link]
7. **Saleem Shahid**, M. Bersanelli, G.G. Gentili, A. Mennella, E. Pagana, L. Stringhetti, "Compact Test Range for Millimetre wave Antennas", *36th ESA Antenna Workshop on Antennas and RF Systems for Space Science*, pp. 1-3, Noordwijk, Netherlands, October 2015
8. A. S. Elkorany, Said M. Elhalafawy, **Saleem Shahid**, G. Guido Gentili, "UWB Integrated Microstrip Patch Antenna with Unsymmetrical Opposite Slots", *International Conference on Electromagnetics in Advanced Applications (ICEAA 2015)*, pp. 426 - 429, Turin, Italy, September 2015 [link]

BIBLIOGRAPHY

[1] Il S. Seo, W. Seok Chin, D. G. Lee, “Characterization of electromagnetic properties of polymeric composite materials with free space method”, Composite Structures, Vol. 66, Issues 1–4, (2004), pp. 533-542

[2] Birch, J. R, Simonis, G. J, Afsar, M. N, and Wells, T. B., “An intercomparison of Measurement techniques for the determination of the dielectric properties of solids at near millimetre wavelengths”, IEEE Trans MTT, June 1994, 42, 6, pp. 956-963

[3] Correia, L., “Material characterization” ch. 8.2 in COST 231 Final report ed. Damosso E and Correia L: Digital mobile radio towards future generation systems, European Commission, Directorate General XIII, Belgium, 1999, pp. 418-425

[4] Jain, R. C. and Voss, W. A. G., “Dielectric measurement methods for industrial scientific and medical applications in the microwave frequency range”, IETE Technical Review, Sept & Dec 1994, 11, 5 & 6, pp 297 - 311

[5] A.J.L. Adam, “Review of Near-Field Terahertz Measurement Methods and Their Applications”, Journal of Infrared, Millimeter, and Terahertz Waves, (2011), 32:976

[6] “Technique of Microwave Measurements” (M.I.T Radiation Laboratory Series, Vol. 11, McGraw-Hill Book Company, Inc., New York, 1947).

[7] Ghodgaonkar, M. F, Varadan, V. V. and Varadan, V. K., “A free space method for measurement of dielectric constants and loss tangents at microwave frequencies”, IEEE Trans. Instr. and measurement, June 1989, 37, 3, pp 789-793

[8] MA, Z. and Okamura, S., “Permittivity determination using amplitudes of transmission and reflection coefficients at microwave frequency”, IEEE Trans. MTT, 1999, 47, pp. 546-550

[9] Kadaba, P. K., “Simultaneous measurement of complex permittivity and permeability in the millimeter region by a frequency domain technique”, IEEE Trans. Instr. and measurement, Dec 1984, IM-33, 4, pp 336–340

[10] Cullen, A. L., “A new free-wave method for ferrite measurement at millimeter wavelengths”, Radio Science, Dec 1987, 22, 7, pp 1168–1170

[11] Lynch, A. C, Griffiyhs, H. D, Appleton, S, Cullen, A. L, Khosrowbeygi, A. and Benjamin, R., “Free wave measurement of permeability and permittivity of ferrites at millimeter-wave frequencies’, IEE Proc. Science and Measurement Technology, March 1995, 142, 2, pp169-175

[12] Shimabukuro, F, Lazar, S, Chernick, M and Dyson, H., “A quasioptical method for measuring the complex permittivity of materials”, IEEE Trans. MTT, 1984, MTT-32, pp 659-665

[13] Y. Yu and L. Carin, "Three-Dimensional Bayesian Inversion With Application to Subsurface Sensing," in IEEE Transactions on Geoscience and Remote Sensing, vol. 45, no. 5, pp. 1258-1270, May 2007

[14] V. Kolehmainen et al., "Parallelized Bayesian inversion for three-dimensional dental X-ray imaging," in IEEE Transactions on Medical Imaging, vol. 25, no. 2, pp. 218-228, Feb. 2006.

[15] Zheng, L, and Ziqiang, Y., “Measurement of complex permittivity and permeability of materials by quasi-optical method”, Int. J. IR & MMW, 1989, 10, 5, pp. 557-563

[16] Friedsam, G. L. and Biebl, E. M., “A broadband free-space dielectric properties measurement system at millimeter wavelengths”, IEEE Trans. Instr. And measurement, Apr 1997, 42, 2, pp. 515-518

[17] Iijima, Y, Tanaka, T, Kimura, M. and Sato, R., “Measurement of complex permittivity and permeability at millimeter wavelength using a free space method”, Int. Symp. Electromagnetic Compatibility, May 1999, pp. 412–415

[18] Koh, G., “Dielectric properties of ice at millimeter wavelengths”, Geophysical research letters, 1997, 24, 18, pp. 2311-2313

[19] Abbas, Z, Pollard, R. D. and Kelsall, R. W., “A rectangular dielectric waveguide technique for determination of permittivity of materials at W-band”, IEEE Trans. MTT, Dec 1998, 46, 2, pp. 2011–2015

[20] Van Loon, R. and Finsy, R., “Measurement of complex permittivity of liquids at frequencies from 60 to 150GHz”, Reviews Sci. Instrum., Apr. 1974, 45, 4, pp 523-525

[21] https://www.britannica.com/science/dielectric Access date: 07 June, 2017

[22] Larry K. Baxter, "Appendix 2: Dielectric Properties of Various Materials," in Capacitive Sensors: Design and Applications , 1, Wiley-IEEE Press, 1997, pp.287-297

[23] Stephen H. Hall; Howard L. Heck, "Electrical Properties of Dielectrics," in Advanced Signal Integrity for High-Speed Digital Designs , 1, Wiley-IEEE Press, 2009, pp.249-295

[24] Ravindra Arora; Wolfgang Mosch, "Solid Dielectrics, their Sources, Properties, and Behavior in Electric Fields," in High Voltage and Electrical Insulation Engineering , 1, Wiley-IEEE Press, 2011, pp.319-370

[25] Silver, S. (ed.), “Microwave Antenna Theory and Design”, New York: McGraw-Hill, 1949.

[26] Jakes, W. C., “Horn Antennas”, Antenna Engineering Handbook, Chap. 10, H. Jasik (ed.), 1st ed., New York: McGraw-Hill, 1961

[27] Olver, A. D., et al., “Microwave Horns and Feeds”, IEE Electromagnetic Waves Series, Vol. 39, IEEE Press, 1994

[28] Balanis, C. A., “Antenna theory”, New York: Harper & Row, 1982

[29] Federal Communications Commission, First report and order, Revision of Part 15 of commission's rule regarding UWB transmission system FCC 02-48,Washington, DC, 2002.

[30] H.Schantz, The Art and Science of Ultra-Wideband Antennas, Artech House, 2005

[31] Hubregt J. Visser, "Dipole Antennas," in Antenna Theory and Applications , 1, Wiley Telecom, 2012, pp.312

[32] C. Y. D. Sim, C. Wen-Tsan, and L. Ching-Her, "Compact Slot Antenna for UWB Applications," Antennas and Wireless Propagation Letters, IEEE, vol. 9, 2010, pp. 63-66

[33] Guha, Debatosh, and Yahia MM Antar, Microstrip and printed antennas: new trends, techniques and applications. John Wiley & Sons, 2011

[34] Schantz, Hans Gregory, "Introduction to ultra-wideband antennas." IEEE conference on ultra-wideband systems and technologies. Vol. 2993. 2003

[35] Yin, Xun-Cai, et al. "A compact ultra-wideband microstrip antenna with multiple notches." Progress In Electromagnetics Research 84 (2008): 321-332

[36] Chen, Zhi Ning, Terence SP See, and Xianming Qing. "Small printed ultra-wideband antenna with reduced ground plane effect" IEEE Transactions on Antennas and Propagation, 55.2 (2007): 383-388

[37] Z. Ahmed, et al. "Ultra-wideband antenna with WLAN band-notch characteristic," 3rd International Conference on Computer, Control & Communication (IC4), 2013, pp.1-5, 25-26 Sept. 2013

[38] Yin, Xun-Cai, et al. "A planar U type monopole antenna for UWB applications." Progress In Electromagnetics Research Letters 2 (2008): 1-10

[39] A. Lazaro, R. Villarino, and D. Girbau, “Design of tapered slot Vivaldi antenna for UWB breast cancer detection,” Microwave Opt. Tech. Lett., vol. 53, no. 3, pp. 639-343, Mar. 2011

[40] A. Atiah and N. Bowring, “Design of flat gain UWB tapered slot antenna for on-body concealed weapons detections,” Prog. In Electromag. Res. Online, vol. 7, no. 5, pp. 491-495, 2011

[41] D. F. Filipovic, S. S. Gearhart and G. M. Rebeiz, Double-slot antennas on extended hemispherical and elliptical silicon dielectric lenses, IEEE Transactions on Microwave Theory and Techniques, vol. 41, no. 10, (1997), pp. 1738-1749

[42] M. K. T. Al-Nuaimi, W. Hong and Y. Zhang, Design of High-Directivity Compact-Size Conical Horn Lens Antenna, IEEE Antennas and Wireless Propagation Letters, vol. 13, (2014), pp. 467-470

[43] Bird, T. S., and A. W. Love, “Horn Antennas.” In Antenna Engineering Handbook, Chap. 14, J. Volakis (ed.), 4th Ed., New York: McGraw-Hill, 2007

[44] Granet, C., and T. S. Bird, “Optimization of Corrugated Horn Radiation Patterns Via a Spline-Profile,” Proc. 9th Int. Symposium on Antenna Technology and Applied Electromagnetics (ANTEM 2002), Montréal, Canada, Jul. 27–29, 2002, pp. 307–310

[45] Granet, C., et al., “A Smooth-walled Spline-Profile Horn as an Alternative to the Corrugated Horn for Wide Band Millimetre-wave Applications,” IEEE Trans. on Antennas and Propagation, Vol. 52, No. 3, Mar. 2004, pp. 848–854

[46] Granet, C., and G. L. James, “Spline-Profile Smooth-walled C-band Horn,” IEEE Antennas and Wireless Propagation Letters, Vol. 6, 2007, pp. 415–418

[47] Bhattacharyya, A. K., and G. Goyette, “A Novel Horn Radiator with High Aperture Efficiency and Low Cross-polarization and Applications in Arrays and Multi-beam Reflector Antennas,” IEEE Trans. on Antennas and Propagation, Vol. AP–52, 2004, pp. 2850–2859

[48] Tsandoulas, G. N., and W. D. Fitzgerald, “Aperture Efficiency Enhancement in Dielectrically Loaded Horns,” IEEE Trans. on Antennas and Propagation, Vol. AP–20, 1972, pp. 69–74

[49] Lier, E., Y. Rahmat-Samii, and S. R. Rengarajan, “Application of Rectangular and Elliptical Dielcore Feed Horns to Elliptical Reflector Antennas,” IEEE Trans. on Antennas and Propagation, Vol. AP–39, 1991, pp. 1592–1597

[50] Wolf, H., “The Scrimphorn, “A New Compact Multimode Horn for Array Application,” Journées Internationales de Nice sur les Antennes (JINA1988), Nice, France, 1988, pp. 446–449.

[51] James, G. L., “Design of Wide-band Compact Corrugated Horns,” IEEE Trans. on Antennas and Propagation, Vol. AP–32, No. 10, Oct. 1984, pp. 1134–1138

[52] Thomas, B. MacA., G. L. James, and K. J. Greene, “Design of Wide-band Corrugated Conical Horns for Cassegrain Antennas,” IEEE Trans. on Antennas and Propagation, Vol. 34, No. 6, Jun. 1986, pp. 750–757

[53] Gonzalo, R., J. Teniente, and C. del Rio, “Very Short and Efficient Feeder Design for Monomode Waveguide,” Proc. IEEE Int. Symposium on Antennas and Propagation, 1997, pp. 468–471

[54] Granet, C., T. S. Bird, and G. L. James, “Compact Multimode Horn with Low Side lobes for Global Earth Coverage,” IEEE Trans. on Antennas and Propagation, Vol. 48, No. 7, July 2000, pp. 1125–1133

[55] Barrow, W. L., and L. J. Chu, “Theory of the Electromagnetic Horn,” Proc. of the Institute of Radio Engineers, IRE, Vol. 27, Jan. 1939, pp. 51–64

[56] Steel, M. C, Sheppard, R. J. and Collins, R., “Precision waveguide cells for the measurement of complex permittivity of lossy liquids and biological tissues at 35GHz”, J. Physics E: Scientific Instruments, 1987, 20, pp. 872-877

[57] Van Loon, R. and Finsy, R., “Measurement of complex permittivity of liquids at frequencies from 5 to 40GHz’, Reviews Sci. Instrum., Sept. 1973, 44, 9, pp. 1204-1208

[58] Hoshi, N, Nikawa, Y, Kawai, K. and Ebisu, S., “Application of microwaves and millimeter waves for the characterisation of teeth for dental diagnosis and treatment’, IEEE Trans. MTT, June 1998, 46, 6, pp. 834-838

[59] Staebell, K. F. and Misra, D., “An experimental technique for in vivo permittivity measurement of materials at microwave frequencies”, IEEE Trans. MTT, March 1990, 38, 3, pp. 337-339

[60] Misra, D. K. and Eungdamrong, D., “Coaxial aperture sensor and its applications – a tutorial overview”, IEEE Int, symposium on circuits and systems, Sydney, NSW, Australia, May 2001

[61] Misra, D, Chabbra, M, Epstein, B. R, Mirotznik, M. and Foster, K. R., “Noninvasive electrical characterization of materials at microwave frequencies using an open-ended coaxial line: test of an improved calibration technique”, IEEE Trans. MTT, Jan 1990, 38, 1, pp. 8 - 14

[62] Rzepecka, M. A., “A cavity perturbation method for routine permittivity measurement”, Journal of microwave power, 1973, 8, pp. 3-11

[63] Campbell, A. M., “Measurement and analysis of the microwave dielectric properties of tissues”, PhD thesis, University of Glasgow, 1990

[64] Gabriel, C. and Gabriel, S., “Compilation of the dielectric properties of body tissue at RF and microwave frequencies”, Final report for AFOSR/NL Bolling AFB DC 20332-0001, June 1996

[65] http://ourworld.cs.com/soundweapon/millivision.htm

[66] Boric-Lubecke, O, Nikawa, Y, Snyder, W, Lin, J. and Mizuno, K., “Novel microwave and millimeter-wave biomedical applications”, IEEE 4th Int. Conf. Telecommunications in Modern Satellite, Cable and Broadcasting Systems 1999 TELSIKS’99, 1, pp. 186-193

[67] Boric-Lubecke, O, Nikawa, Y, Snyder, W, Lin, J. and Mizuno, K., “Skin properties at millimeter waves”, Proc. Asia Pacific Microwave Conference 1998 APMC’98, 2, pp. 877–880

[68] Gabriel, C, Sheppard, R. J. and Grant, E. H., “Dielectric properties of ocular tissues at 370C”, Phys. Med. Biol., 1983, 28, 1, pp. 43–49.

[69] Guillermo Carpintero; Enrique Garcia-Munoz; Hans Hartnagel; Sascha Preu; Antti Raisanen, "Selected Photonic THz Technologies," in Semiconductor TeraHertz Technology: Devices and Systems at Room Temperature Operation , 1, Wiley-IEEE Press, 2015, pp.408

[70] M. E. Hines and H. E. Stinehelfer Sr., “Time domain oscillographic microwave network analysis using frequency domain data,” IEEE Trans. Microwave Theory Tech., vol. 22, no. 3, 1974

[71] Z. A. Maricevic, T. K. Sarkar, Y. Hua and A. R. Djordjevic, “Time domain measurements with the Hewlett-Packard network analyzer HP8510 using the matrix pencil method,” IEEE Trans. Microwave Theory Tech., vol. 39, no. 3, pp. 538–547, 1991

[72] G. G. Gentili, P. Bolli, R. Nesti, G. Pelosi and L. Toso, “High-Order FEM Mode Matching Analysis of Circular Horns With Rotationally Symmetric Dielectrics”, IEEE Transactions on Antennas and Propagation, vol. 55, no. 10, (Oct. 2007), pp. 2915-2918

[73] Tarantola A. 2005. Inverse Problem Theory

[74] J. C. Martínez-Antón, “Determination of optical parameters in general film–substrate systems: A reformulation based on the concepts of envelope extremes and local magnitudes,” Appl. Opt., vol. 39, no. 25, pp. 4557–4568, Sep. 2000.

[75] “Assessing the Reliability of Complex Models: Mathematical and Statistical Foundations of Verification, Validation, and Uncertainty Quantification”, 2012: The National Academies Press.

[76] E. C. Fear, J. Sill, and M. A. Stuchly, “Experimental feasibility study of confocal microwave imaging for breast tumor detection,” IEEE Trans. Microw. Theory Tech., vol. 51, pp. 887–892, 2003

[77] L. Xu, S. K. Davis, S. C. Hagness, D. W. van der Weide, and B. D. Van Veen,"Microwave imaging via space-time beamforming: Experimental investigation of tumor detection in multilayer breast phantoms," IEEE Trans. Microw. Theory Tech., vol. 52, no. 2, pp. 1856–1865, 2004

[78] J. M. Sill and E. C. Fear, "Tissue sensing adaptive radar for breast cancer detection: experimental investigation of simple tumor models," IEEE Trans. Microw. Theory Tech., vol. 53, no. 11, pp. 3312–3319, 2005

[79] G. Bindu, A. Lonappan, V. Thomas, C. K. Aanandan, and K. T. Mathew, "Acitve microwave imaging for breast cancer detection," Progress in Electromagnetics Research, vol. 58, pp. 149–169, 2006

[80] S. M. Salvador and G. Vecchi, "Experimental tests of microwave breast cancer detection on phantoms," IEEE Trans. Antennas Propagat., vol. 57, no. 6, pp. 1705–1712, 2009

[81] M. E. Hines and H. E. Stinehelfer Sr., "Time domain oscillographic microwave network analysis using frequency domain data," IEEE Trans. Microwave Theory Tech., vol. 22, no. 3, 1974

[82] Z. A. Maricevic, T. K. Sarkar, Y. Hua and A. R. Djordjevic, "Time domain measurements with the Hewlett-Packard network analyzer HP8510 using the matrix pencil method," IEEE Trans. Microwave Theory Tech., vol. 39, no. 3, pp.538–547, 1991

[83] Carcione J.M., Ursin B. and Nordskag J.I. 2007. Cross-property relations between electrical conductivity and the seismic velocity of rocks. Geophysics 72, 193–204

[84] Cerney B. and Bartel D.C. 2007. Uncertainties in low-frequency acoustic impedance models. The Leading Edge 26, 74– 87.

[85] Chen J. and Dickens T.A. 2009. Effects of uncertainty in rock-physics models on reservoir parameter estimation using seismic amplitude variation with angle and controlled-source electromagnetics data. Geophysical Prospecting 57, 61–74

[86] Chen J., Hoversten G.M., Vasco D., Rubin Y. and Hou Z. 2007. A Bayesian model for gas saturation estimation using marine seismic AVA and CSEM data. Geophysics 72, 85–95

[87] Harris P. and MacGregor L. 2006. Determination of reservoir properties from the integration of CSEM, seismic and well log data. First Break 24, 53–59

[88] Jupp D.L.B. and Vozoff K. 1975. Stable iterative methods for the inversion of geophysical data. Geophysical Journal of the Royal Astronomical Society 42, 957–976

[89] Kachanov M., Sevostianov I. and Shafiro B. 2001. Explicit cross property correlations for porous materials with anisotropic microstructures. Journal of the Mechanics and Physics of Solids 49, 1–25

[90] Keller G.V. 1987. Rock and mineral properties. In: Electromagnetic Methods in Applied Geophysics, Part A (ed. M.C. Nabighian), pp. 13–52

[91] S. J. Moon, X. Ye and R. Smith, "Comparison of TRL calibration vs. 2x thru de-embedding methods", IEEE Symposium on Electromagnetic Compatibility and Signal Integrity, Santa Clara, CA, (2015), pp. 176-180

[92] M. Wojnowski, V. Issakov, G. Sommer and R. Weigel, “Multimode TRL Calibration Technique for Characterization of Differential Devices”, IEEE Transactions on Microwave Theory and Techniques, vol. 60, no. 7, (2012), pp. 2220-2247